2021년 2월

박사학위 논문

Study on the anti-aging effects of Compounds isolated from the flowers of *Rudbeckia bicolor* Nutt. and *Coreopsis lanceolata* L.

조선대학교 대학원

약 학 과

이 환

Study on the anti-aging effects of Compounds isolated from the flowers of *Rudbeckia bicolor* Nutt. and *Coreopsis lanceolata* L.

원추천인국과 큰금계국의 꽃으로부터 분리한
화합물의 항노화 효능 연구

2021년 2월 25일

조선대학교 대학원

약 학 과

이 환

Study on the anti-aging effects of Compounds isolated from the flowers of *Rudbeckia bicolor* Nutt. and *Coreopsis lanceolata* L.

지도교수 이 동 성

이 논문을 약학 박사학위신청 논문으로 제출함

2020년 10월

조선대학교 대학원

약 학 과

이 환

이환의 박사학위논문을 인준함

위원장	조선대학교	교 수	우 은 란	(인)
위 원	조선대학교	교 수	홍 준 희	(인)
위 원	원광대학교	교 수	김 윤 철	(인)
위 원	광주대학교	교 수	김 승	(인)
위 원	조선대학교	교 수	이 동 성	(인)

2020년 12월

조선대학교 대학원

Contents

List of Schemes

List of Figures

List of Tables

List of Abbreviations

AD: Alzheimer’s disease

AD: Atopic dermatitis

Alpha-MEM: Minimum Essential Medium Eagle - alpha modification

BuOH: Butyl alcohol

C. C.: Column chromatography

***C. lanceolata*:** *Coreopsis lanceolata* L.

CD spectra: Circular dichroism

$CDCl_3$: Deuterated chloroform

CD_3OD: Deuterated methanol

CH_2Cl_2: Dichloromethane

CNS: Central nervous system

COSY: Correlation spectroscopy

COX-2: Cyclooxygenase-2

DEPT: Distortionless Enhancement by Polarization Transfer

DMEM: Dulbecco's Modified Eagle's Medium

DMSO: Dimethyl sulfoxide

ECL: Enhanced Chemiluminescence

EIMS: Electron impact mass spectroscopy

EtOAc: Ethyl acetate

FBS: Fetal bovine serum

HMBC: Heteronuclear Multiple Bond Correlation

HPLC: High performance liquid chromatography

HREIMS: High resolution electro impact mass spectroscopy

HSQC: Heteronuclear Single Quantum Coherence

H_2O: Water

H_2O_2: Hydrogen peroxide

IFN-γ: interferon-gamma

IL-6: Interleukin-6

IL-8: Interleukin-8

iNOS: Inducible nitric oxide synthase

IR: Infrared spectroscopy

KCl: Potassium Chloride

LOD: Limit of detection

LOQ: Limit of quantitation

LPS: Lipopolysaccharide

M. W.: Molecular weight

MHz: Mega hertz

MS: Mass spectrum

MTT: 3-(4,5-dimethylthiazol-2-yl)-2,5-diphenyltetrazolium bromide

NaCl: Sodium Chloride

NF-κB: Nuclear factor-kappa B

NMR: Nuclear magnetic resonance

NO: Nitric oxide

NP: Normal phase

OH: Hydroxy radical

O_2^-: Superoxide

$^1O_2$: Singlet oxygen

PBS: Phosphate-buffered saline

PGE_2: Prostaglandin E2

***R. bicolor*:** *Rudbeckia bicolor* Nutt.

RANTES: Regulated upon activation, normal T cell expressed and secreted

RNS: Reactive nitrogen species

ROS: Reactive oxygen species

RP: Reverse phase

RPMI: Roswell Park Memorial Institute

RT: Retention time

S: Slope calibration curve

SD: Standard deviation

SDS-PAGE: Sodium dodecyl sulfate-polyacrylamide gel electrophoresis

SE: Standard error

TARC: Thymus and activation-regulated chemokine

TLC: Thin layer chromatography

TNF-*α*: Tumor necrosis factor-alpha

UV: Ultraviolet

FD-MS: Field desorption mass spectrometry

^{1}H NMR: Proton NMR

^{13}C NMR: Carbon NMR

br: Broad (in connection with NMR data)

d: Doublet (in connection with NMR data)

***J*:** Spin-spin coupling constant [Hz]

m: Multiplet (in connection with NMR data)

ppm: Parts per million

s: Singlet (in connection with NMR data)

t: Triplet (in connection with NMR data)

국문 초록

원추천인국(*Rudbeckia bicolor* Nutt.)과 큰금계국(*Coreopsis lanceolata* L.)의 꽃으로부터 분리한 화합물의 항노화 효능 연구

이 환
지도교수 : 이 동 성
약학과
조선대학교 대학원

고령화 사회가 급속도로 진행됨에 따라 사람들의 건강관리도 관심이 높아지고 있다. 고령화가 진행될수록 노화에 관한 발병률이 증가하고 있으며, 노화 예방관련 식품, 의약품, 화장품들도 무수히 연구되고 있다. 노화는 면역조절, 산화스트레스 등과 관련이 있으며, 이는 염증으로 이어지고 신경퇴행성질환 및 피부노화로 이어진다. 신경퇴행성질환의 종류로는 알츠하이머, 헌팅턴, 파킨슨 병이 포함되며, 이들은 모두 염증과 관련이 있다. 신경퇴행성질환과 관련된 또 다른 반응은 아폽토시스, 염증성사이토카인 등 아직까지도 밝혀지지 않은 다양한 발병기전들이 존재한다.

시간이 지남에 따라 인간의 피부는 자연적인 노화, 외부적 손상 등의 과정을 거치며 노화가 일어난다. 피부 노화는 크게 내인성요인과 외인성요인으로 구분되며, 주름형성, 색소침착, 피부건조, 두꺼운 피부, 탄력저하 등의 증상이 발생한다. 피부노화의 대표적인 질환은 건선, 아토피성 피부염, 알

레르기성 접촉 피부염과 같은 염증성 피부질환이 있으며, 이들은 염증과도 밀접한 관련이 있다.

국화과(Compositae) 식물은 세계에 널리 분포하고 있으며, 약 920속 20000종이 알려져있고, 오래전부터 약용소재로써 사용되어왔다. 그 중 원추천인국(*Rudbeckia bicolor* Nutt.)과 큰금계국(*Coreopsis lanceolata* L.)은 길가에 흔히 보이는 생존력이 높은 식물로 알려져 있다. 하지만 원추천인국과 큰금계국의 꽃 함유성분에 대한 연구와 항노화에 관련된 연구는 거의 보고된 바가 없다. 이에 본 연구에서는 원추천인국과 큰금계국 추출물과 하위 분획물의 항노화 활성을 확인하였고, 그 활성성분을 분리하고자 하였다. 원추천인국과 큰금계국의 꽃 70% EtOH 추출물로부터 9개의 화합물 (patulitrin, eupatolitin-3-*O*-glucoside, eupatolin, beta-amyrin, phenylheptatryine, 2'-hydroxy-3,4,4'-trimethoxy chalcone, 4 ', 7-dimethoxyflavanone, 8-methoxybutin, leptosidin)을 분리하고 구조동정하였으며, 이들 화합물이 BV2, RAW264.7, HT22, HaCaT 세포주에서 염증성 사이토카인 생성 억제 및 NO, 세포보호효과 등의 효과를 확인하였다. 그 결과 원추천인국 H_2O 분획물을 제외한 추출물과 모든 분획물 및 큰금계국 추출물과 EtOAc, BuOH 분획물은 HT22 해마세포에서 산화스트레스에 의한 신경독성으로부터 신경세포보호효과가 확인되었으며, 원추천인국과 큰금계국의 추출물 및 모든 분획물은 LPS로 유도한 BV2 미세아교세포에서 항신경염증 효과를 확인하였다. 또한 원추천인국과 큰금계국의 BuOH 분획물을 제외한 추출물 및 모든 분획물에서 LPS

로 유도한 RAW264.7 대식세포에서 항염증 효과를 확인하였으며, 피부노화와 관련된 HaCaT 각질세포에서는 원추천인국의 EtOAc 분획물을 제외한 추출물과 분획물에서, 큰금계국의 BuOH 분획물을 제외한 추출물과 분획물에서 피부염증 억제효과를 나타내었다. 또한, 분리한 화합물 9종 중 5종(patulitrin, beta-amyrin, phenylheptatryine, 8-methoxybutin, leptosidin)에 대해 항노화와 관련된 염증억제효과를 확인한 결과 phenylheptatryine과 8-methoxybutin은 BV2 미세아교세포와 RAW264.7 대식세포에서 항신경염증 및 항염증 효과가 가장 우수하였다. 추가적으로, 분리된 화합물을 이용하여 원추천인국과 큰금계국 추출물의 지표성분에 대한 정성 및 정량평가를 진행한 후, 표준화 연구를 수행하였다. 이에 원추천인국과 큰금계국은 항노화와 관련된 천연 소재로써 개발 가능성이 있음을 시사한다.

Abstract

Study on the anti-aging effects of Compounds isolated from the flowers of *Rudbeckia bicolor* Nutt. and *Coreopsis lanceolata* L.

Lee, Hwan

Advisor: Prof. Lee, Dong-Sung

College of Pharmacy

Graduate School of Chosun University

Because of a rapidly aging society, people's interest in health care is also increasing. With the progress of the aging process, the incidence of aging-related issues also increases; therefore, foods, medicines, and cosmetics related to aging are being studied extensively. Aging is related to immune regulation and oxidative stress, which lead to inflammation, neurodegenerative diseases, and skin aging. Neurodegenerative diseases include Alzheimer's, Huntington's, and Parkinson's, all of which are associated with inflammation. Another reaction associated with neurodegenerative diseases is apoptosis induced by inflammatory cytokines and other processes that have not yet been identified. Skin diseases related to aging also exist. Over time, human skin ages through processes such as natural aging and external damage. Skin aging is largely categorized as owing to endogenous and exogenous factors, and results in symptoms such as wrinkle formation, pigmentation, xeroderma, thick skin, and loss of elasticity. Representative diseases of skin aging include inflammatory skin diseases such as psoriasis, atopic dermatitis, and allergic

contact dermatitis, which are also closely related to inflammation.

Compositae are widely distributed globally, comprising approximately 920 genera and 20,000 species and are known to have been used as medicinal materials for a long time. Among them, *Rudbeckia bicolor* Nutt. and *Coreopsis lanceolata* L. are plants belonging to Compositae, which are commonly seen on the roadside. However, not much is known about both plants to date. Thus, the 70% EtOH extract of *R. bicolor* was investigated and compounds patulitrin, eupatolitin-3-*O*-glucoside, eupatolin, and beta-amyrin were isolated and their structures determined. In addition, the compounds phenylheptatryine, 2'-hydroxy-3,4,4'-trimethoxy chalcone, 4',7-dimethoxyflavanone, 8-methoxybutin, and leptosidin were isolated and structures determined from the 70% EtOH extract of *C. lanceolata*. The effects of the isolated compounds were investigated in BV2, RAW264.7, HT22, and HaCaT cell lines, and the inhibition of inflammatory cytokine and nitrite production and cytotoxicity were confirmed. In this study, natural compounds contained in the Compositae plants *R. bicolor* and *C. lanceolata* were identified, and the inhibitory effect of these compounds on the production of inflammatory substances related to aging was confirmed *in vitro* models. As a result, 70% extracts and EtOAc fractions of *R. bocolor* and *C. lanceolata* showed superior anti-aging effect compared to other fractions. Among the isolated compounds, phenylheptatryine and 8-methoxybutin showed the best anti-neuroinflammatory and anti-inflammatory effect compared to other compounds. In addition, standardization studies were conducted by evaluating the content of major components in extracts *R. bocolor* and *C. lanceolata* as isolated compounds. This suggests that the 70% EtOH extracts of *R. bicolor* and *C. lanceolata* have potential as anti-aging treatments.

Chapter 1.

General Information

Ⅰ. *Rudbeckia bicolor* Nutt.

R. bicolor belongs to the Compositae family and is widely cultivated as an ornamental crop and occurs commonly in the wild [1]. Another name is the 'pinewood coneflower,' as the capitulum has a conical shape. The height of the plant is approximately 30-50 cm, and the flowers are approximately 5-8 cm in diameter. Compositae are widely distributed globally, with approximately 920 genera and 20,000 species known, many of which have been previously studied [2]. In addition, Compositae species have long been known to be effective for colds, stomachache, headache, and hypertension, and have been used as a medicinal material such as antibacterial, antiviral, and anti-inflammatory [3-5]. Among them, *R. bicolor* is not yet known, although there is a precedent for a member of the same genus being used traditionally as a medicinal plant. For example, *Rudbeckia hirta* L., called the 'black-eyed Susan,' has been used by Native Americans to treat colds and inflammation, and studies have been conducted on its antioxidant, anti-inflammatory, and immunomodulation activities [6]. In addition, *Rudbeckia laciniata* L., called the 'cutleaf coneflower,' was used by Native Americans to treat burns, and studies have isolated natural compounds such as flavonoids and sesquiterpenoids [7]. The purpose of this study was to isolate natural compounds contained in *R. bicolor* belong to the Compositae family and evaluate their anti-aging activities.

Fig. 1: *Rudbeckia bicolor* Nutt. (Compositae)

Ⅱ. *Coreopsis lanceolata* L.

C. lanceolata is a perennial plant belonging to the Compositae family, that is native to North America and is distributed in East Asia, Oceania, North America, Central America, and South America [8]. The leaves are green and spear-shaped, flowers 4-6 cm in diameter, and petals are yellow and obovate-shaped [9]. The name *Coreopsis* is derived from the Greek words “koris” and “opsis” that describe the shape of the achene and *lanceolata* is derived from the Latin word for the shape of a long spear [10, 11]. Over a 100 species belong to this genus, including *Coreopsis tinctoria* Nutt., *Coreopsis grandiflora* Hogg ex Sweet, *Coreopsis tripteris* L., and *Coreopsis basalis* (A.Dietr.) S.F.Blake [12]. *C. tinctoria*, a well-known plant of the genus, has been traditionally used in Xinjiang, China as a herbal tea to treat hypertension and diarrhea [13]. In addition, North American Indians used it to treat a number of conditions, including diarrhea, bleeding, vomiting, and for blood strengthening [14]. *C. lanceolata*, which blooms in summer, is known for its use as an ornamental plant. However, owing to its aggressive spread, it is recognized as an ecological disturbance plant in Japan [15]. A previous study isolated various compounds including β-sitosterol, lanceoletin, leptosidin, and luteolin from *C. lanceolata*, and these have been reported to have various effects such as antioxidant, anti-inflammatory, and anti-cancer activity [16-20]. This study aimed to isolate and identify compounds present in *C. lanceolata* and to evaluate their anti-aging related activity.

Fig. 2: *Coreopsis lancelolata* L. (Compositae)

Ⅲ. Chromatography

Extracts from natural products have long been used in traditional medicine for a variety of purposes [21]. However, according to the needs of modern times, a scientific basis for traditional medicine is required. Accordingly, many scientists have employed the chemical separation and analysis method known as chromatography to provide a reasonable scientific basis for natural products used in traditional medicine [22]. Natural product extracts consist of various compounds, the characteristics of which are utilized in chromatography to present a scientific basis for traditional medicines. For example, Taxol isolated from *Taxus cuspidata*, is a proven traditional medicine [23]. There are several types of chromatographic techniques. Liquid chromatography, which is typically used, includes both normal- and reversed-phase chromatography that can separate chemical substances according to their polarity. Similarly, ion exchange chromatography uses ionic interaction for separation and size exclusion chromatography separates compounds according to size [22]. The method used in this study was both normal- and reversed-phase chromatography and size exclusion chromatography, and fractions were additionally purified using a preparative column linked to a high-performance liquid chromatograph.

Ⅳ. Anti-aging and neurodegenerative diseases

Representative diseases of aging include Alzheimer's, Parkinson's, and Huntington's diseases, which are neurodegenerative diseases related to the brain [24, 25]. Generally, aging-related neurodegenerative and neuroinflammatory disorders are caused by various conditions, such as disruption in neurotransmitters, electrophysiology, and neuroimaging [26]. The human brain has various neurons. Microglia, residing in the central nervous system (CNS), play an important role in the innate immune response and protect against exogenous toxins and pro-inflammatory reactions [27, 28]. These cells also remove CNS debris such as damaged neurons and pathogens and maintains synaptic homoeostasis [29]. However, overactivated microglia accelerate neuroinflammation and neurotoxic reactions by releasing various pro-inflammatory cytokines and mediators such as interleukin (IL)-1β, tumor necrosis factor (TNF)-α, cyclooxygenase-2, and inducible nitric oxide synthase [30]. Overexpression of these factors causes apoptosis and damage in midbrain dopaminergic neurons [31]. There are various unknown molecular mechanisms for apoptosis associated with neurodegenerative diseases [32, 33]. The molecular mechanism involved in oxidative stress is the over-accumulation of reactive oxygen species (ROS) and reactive nitrogen species (RNS) leading to lipid, protein, and mitochondrial dysfunction [34]. Associated with mitochondrial dysfunction, there is a further increase in the over-release of ROS and other factors into the cytoplasm, including RNS (H_2O_2, O_2^-, NO, $ONOO^-$ / ONOOH), triggering cellular apoptosis [35, 36]. Abnormally high levels of neuron damage by glutamate, a neurotransmitter in the CNS, is closely related to ROS and RNS accumulation. Currently, an lipopolysaccharide (LPS)-activated experimental model of microglia is used to mimic the inflammatory environment related to neurodegenerative diseases in vitro [37]. When cells are stimulated with LPS, toll-like receptor 4 is

activated, activating the NF-κB pathway, leading to the production of inflammatory mediators, neuroinflammation, and neurodegeneration [38]. Therefore, LPS-induced and abnormally activated microglia can be an effective approach as a therapeutic model for neuroinflammation and neurotoxic reactions [39, 40]. In addition, a hippocampal cell model that causes excitotoxicity is used to mimic apoptosis [41]. Accumulation of glutamate causes oxidative damage and neuronal cell death owing to excessive neuronal activation [42]. In this regard, the hippocampal cell model activated by treatment with glutamate can be an effective approach as a model for suppressing apoptosis. The combination of these two models is thus appropriate as a research method for neurodegenerative diseases [43].

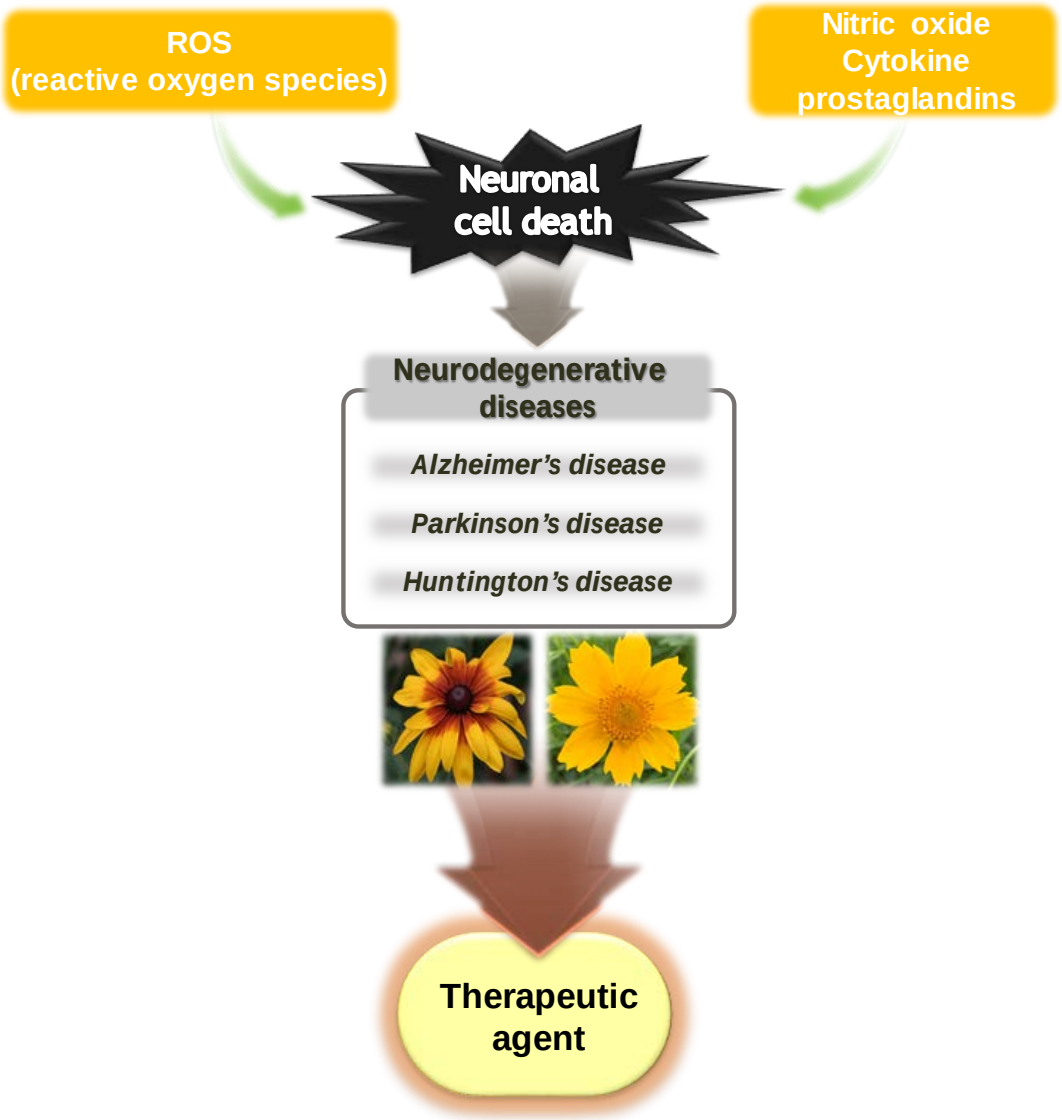

Fig. 3: Oxidative Stress & neuroinflammation

Ⅴ. Anti-aging and skin disease

Human skin undergoes natural aging over time [44]. In addition, human skin continues to suffer harmful damage owing to environmental factors [45]. Skin aging is caused by endogenous and exogenous factors. Endogenous factors include cell metabolism, hormonal changes, and genetic mutations, and exogenous factors include toxins, chemicals, and ultraviolet (UV) radiation [46-48]. In the aging skin, the number of epidermal and dermal cells decreases and the function of the cells decreases, resulting in wrinkles, pigmentation, xeroderma, thick skin, and loss of elasticity. The epidermis protects the skin from external stimuli and various pathogens and plays a role in maintaining moisture and lipid components [49]. Keratinocytes are cells that constitute approximately 95% of epidermal cells. These cells primarily defend against the environment, such as pathogenic bacteria, viruses, UV rays, and allergies, and when they fail to regulate the production of pro-inflammatory mediators, skin inflammation ensues [50, 51]. Excessive production of TNF-α has been linked to inflammatory skin diseases such as psoriasis, atopic dermatitis, and allergic contact dermatitis [52]. Atopic dermatitis is a chronic inflammatory skin disease with allergies and genetic causes. Symptoms of atopic dermatitis include itching, eczema, and hyperkeratosis, and inflammatory cells such as Th2 type cells, eosinophils, and macrophages that penetrate the lesioned skin [53]. TNF-α, an immune cytokine, binds to receptors on the cell surface and activates MAPK, ERK1/2, JNK, and p38 [54]. Moreover, the transcription factor NF-κB induces the expression of genes including those of various cytokines and is involved in inflammatory conditions [55, 56]. Currently, an experimental model of a keratinocyte treated with TNF-α/IFN-γ is used to imitate in vitro the inflammatory environment associated with atopic dermatitis [57]. When epidermal keratinocytes are activated by cytokines, they can produce IL-6 and IL-8, which mediate the entry of Th2-type cells and neutrophils into the epidermis [58]. Thymus and activation-

regulated chemokine (TARC/CCL17) secreted by keratinocytes and regulated upon activation, normal T cell expressed and secreted (RANTES/CCL5) play an important role in the penetration of Th2 cells into inflammatory tissue [59-62]. Therefore, the use of abnormally activated keratinocytes and macrophages can be an effective approach as a therapeutic model that modulates inflammatory factors related to atopic dermatitis.

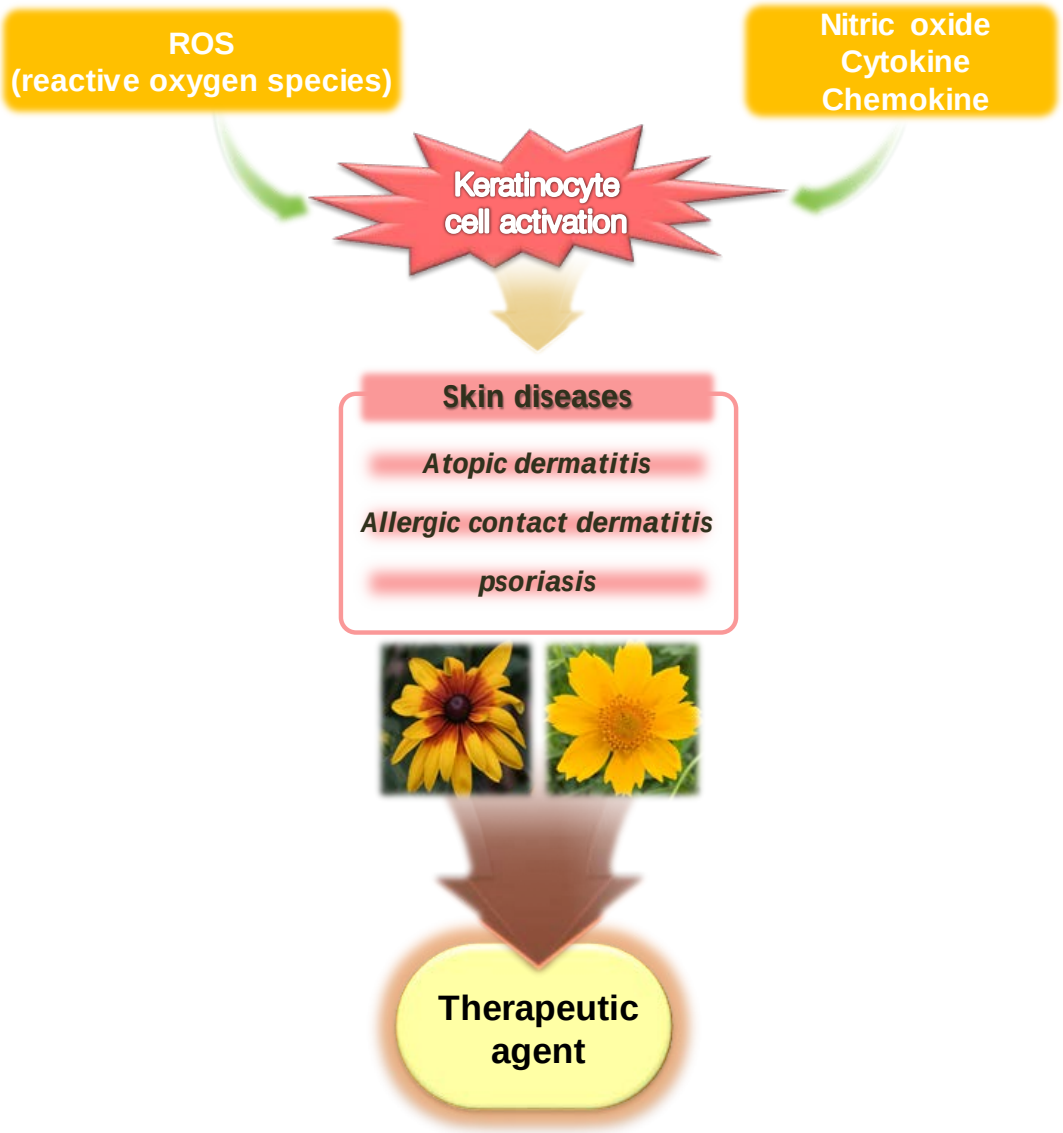

Fig. 4: Oxidative Stress & skin inflammation

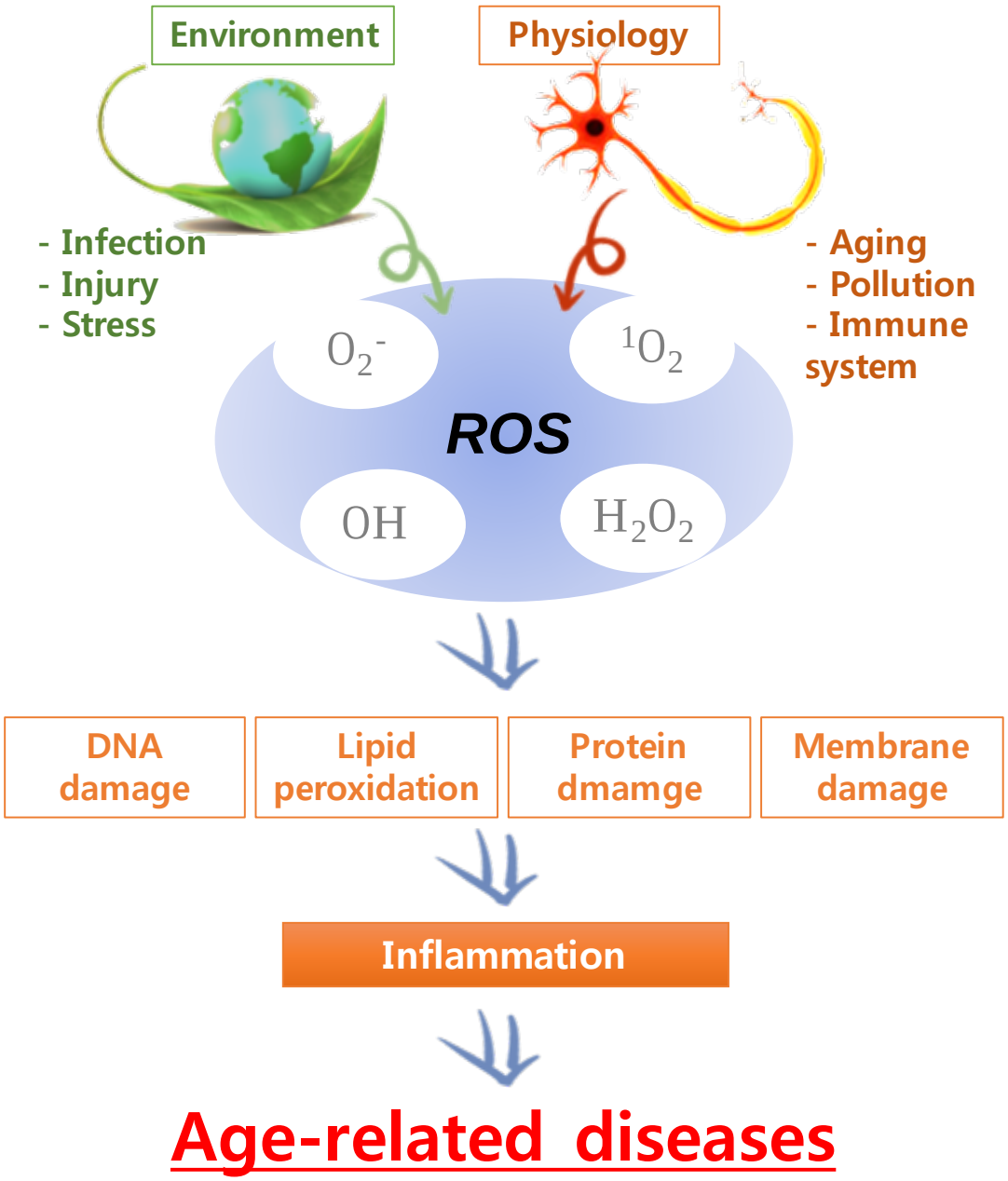

Fig. 5: Inflammatory pathogenesis of age-related diseases

Ⅵ. *In vitro* cell lines for the anti-aging effects

1. Mouse-derived HT22 hippocampal neuronal cell line

The hippocampus plays a memory-related role in the brain [63]. HT22 is a hippocampal neuron cell line that does not express cholinergic and glutamate receptors as do mature hippocampal neurons in vivo [64]. Excessive levels of glutamate cause oxidative stress in HT22 cells, resulting in neuronal cell death [65]. Therefore, the HT22 hippocampal cell model, in which the protective effect from neuronal cell death caused by excessive processing of glutamate can be confirmed, is adopted as an in vitro model in relation to neurodegenerative diseases.

2. Mouse-derived BV2 microglia cell line

Microglia are resident immune cells that regulate the immune response in the central nervous system (CNS) and known to play an important role in defending against pathogenic bacteria in the CNS [66, 67]. However, when they are stimulated by damage or infection, they are abnormally activated and secrete inflammatory mediators and inflammatory cytokines [68]. Overproduction of inflammatory mediators and inflammatory cytokines can lead to nerve cell damage and death [69]. Thus, BV2 microglia, in which abnormal activation can be induced by LPS, is an in vitro model adopted for neurodegenerative diseases.

3. Mouse-derived RAW264.7 macrophage cell line

Macrophages are immune cells that play an important role in immune responses such as phagocytosis, antigen supply, and secretion of cytokines and chemokines [70]. However, when abnormally activated by external stimulation and damage, they produce inflammatory cytokines and inflammatory mediators. This destroys the immune system of macrophages, leading to cell damage and death. Thus, RAW264.7 macrophages, in which LPS treatment can induce abnormal activation, is an in vitro model adopted for inflammation

4. Human-derived HaCaT keratinocyte cell line

The epidermis protects against damage caused by various external factors and plays a role in continuous self-regeneration [71]. Therefore, it has been a focus of intensive medical research for tissue differentiation, wounds, tumors, skin dysfunction, and infection [72]. Keratinocytes are the major cells of the epidermis and are known to be the subject of research in various skin diseases such as atopic dermatitis and psoriasis. HaCaT cells are naturally immortalized human keratin systems and have been widely used in skin biology and differentiation [73]. The characteristic of atopic dermatitis is an environmental imbalance owing to elevated levels of inflammatory cytokines, chemokines, and monokines, and a complex inflammatory network regulates the pathogenesis of atopic dermatitis [74]. Accordingly, HaCaT keratinocytes that have been activated by inflammatory cytokines are an in vitro model adopted for atopic dermatitis.

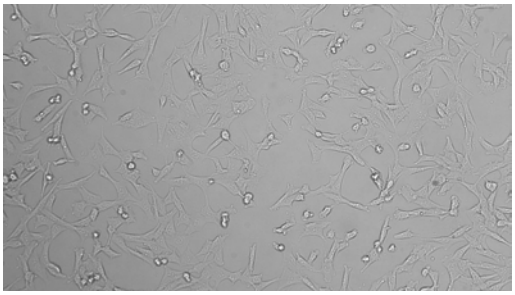

HT22 murine hippocampal

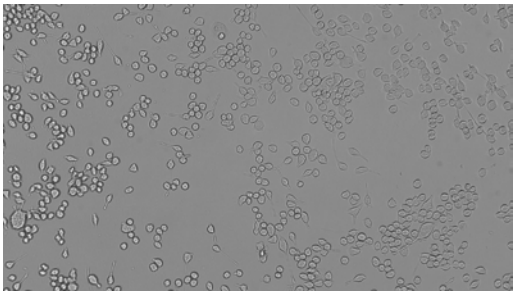

BV2 murine microglia

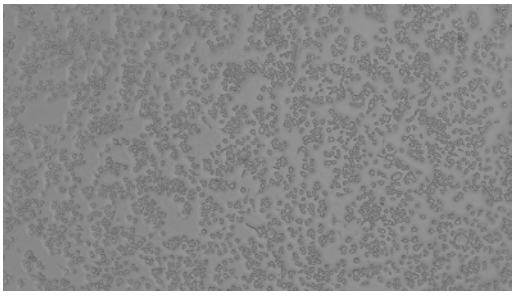

RAW264.7 murine macrophage

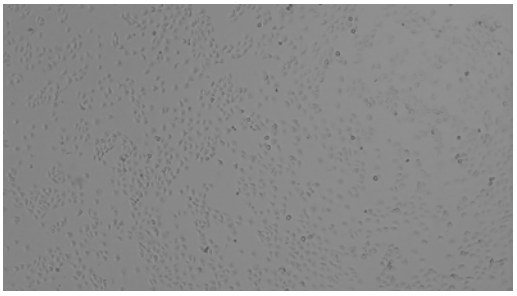

HaCaT human keratinocyte

Fig. 6: Morphology of the cell lines captured by microphotography

Chapter 2.

Isolation of natural compounds from the flowers of *R. bicolor* Nutt. and *C. lanceolata* L.

Ⅰ. Introduction

The range of natural products is broad, including those obtained from plants, animals, microorganisms, and marine organisms, and these have been used as medicine for thousands of years [75]. As evidence, in ancient Egypt, saw palmetto (*Serenoa repens*) was used for urinary symptoms, and a classic Chinese book called 'Huangdi Neijing' describes it as a traditional herbal medicine [76, 77]. In addition, this product has been sold as a medicinal herb for more than 2200 years and has been used for disease treatment [21]. Previously, natural products were used in the form of traditional medicine in each country; however, in Europe, they are legalized and regulated based on Directive 2004/24/EC [78]. In the United States, in 2004, the Food and Drug Administration published industry guidelines for botanical drugs incorporated in the existing system of food ingredients [79]. Unlike previously, modern natural products are used to treat diseases in the form of foods and medicines, and not in the form of herbs. Representative natural medicines include aspirin (Bayer, Germany), Taxol (BMS, USA), and Tamiflu (Gilead, USA).

Compared to synthetic compounds, natural products are a promising source for discovering new drugs based on their diverse structures and broad biological activities [80]. Chromatography has been used to separate compounds from natural products. In the past decades, natural products have functioned as potential sources of various scaffolds in the development of new drugs and have provided innovative leads in a variety of medical fields [81, 82].

Compositae is widely distributed globally, and approximately 920 genera and 20,000 species are known [2]. Compositae members have been used as sources of traditional medicine for colds, stomachache, headache, and hypertension [3-5]. *R. bicolor* and *C. lanceolata* of the Compositae family have been used as ornamental

crops, and many studies have not yet been conducted on this species. However, previous studies conducted on medicinal plants of the Compositae predict that *R. bicolor* and *C. lanceolata* also have various active components. In this study, the components contained in the 70% EtOH extract of *R. bicolor* and *C. lanceolata* were isolated and identified, and determination of a marker compound was attempted.

Ⅱ. Materials and Methods

1. Materials

(1) Plant Material

Rudbeckia bicolor Nutt. was collected at Chosun University Herb Garden (Aug. 2018), Gwangju, Republic of korea in August 2019 and identified by Professor Dong-Sung Lee of the Department of Pharmacy at Chosun University. The voucher specimen (RB19-001) is stored in the Department of Natural Products Chemistry, College of Pharmacy, Chosun University. *Coreopsis lanceolata* L. was collected in Bulgap-myeon, Yeonggwang, Jeollanam-do (Aug. 2017), Republic of korea in August 2019, and was identified by Professor Dong-Sung Lee of the Department of Pharmacy at Chosun University. The voucher specimen (CL19-001) is stored in the Natural Products Chemistry Laboratory, College of Pharmacy, Chosun University.

(2) Chemicals, reagents and chromatography for isolation

TLC used pre-coated silica gel F plates (Merck, art. 5715, darmstadt, Germany), RP-18F plates (Merck, art. 15389, darmstadt, Germany). Resins used for open column chromatography (C. C.) were Silica gel 60 (40-63 and 63-200 μm, Merck, darmstadt, Germany), LiChroprep RP-18 (40-63 μm, Merck, darmstadt, Germany), Sephadex LH-20 (25-100 μm, Sigma-aldrich, Saint Louis, MO, USA) and ODS-A (12 nm, S-75 μm, YMC, Kyoto, Japan) was used, and Sand (50-70 mesh, Sigma-aldrich, Saint Louis, MO, USA) was used to fix the sample.

(3) High-performance liquid chromatography

Analytical high performance liquid chromatography (HPLC) was performed using the Waters 1525 binary HPLC pump (MA, USA) and detected with a 996 photodiode array (PDA) detector (MA, USA). Preparative HPLC was performed using a 600 controller manufactured by Waters (MA, USA) and detected with a 2487 dual λ absorbance detector (MA, USA). The analytical column was YMC-Triart C18 ExRS (5 μm, 4.6 × 250 mm I.D., YMC), and the preparative column was YMC-Triart C18 ExRS (5 μm, 10.0 × 250 mm I.D., YMC), Kinetex® 5 μm EVO C18 100 Å LC column (5 μm, 150 × 21.2 mm, Phenomenex) was used.

(4) Nuclear magnetic resonance

Nuclear magnetic resonance (NMR) spectra (1- and 2-dimensional) 400 MHz (400 MHz for ^{1}H, 100 MHz for ^{13}C) were used as a JEOL JNM ECP-400 spectrometer. Correlation spectroscopy (COSY), distortionless enhancement by polarization transfer (DEPT), heteronuclear single quantum correlation (HSQC), and heteronuclear multiple bond correlation (HMBC) were recorded using standard JEOL pulse sequences. 600 MHz NMR spectra were recorded on a Varian VNMRS 600MHz NMR spectrometer (KBSI-Gwangju Center) and chemical shifts are given in ppm (δ). The solvents used in the analysis, $CDCl_3$, pyridine-d_5, DMSO-d_6, and CD_3OD, were purchased from Sigma (MO, USA).

2. Methods

(1) Extract and fraction of *R. bicolor* Nutt.

400 g of dried *R. bicolor* was extracted twice with 3 L of 70% ethanol at 80 °C to obtain 17 g of extract. The extract was sequentially fractionated using CH_2Cl_2, EtOAc, *n*-BuOH, and H_2O to obtain 2.373 g of a CH_2Cl_2 fraction, 1.078 g of an EtOAc fraction, 4.099 g of a *n*-BuOH fraction, and 9.855 g of a H_2O fraction (Scheme 1).

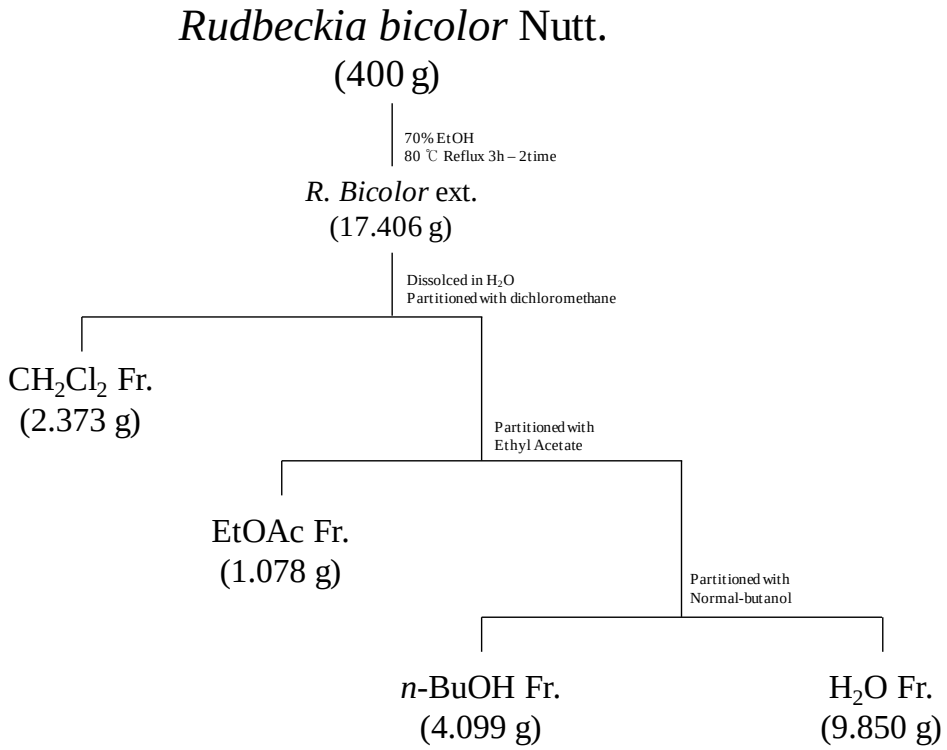

Scheme 1: Scheme of *R. bicolor* Nutt. extraction and fractions

(2) Isolation of compounds from *R. bicolor* Nutt.

The EtOAc fraction (900 mg) was subjected to C-18 column chromatography (C. C.) eluting with a MeOH-H_2O gradient system to give 17 subfractions (EA1-EA17). Fraction EA-1- EA-2 was further chromatographed at C-18 C. C. using a MeOH-H_2O gradient system to give compound **1** (EA-2-2, 60 mg). Compound **1** (EA-2-1-2, 2.1 mg) was obtained once more from fraction EA-2-1 eluted with MeOH-H_2O gradient system. Subsequently, fraction EA-3 was prepared by HPLC combined with a Kinetex® 5 µm EVO C18 100 Å LC column using a MeOH-H_2O gradient system to obtain compounds **2** (EA-3-3, 2.4 mg). Next, the fraction EA-3-2 was applied to the same system as EA-3 to obtain compound **2** (EA-3-2-3, 3.4 mg) and compound **3** (EA-3-2-5, 2.4 mg). Fraction EA15 was obtained using a $CHCl_3$-MeOH isocratic system to obtain compound **4** (EA-15-1, 2.0 mg) (Scheme 2).

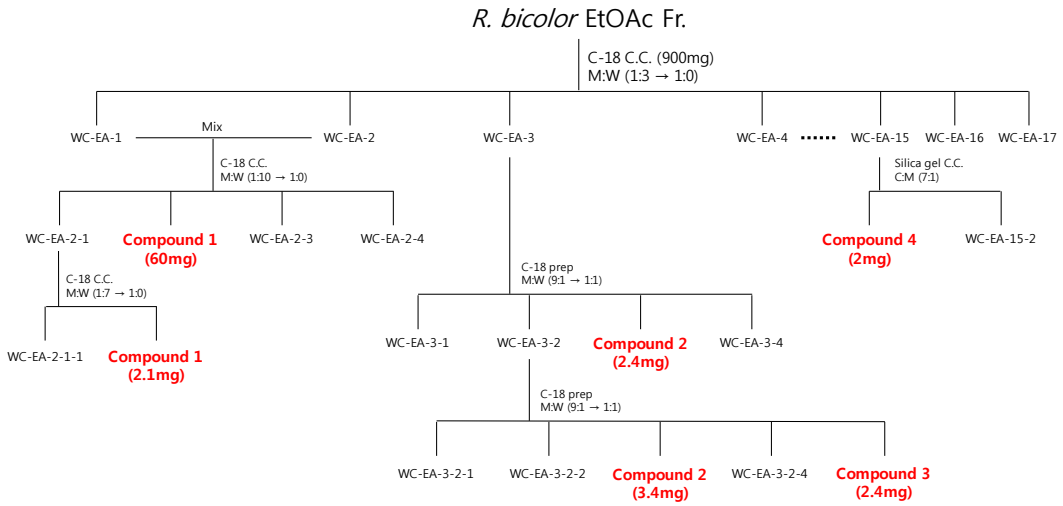

Scheme 2: Isolation scheme of *R. bicolor* EtOAc fraction derived compounds

Compound **1** was obtained as a yellow gum. Based on the analysis of ^1H and ^{13}C NMR data, its molecular formula was determined as $C_{22}H_{22}O_{13}$. ^1H-NMR (CD_3OD,

400 MHz): δ: 7.73 (1H, s, H-2′), 7.63 (1H, d, *J* = 8.0 Hz, H-5′), 6.86 (1H, d, *J* = 8.8 Hz, H-3′), 6.83 (1H, s, H-8), 5.09 (1H, d, *J* = 6.8 Hz, H-1″), 3.88 (3H, s, OCH_3), 3.72 (1H, m, H-6″); ^{13}C-NMR (CD_3OD, 100 MHz): δ: 176.1 (C-4), 131.9 (C-6), 156.3 (C-7), 94.1 (C-8), 151.7 (C-9), 105.4 (C-10), 122.6 (C-1′), 120.6 (C-2′), 114.8 (C-3′), 147.5 (C-4′), 144.7 (C-5′), 114.9 (C-6′), 60.1 (OCH_3), 100.7 (C-1″), 61.2 (C-6″).

Compound **2** was obtained as a yellow gum. Based on the analysis of ^{1}H and ^{13}C NMR data, its molecular formula was determined as $C_{23}H_{24}O_{13}$. ^{1}H-NMR (DMSO-*d*$_6$, 600 MHz): δ: 12.60 (1H, s, 5-OH), 7.61 (2H, m, H-2′ and 6′), 6.86 (2H, s, H-8), 6.84 (1H, d, *J* = 9.0 Hz, H-5′), 5.48 (1H, d, *J* = 7.2 Hz, H-1″), 3.92 (3H, s, 7-OCH_3), 3.73 (3H, s, 6-OCH_3), 3.57 (1H, m, H-5″), 3.27 (1H, m, H-3″), 3.09 (1H, m, H-4″); ^{13}C-NMR (DMSO- *d*$_6$, 150 MHz): δ: 156.6 (C-2), 133.3 (C-3), 177.6 (C-4), 151.7 (C-5), 131.6 (C-6), 158.2 (C-7), 91.2 (C-8), 151.7 (C-9), 105.3 (C-10), 121.1 (C-1′), 116.3 (C-2′), 144.8 (C-3′), 148.6 (C-4′), 115.2 (C-5′), 121.6 (C-6′), 100.7 (C-1″), 76.5 (C-2″), 69.9 (C-3″), 74.1 (C-4″), 77.6 (C-5″), 60.9 (C-6″), 60.1 (6-OCH_3), 56.5 (7-OCH_3).

Compound **3** was obtained as a yellow gum. Based on the analysis of ^{1}H and ^{13}C NMR data, its molecular formula was determined as formula was determined as $C_{23}H_{24}O_{13}$. ^{1}H-NMR (DMSO-*d*$_6$, 600 MHz): δ: 7.34 (1H, d, *J* = 2.4 Hz, H-2′), 7.29 (1H, dd, *J* = 10.8, 2.4 Hz, H-5′), 6.86 (1H, d, *J* = 8.4 Hz, H-3′), 6.84 (1H, s, H-8), 5.29 (1H, d, *J* = 1.2 Hz, H-1″), 3.91 (3H, s, 7-OCH_3), 3.73 (3H, s, 6-OCH_3), 3.53 (1H, m, H-5″), 3.51 (1H, m, H-3″), 3.23 (1H, m), 3.21 (1H, m), 3.17 (1H, m), 3.14 (1H, m), 0.82 (3H, d, 6.0 Hz, Rh-OCH_3) ; ^{13}C-NMR (DMSO-*d*$_6$, 150 MHz): δ: 156.6 (C-2), 133.3 (C-3), 177.6 (C-4), 151.7 (C-5), 131.6 (C-6), 158.2 (C-7), 91.2 (C-8), 151.7 (C-9), 105.3 (C-10), 121.1 (C-1′), 116.3 (C-2′), 144.8 (C-3′), 148.6 (C-4′),

115.2 (C-5′), 121.6 (C-6′), 100.7 (C-1″), 76.5 (C-2″), 69.9 (C-3″), 74.1 (C-4″), 77.6 (C-5″), 60.9 (C-6″), 60.1 (6-OCH_3), 56.5 (7-OCH_3), 17.5 (Rh-OCH_3).

Compound **4** was obtained as a white gum. Based on the analysis of ^1H and ^{13}C NMR data, its molecular formula was determined as $C_{30}H_{50}O$. ^1H-NMR ($CDCl_3$, 400 MHz): δ: 5.17 (1H, t, *J* = 7.2 Hz, H-12), 2.01 (1H, dd, *J* = 13.2, 4.4 Hz, H-19), 3.21 (1H, m, OH), 1.96 (1H, td, *J* = 17.6, 4.0 Hβ, H-15), 1.90 (1H, td, *J* = 16.0, 2.8 Hβ, H-16), 1.85 (1H, dd, *J* = 10.4, 4.0 Hz, H-22), 1.24 (3H, s, 27-OCH_3), 1.12 (3H, s, 28-OCH_3), 0.99 (3H, s, 26-OCH_3), 0.96 (3H, s, 24-OCH_3), 0.93 (3H, s, 29-OCH_3), 0.86 (3H, s, 30-OCH_3), 0.82 (3H, s, 23-OCH_3), 0.78 (3H, s, 25-OCH_3), 0.71 (1H, d, *J* = 4.0 Hz, H-5); ^{13}C-NMR (DMSO-d_6, 100 MHz): δ: 38.9 (C-1), 27.5 (C-2), 77.4 (C-3), 38.7 (C-4), 55.3 (C-5), 18.5 (C-6), 32.7 (C-7), 39.0 (C-8), 47.6 (C-9), 37.0 (C-10), 23.6 (C-11), 122.1 (C-12), 145.1 (C-13), 41.8 (C-14), 26.3 (C-15), 26.2 (C-16), 32.8 (C-17), 47.2 (C-18), 46.9 (C-19), 31.3 (C-20), 34.7 (C-21), 37.1 (C-22), 28.6 (C-23), 17.1 (C-26), 28.7 (C-28), 33.6 (C-29), 24.0 (C-30).

(3) Extract and fraction of *C. lanceolata* L.

400 g of dried *C. lanceolata* was extracted twice with 3 L of 70% ethanol at 80 ℃. to obtain 40 g of an extract. The extract was sequentially fractionated using CH_2Cl_2, EtOAc, *n*-BuOH, and H_2O to obtain 4.482g of a CH_2Cl_2 fraction, 3.663 g of an EtOAc fraction, 8.051 g of a *n*-BuOH fraction, and 22.273 g of a H_2O fraction (Scheme 3).

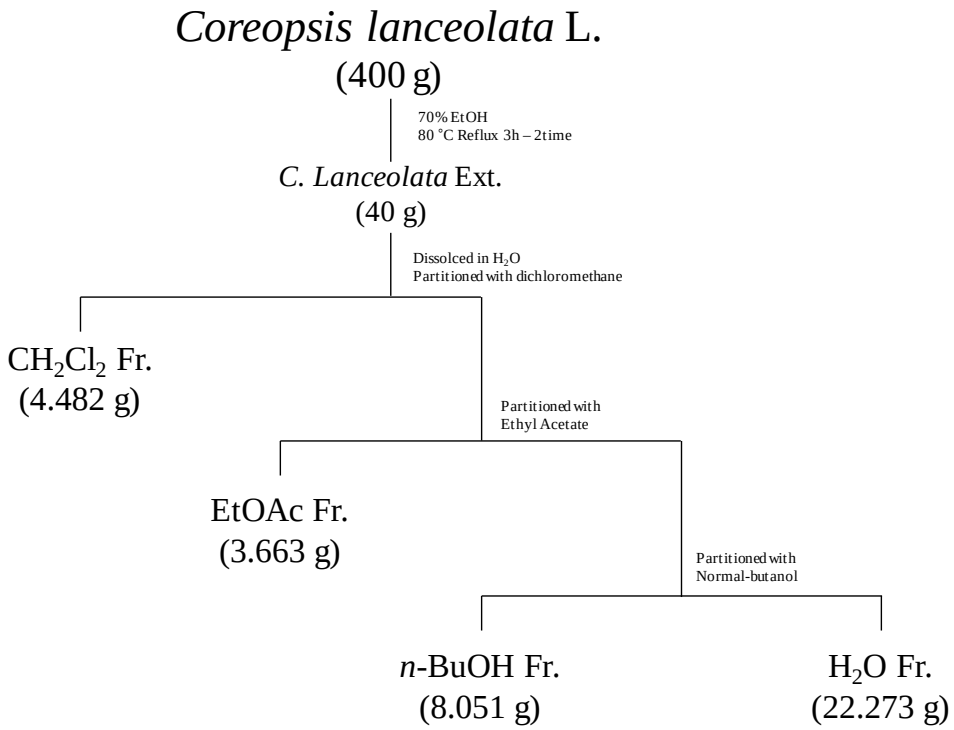

Scheme 3: Scheme of *C. lanceolata* L. extraction and fractions

(4) Isolation of compounds from *C. lanceolata* L.

The CH_2Cl_2 fraction (4445 mg) was applied to silica gel C. C. eluting with a Hexane-Acetone gradient system to obtain 7 subfractions (DM1-DM7). Fraction DM-1 was further chromatographed on silica gel C. C. using a $CHCl_3$-Acetone gradient system to obtain 4 subfractions (DM11-DM14). Fraction DM11 was further chromatographed on silica gel C. C. using a $CHCl_3$-Acetone gradient system to obtain compound **5** (DM113, 54.5 mg). Subsequently, fraction DM-2 was further chromatographed on silica gel C. C. using a Hexane-Acetone gradient system to obtain 7 subfractions (DM21-DM27). Fraction DM24 was further chromatographed on silica gel C. C. using a Hexane-Acetone isocratic system to obtain 7 subfractions (DM241-DM247). Fraction DM241 was further chromatographed at C-18 C. C. using a MeOH-H_2O gradient system to give two subfractions (DM2411-DM2412). Fraction DM2411 was further chromatographed at C-18 C. C. using a MeOH-H_2O gradient system to give 7 subfractions (DM24111-DM24117), and compound **6** (DM24117, 0.5 mg) was obtained. Subsequently, fraction DM24116 was preparated by HPLC combined with a Kinetex® 5 μm EVO C18 100 Å LC column using a MeOH-H_2O gradient system to obtain compound **7** (DM241161, 0.8 mg) (Scheme 4).

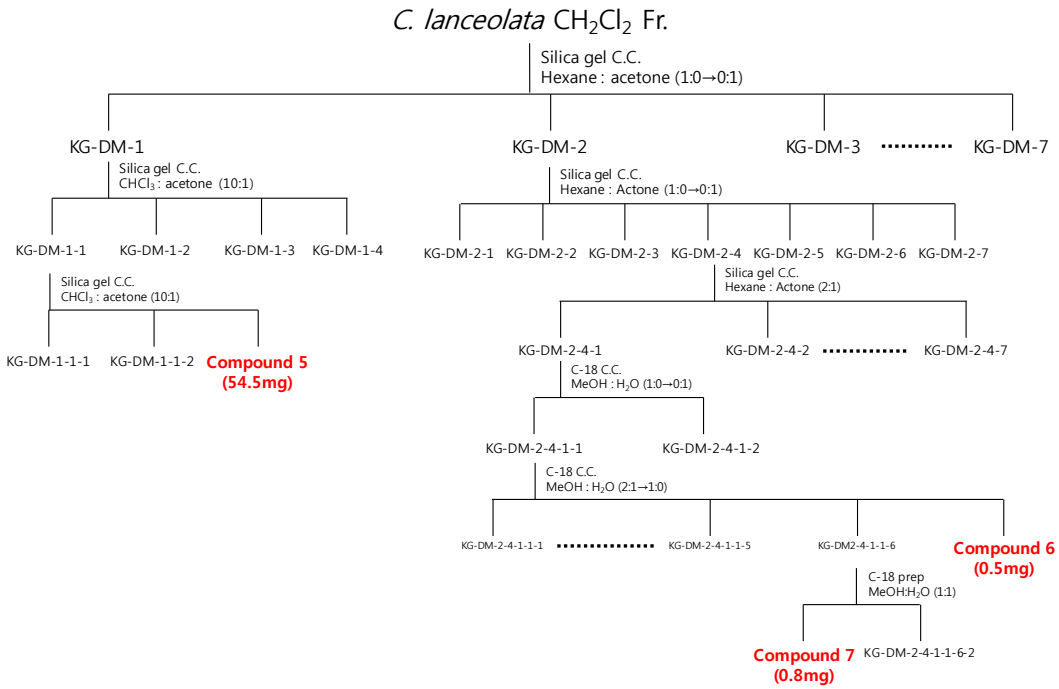

Scheme 4: Isolation scheme of *C. lanceolata* CH_2Cl_2 fraction derived compounds

The EtOAc fraction (1500 mg) was applied to silica gel C. C. eluting with a $CHCl_3$-MeOH-H_2O gradient system to obtain two subfractions (EA1-EA2). Fraction EA-1 was further chromatographed on ODS-A C. C. using a MeOH-H_2O gradient system to give 6 subfractions (EA11-EA16), and compound **8** (EA12, 15 mg) was obtained. Subsequently, fraction EA14 was further chromatographed on ODS-A C. C. using a MeOH-H_2O isocratic system to give 9 subfractions (EA141-EA149). Fraction EA142 was further chromatographed on LH-20 C. C. using a $CHCl_3$-MeOH isocratic system to obtain 4 subfractions (EA1421-EA1424). Fractional EA1422 was further chromatographed at C-18 C. C. using a MeOH-H_2O isocratic system to obtain compound **9** (EA14223, 20.3 mg) (Scheme 5).

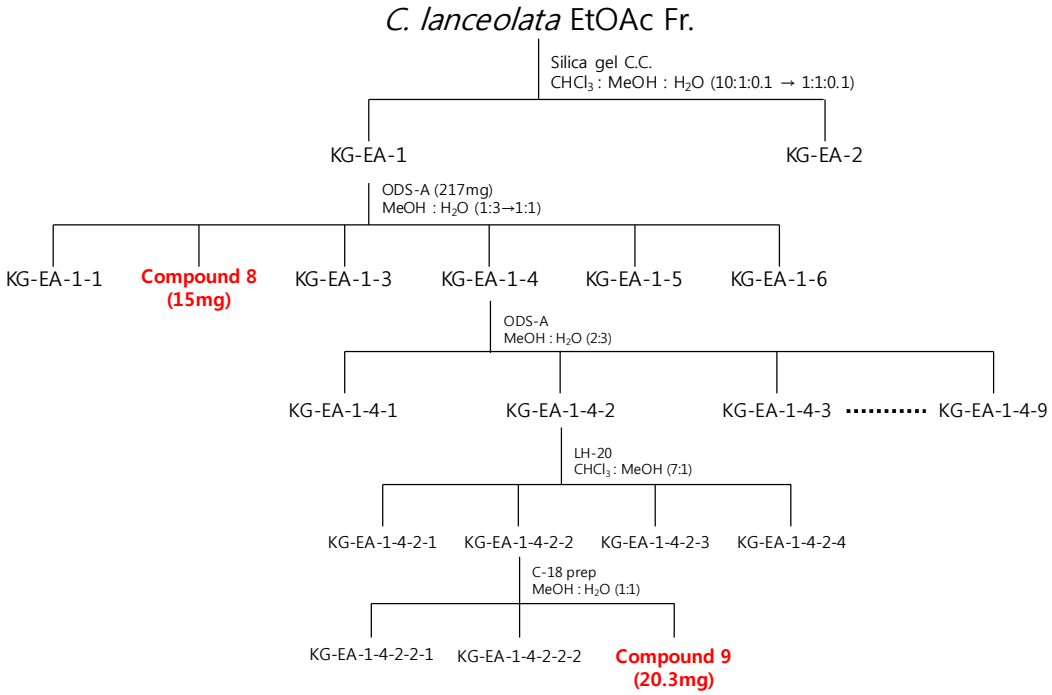

Scheme 5: Isolation scheme of *C. lanceolata* EtOAc fraction derived compounds

Compound **5** was obtained as a yellow gum. Based on the analysis of ^{1}H and ^{13}C NMR data, its molecular formula was determined as $C_{13}H_8$. ^{1}H-NMR ($CDCl_3$, 400 MHz): δ: 7.51-7.49 (2H, m, H-2′ and 6′), 7.39-7.29 (3H, m, H-3′, 4′ and 5′), 2.0 (3H, s, H-1); ^{13}C-NMR ($CDCl_3$, 100 MHz): δ: 4.7 (C-1), 75.3 (C-2), 65.0 (C-3), 67.5 (C-4), 59.0 (C-5), 74.7 (C-6), 78.3 (C-7), 133.0 (C-2′), 128.5 (C-3′), 129.5 (C-4′), 128.5 (C-5′), 133.0 (C-6′).

Compound **6** was obtained as a green gum. Based on the analysis of ^{1}H and ^{13}C NMR data, its molecular formula was determined as $C_{18}H_{18}O_5$. ^{1}H-NMR ($CDCl_3$, 600 MHz): δ: 13.54 (1H, s, 2′-OH), 7.86 (1H, d, *J* = 8.4 Hz, H-7), 7.84 (1H, d, *J* = 1.8 Hz, H-6′), 7.44 (1H, d, *J* = 15.6 Hz, H-8) 7.26 (1H, d, *J* = 1.8 Hz, H-2), 7.17 (1H, d,

J = 1.8 Hz, H-6), 6.50 (1H, d, *J* = 2.4 Hz, H-3′), 6.49 (1H, dd, *J* = 7.2 Hz, H-5′), 3.97 (3H, s, 5-OCH_3), 3.94 (3H, s, 4-OCH_3), 3.87 (3H, s, 4′-OCH_3); ^{13}C-NMR ($CDCl_3$, 150 MHz): δ: 127.8 (C-1), 151.6 (C-4), 149.3 (C-5), 144.6 (C-7), 123.3 (C-8), 191.7 (C-9), 166.1 (C-1′), 168.6 (C-2′), 101.1 (C-3′), 107.6 (C-4′), 114.1 (C-5′), 110.1 (C-6′).

Compound **7** was obtained as a yellow gum. Based on the analysis of ^{1}H and ^{13}C NMR data, its molecular formula was determined as $C_{17}H_{16}O_4$. ^{1}H-NMR ($CDCl_3$, 600 MHz): δ: 7.87 (1H, d, *J* = 8.8 Hz, H-5), 7.41 (2H, d, *J* = 8.4 Hz, H-2′ and 6′), 6.96 (2H, d, *J* = 8.4 Hz, H-3′ and 5′), 6.62 (1H, dd, *J* = 8.8, 2.4 Hz, H-6) 6.48 (1H, d, *J* = 2.4 Hz, H-8), 5.42 (1H, dd, *J* = 16.2, 3.0 Hz, H-2), 3.84 (3H, s, 7-OCH_3), 3.83 (3H, s, 4′-OCH_3), 3.06 (1H, dd, *J*= 16.8, 13.3 Hz, H-3a), 2.80 (1H, dd, *J* = 16.8, 2.9 Hz, H-3b); ^{13}C-NMR ($CDCl_3$, 150 MHz): δ: 79.8 (C-2), 44.1 (C-3), 190.9 (C-4), 128.7 (C-5), 110.2 (C-6), 166.1 (C-7), 100.8 (C-8), 163.6 (C-9), 114.7 (C-10), 130.6 (C-1′), 127.7 (C-2′ and C-6′), 114.0 (C-3′ and C-5′), 159.9 (C-4′), 55.6 (7′-OCH_3), 55.4 (4′-OCH_3).

Compound **8** was obtained as a red gum. Based on the analysis of ^{1}H and ^{13}C NMR data, its molecular formula was determined as $C_{16}H_{14}O_6$. ^{1}H-NMR (DMSO-d_6, 400 MHz): δ: 7.40 (1H, d, *J* = 9.0 Hz, H-5), 6.92 (1H, d, *J* = 1.2 Hz, H-6′), 6.77 (2H, d, *J* = 3.2 Hz, H-2′ and 3′), 6.57 (1H, d, *J* = 8.8 Hz, H-6) 5.42 (1H, dd, *J* = 14.8, 2.4 Hz, H-2), 3.70 (3H, s, 7-OCH_3), 3.05 (1H, dd, *J* = 29.2, 12.4 Hz, H-3a), 2.66 (1H, dd, *J* = 19.6, 2.8 Hz, H-3b); ^{13}C-NMR (DMSO-d_6, 100 MHz): δ: 79.8 (C-2), 43.7 (C-3), 190.8 (C-4), 122.6 (C-5), 110.8 (C-6), 157.2 (C-7), 135.9 (C-8), 155.3 (C-9), 114.9 (C-10), 130.5 (C-1′), 118.3 (C-2′), 115.9 (C-3′), 145.7 (C-4′), 146.2 (C-5′), 114.8 (C-6′), 60.7 (OCH_3).

Compound **9** was obtained as a red gum. Based on the analysis of ^{1}H and ^{13}C NMR data, its molecular formula was determined as $C_{16}H_{12}O_6$. ^{1}H-NMR (DMSO-d_6, 400

MHz): δ: 10.84 (1H, s, OH), 9.73 (1H, s, OH), 9.35 (1H, s, OH), 7.45 (1H, d, *J* = 2.0 Hz, H-2′), 7.34 (1H, d, *J* = 8.4 Hz, H-4), 7.26 (1H, dd, *J* = 10.0, 1.6 Hz, H-6′), 6.86 (1H, d, *J* = 8.4 Hz, H-5′), 6.78 (1H, d, *J* = 8.4 Hz, H-5), 4.03 (3H, s, OCH_3); ^{13}C-NMR (DMSO-d_6, 100 MHz): δ: 181.9 (C-3), 158.6 (C-8), 158.3 (C-6), 148.7 (C-2), 146.14 (C-3′), 146.06 (C-4′), 132.8 (C-7), 125.1 (C-6′), 123.8 (C-1′), 119.9 (C-2′), 118.4 (C-5′), 116.6 (C-4), 115.3 (C-9), 113.9 (C-10), 112.8 (C-5), 61.3 (7-OCH_3).

(5) LOD (Limit of detection) and LOQ (Limit of quantitation)

To establish the LOD and LOQ for an isolated compound, you need to calculate the linearity and standard deviation of the compound. Linearity is the ability to achieve results that are directly proportional to the amount of analyte in a sample. For the linearity setting method, 5 or more concentrations are recommended. In this study, linearity was established by injecting 7 standard solutions to evaluate linearity. Then use regression to calculate the standard error. Then, substituting the function for the standard error, calculates the standard deviation and calculates as follows: LOD = 3.3 * δ / S, LOQ = 10 * δ / S23 (δ: standard deviation of the intercept, S: slope calibration curve).

(6) Quantitative evaluation of the isolated compounds in extracts

To proceed with a quantitative evaluation, it is necessary to establish the linearity of the standard solution. Linearity is the ability to achieve results that are directly proportional to the amount of analyte in a sample. The linearity setting method was set in the same way as LOD and LOQ. Then I calculated the regression equation as follows: y = Ax + B (y: peak area, x: sample volume). All samples analyzed were quantified through 3 replicate injections.

Ⅲ. Results and Discussion

1. Structural identification of compounds isolated from *R. bicolor*

(1) Structure identification of compound 1

Compound **1** was obtained as a yellow gum. Analysis of the ^{1}H and ^{13}C NMR (CD_3OD) data determined the molecular formula to be $C_{22}H_{22}O_{13}$.

The ^{1}H NMR data of compound **1** showed four olefin protons (δ 6.83, 6.86, 7.63 and 7.73), anomeric proton (δ 5.09) with glucose moiety protons (δ 3.95-3.39) and a methoxy protons (δ 3.88). The ^{13}C and DEPT NMR data showed the presence of 21 signals including a carbonyl carbon (δ 176.1), four olefinic carbons (δ 94.1, 114.8, 114.9 and 120.6), an anomeric carbon (δ 100.7), four oxygenated methine carbons (δ 70.7, 73.5, 76.7 and 77.2), oxygenated methylene carbon (δ 61.2), and a methoxy carbon (δ 60.1). From the analysis of ^{1}H and ^{13}C NMR data, the structure of this compound was conjectured as having skeleton of flavonoid glucoside.

From the comparison with ^{1}H and ^{13}C NMR data in previous literature, the structure of compound **1** was determined as 2-(3,4-dihydroxyphenyl)-3,5-dihydroxy-6-methoxy-7-[(2S,3R,4S,5S,6R)-3,4,5-trihydroxy-6-(hydroxymethyl)oxan-2-yl]oxychromen-4-one (patulitrin) (Fig. 7) [83].

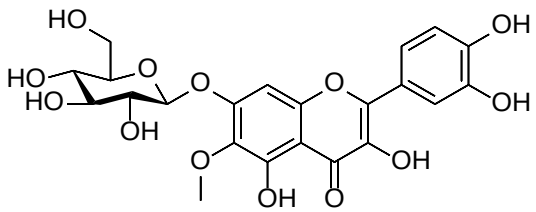

Fig. 7: Structure of compound 1

(2) Structure determination of compound 2

Compound **2** was obtained as a yellow gum. Analysis of the ^{1}H and ^{13}C NMR (DMSO-d_6) data determined the molecular formula to be $C_{23}H_{24}O_{13}$.

The ^{1}H and ^{13}C NMR data of compound **2** suggested that its structure was closely similar with compound **1**, except for finding additional a methoxy group. In addition, the presence of the β-D-glucopyranosyl group (δ 100.7, 77.6, 76.5, 74.1, 69.9 and 60.9) was similar. From the analysis of HMBC data, correlation between H-1"(δ 5.48) of glucoside moiety with C-3 (δ 133.3) of flavonoid moiety was suggested that glucose was attached to position 3 unlike compound **1**.

From the comparison with ^{1}H and ^{13}C NMR data in previous literature, the structure of compound **2** was determined as 2-(3,4-dihydroxyphenyl)-5-hydroxy-6,7-dimethoxy-3-[(2R,5S,6R)-3,4,5-trihydroxy-6-(hydroxymethyl)oxan-2-yl]oxychromen-4-one (eupatolitin-3-*O*-glucoside) (Fig. 8) [84, 85].

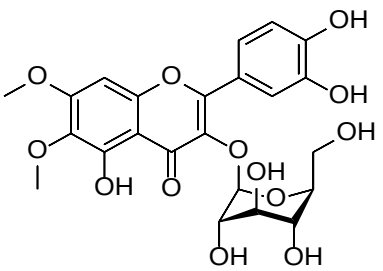

Fig. 8: Structure of compound 2

(3) Structure determination of compound 3

Compound **3** was obtained as a yellow gum. Analysis of the ^{1}H and ^{13}C NMR (DMSO-d_6) data determined the molecular formula to be $C_{23}H_{24}O_{13}$.

The ^{1}H and ^{13}C NMR data of compound **3** suggested that its structure was closely similar with compound **2**, except for oxymethylene group in glucose was substituted with a methyl group. From the analysis of NMR data, unlike compound **2**, this compound has rhamnose moiety attached in position 3.

From the comparison with ^{1}H and ^{13}C NMR data in previous literature, the structure of compound **3** was determined as 2-(3,4-dihydroxyphenyl)-5-hydroxy-6,7-dimethoxy-3-[(2S,3R,4R,5R,6R)-3,4,5-trihydroxy-6-methyloxan-2-yl]oxychromen-4-one (eupatolin) (Fig. 9) [86].

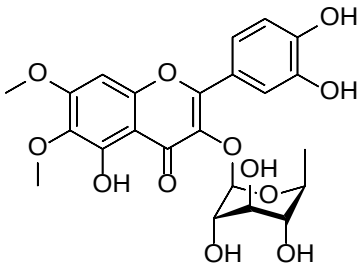

Fig. 9: Structure of compound 3

(4) Structure determination of compound 4

Compound **4** was obtained as a white gum. Analysis of the ^{1}H and ^{13}C NMR (DMSO-d_6) data determined the molecular formula to be $C_{30}H_{50}O$.

The ^{1}H NMR data of compound **4** (DMSO-d_6) shows eight methoxy protons (δ 0.78, 0.82, 0.86, 0.93, 0.96, 0.99, 1.12 and 1.24). The ^{13}C NMR data showed the presence of 30 carbon signals. Additionally, the presence of a hydroxyl group was confirmed in C-3 (δ 77.4), and the double bond was confirmed in C-12 (δ 122.1) and C-13 (δ 145.1). From the analysis of ^{1}H and ^{13}C NMR data, the structure of this compound was conjectured as having skeleton of triterpene group.

Therefore, the structure of compound **4** was determined as (3S,4aR,6aR,6bS,8aR,12aR,14aR,14bR)-4,4,6a,6b,8a,11,11,14b-octamethyl-1,2,3,4a,5,6,7,8,9,10,12,12a,14,14a-tetradecahydropicen-3-ol (beta-amyrin) (Fig. 10) [87].

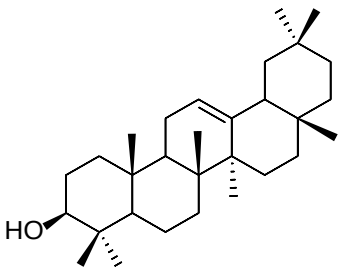

Fig. 10: Structure of compound 4

2. Structural identification of compounds isolated from *C. lanceolata*

(1) Structure determination of compound 5

Compound **5** was obtained as a yellow gum. Analysis of the ^{1}H and ^{13}C NMR ($CDCl_3$) data determined the molecular formula to be $C_{13}H_8$.

The ^{1}H NMR data of compound **5** shows five olefin protons (δ 7.51-7.49 and 7.39-7.29). a methyl proton (δ 2.0). The ^{13}C NMR and DEPT data show five olefinic carbons (δ 128.5, 129.5 and 133.0), an aromatic quaternary carbon (δ 121.2), six sp carbons (δ 59.0, 65.0, 67.5, 74.7, 75.3 and 78.3), a methyl carbon (δ 4.7). From the analysis of ^{1}H and ^{13}C NMR data, the structure of this compound was conjectured as having methyltriacetylene group attached phenyl group.

From the comparison with ^{1}H and ^{13}C NMR data in previous literature, the structure of compound **5** was determined as hepta-1,3,5-triynylbenzene (phenylheptatriyne) (Fig. 11) [88].

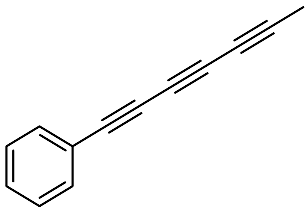

Fig. 11: Structure of compound 5

(2) Structure determination of compound 6

Compound **6** was obtained as a yellow gum. Analysis of the ^{1}H and ^{13}C NMR ($CDCl_3$) data determined the molecular formula to be $C_{18}H_{18}O_5$.

The ^{1}H NMR data of compound **6** shows a hydroxyl group (δ 13.54), two trans olefinic protons (δ 7.44 and 7.86, J = 15.6 Hz), six olefinic proton (δ 6.49, 6.50, 6.91, 7.17, 7.26 and 7.84) and three methoxy protons (δ 3.87, 3.94 and 3.97). The ^{13}C NMR data showed the presence of 18 signals including a carbonyl carbon (δ 191.8), four oxygenated aromatic carbons (δ 149.3, 151.6, 166.1 and 166.6) two α,β-unsaturated carbons (δ 144.6 and 131.1), and three methoxy carbon (δ 55.6, 56.00 and 56.02). From the analysis of ^{1}H and ^{13}C NMR data, the structure of this compound was conjectured as having skeleton of chalcone. Further analysis of HMBC data, the position of methoxy and hydroxy group were confirmed.

From the comparison with ^{1}H and ^{13}C NMR data in previous literature, the structure of compound **6** was determined as (E)-3-(3,4-dimethoxyphenyl)-1-(2-hydroxy-4-methoxyphenyl)prop-2-en-1-one (2′-Hydroxy-3,4,4′-trimethoxychalcone) (Fig. 12) [89].

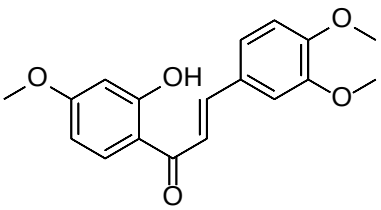

Fig. 12: Structure of compound 6

(3) Structure determination of compound 7

Compound **7** was obtained as a yellow gum. Analysis of the ^{1}H and ^{13}C NMR ($CDCl_3$) data determined the molecular formula to be $C_{17}H_{16}O_4$.

The ^{1}H NMR data of compound **7** shows seven olefinic proton [δ 6.48, 6.62, 6.96 (2H), 7.41 (2H) and 7.87], a oxygenated methine proton (δ 5.42), two methoxy protons (δ 3.84 and 3.83) and a methylene protons (δ 3.06 and 2.80). The ^{13}C NMR data showed the presence of 17 signals including a carbonyl carbon (δ 190.9), three oxygenated aromatic carbons (δ 159.9, 163.6 and 166.1), an oxygenated methine carbon (δ 79.8), two methoxy carbon (δ 55.4 and 55.6) and a methylene carbon (δ 44.1). From the analysis of ^{1}H and ^{13}C NMR data, the structure of this compound was conjectured as having skeleton of flavanone.

From the comparison with ^{1}H and ^{13}C NMR data in previous literature, the structure of compound **7** was determined as 7-methoxy-2-(4-methoxyphenyl)chromen-4-one (4′,7-dimethoxyflavanone) (Fig. 13) [90].

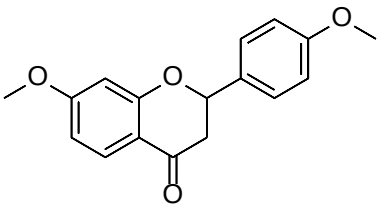

Fig. 13: Structure of compound 7

(4) Structure determination of compound 8

Compound **8** was obtained as a red gum. Analysis of the ^{1}H and ^{13}C NMR (DMSO-d_6) data determined the molecular formula to be $C_{16}H_{14}O_6$.

The ^{1}H and ^{13}C NMR data of compound **8** suggested that its structure was closely similar with compound **7**, except for a methoxy group was missing and three hydroxyl group was added. From the analysis of HMBC data, unlike compound **7**, this compound has two hydroxy group attached in position 7 and 3′, and methoxy group in position 4′ was substituted with hydroxy group.

From the comparison with ^{1}H and ^{13}C NMR data in previous literature, the structure of compound **8** was determined as 2-(3,4-dihydroxyphenyl)-7-hydroxy-8-methoxy-2,3-dihydrochromen-4-one (8-Methoxybutin) (Fig. 14) [91].

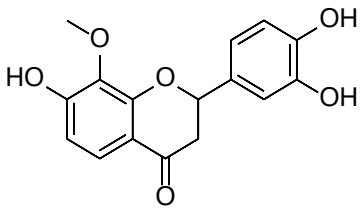

Fig. 14: Structure of compound 8

(5) Structure determination of compound 9

Compound **9** was obtained as a red gum. Analysis of the ^{1}H and ^{13}C NMR (DMSO-d_6) data determined the molecular formula to be $C_{16}H_{12}O_6$.

The ^{1}H NMR data of compound **9** shows three hydroxy group (δ 9.35, 9.73 and 10.84), six olefinic proton (δ 6.68, 6.78, 6.86, 7.26, 7.34 and 7.45) and a methoxy protons (δ 4.03). The ^{13}C NMR data showed the presence of 16 signals including a carbonyl carbon (δ 181.9), five oxygenated olefinic carbons (δ 146.05, 146.14, 148.8, 158.3 and 158.6) and a methoxy carbon (δ 61.3). From the analysis of ^{1}H and ^{13}C NMR data, the structure of this compound was conjectured as having skeleton of aurone. Further HMBC analysis, three hydroxy group and a methoxy group position was confirmed.

From the comparison with ^{1}H and ^{13}C NMR data in previous literature, the structure of compound **9** was determined as (2Z)-2-[(3,4-dihydroxyphenyl)methylidene]-6-hydroxy-7-methoxy-1-benzofuran-3-one (leptosidin). (Fig. 15) [91].

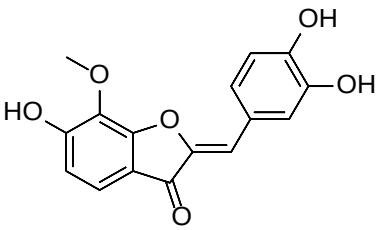

Fig. 15: Structure of compound 9

3. LOD and LOQ of isolated compounds

HPLC analysis of 70% EtOH extracts of *R. bicolor* and *C. lanceolata* with various columns showed that the YMC-triart C-18 exrt column showed superior separation compared to other columns. Therefore, LOD and LOQ values were calculated using the YMC-triart C-18 exrt column. Some compounds could not be analyzed due to their low yield, and analysis was attempted on a total of 4 compounds. Area values were obtained by injecting 20 μL with 7 different concentrations to establish the LOD and LOQ of the isolated compounds. After calculating the standard error and standard deviation, I have calculated the LOD and LOQ. The detection limit of patulitrin was set at 26.31 μg/mL and the limit of quantification was set at 79.74 μg/mL. Then, LOD of the eupatolitin 3-*O*-glucoside was set to 30.94 μg/mL and the LOQ was set to 93.77 μg/mL. Next, the LOD for eupatolin was 13.60 μg/mL, the LOQ was 41.21 μg/mL, the LOD for leptosidin was 1.20 μg/mL, and the LOQ was 3.64 μg/mL (Table 1).

Compound	Range (μg/ml)	Regression equation	Determination coefficient (R^2)	SE of intercept	SD of intercept	LOD (μg/ml)	LOQ (μg/ml)
Patulitrin	7.8125–500	y=43175x + 72683	0.999	130133.19	344300.08	26.31	79.74
Eupatolitin 3-O-glucoside	7.8125–500	y=29513x + 169271	0.9987	104604.10	276756.40	30.94	93.77
Eupatolin	3.90625–250	y=27930x − 70246	0.9989	43756.76	115769.50	13.60	41.21
Leptosidin	0.625–40	y=43845x − 2997.8	0.9997	6034.74	15966.43	1.20	3.64

Table 1: LOD and LOQ analysis of compounds. It was calculated from the area values obtained by analysis with 7 concentrations for patulitrin, eupatolitin 3-*O*-glucoside, eupatolin and leptosidin.

(SE of intercept: Standard error of intercept, SD of intercept: Standard deviation of intercept)

4. Quantitative evaluation of *R. bicolor*

Patulitrin, eupatolitin 3-*O*-glucoside, eupatolin isolated from *R. bicolor* were evaluated qualitatively and quantitatively. The extract was dissolved at 5 mg/mL and injected, and patulin, eupatolitin 3-*O*-glucoside, eupatolin were injected to compare the retention times (RT). The stationary phase was a YMC-triart C-18 exrt column and the mobile phase was a gradient system using 10% to 100% methanol (0.1% formic acid) for 40 minutes. The flow rate was analyzed as 1 mL/min and detected at a wavelength of 254 nm. In the *R. bicolor* 70% ethanol extract (Rb-70%E), 8 peaks predicted as major compounds were detected, and 3 of them were evaluated quantitatively. The RTs of the compounds were found at 21.30 min in patulitrin, 24.40 min in eupatolitin 3-*O*-glucoside and 26.41 min in eupatolin. It was found that Rb-70%E was also detected at the same RT as the 3 compounds (Fig. 16).

The compounds were then injected at 7 different concentrations to detect the area values and calculate the calibration curve. As a result of quantitative evaluation for each compound, the patulitrin contained in Rb-70%E was 0.628 (±0.004) %, eupatolitin 3-*O*-glucoside was 1.045 (±0.034) %, and eupatolin was 0.650 (±0.041) % (Table 2).

As a result of qualitative evaluation, all three compounds were found as the major compounds of Rb-70%E, and of the 3 isolated compounds, eupatolitin 3-*O*-glucoside was found to be the most abundant in Rb-70%E.

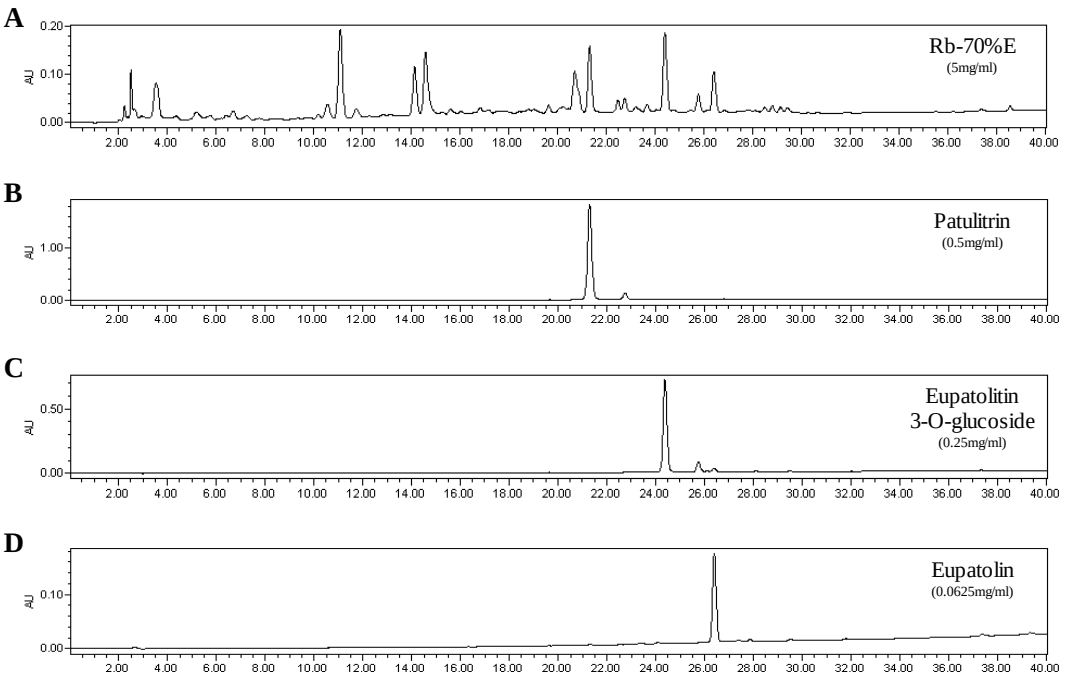

Fig. 16: Comparative analysis of *R. bicolor* and compounds in HPLC. Qualitative analysis of the compound using HPLC. *R. bicolor* 70% EtOH extract (A) and the isolated compounds patulitrin (B), eupatolitin 3-*O*-glucoside (C), eupatolin (D) were analyzed with the same mobile phase and column.

A

	1st	2nd	3rd	mean	O.D.
Rb-70E (uV*sec)	1421725	1427587	1438537	1429283	8533.355
X (ug)	31.24591	31.38168	31.635298	31.42096	0.197646
Content	0.62%	0.63%	0.63%	0.628%	0.004%

B

	1st	2nd	3rd	mean	O.D.
Rb-70E (uV*sec)	1711096	1761481	1660148	1710908	50666.76
X (ug)	52.24223	53.94945	50.51594	52.23587	1.716761
Content	1.04%	1.08%	1.01%	1.045%	0.034%

C

	1st	2nd	3rd	mean	O.D.
Rb-70E (uV*sec)	880356	790474	774828	815219.3	56949.88
X (ug)	34.80364	31.6034	31.04632201	32.48445	2.027696
Content	0.70%	0.63%	0.62%	0.650%	0.041%

Table 2: Evaluation of the content of compounds isolated from *R. bocolor*. All quantitative evaluations were calibrated through three independent analysis and the area values obtained through the analysis were calculated. The compounds used in the quantitative evaluation were patulitrin (A), eupatolitin 3-*O*-glucoside (B) and eupatolin (C).

5. Quantitative evaluation of *C. lanceolata*

The compound leptosidine isolated from *C. lanceolata* was evaluated qualitatively and quantitatively. The stationary phase was a YMC-triart C-18 exrt column and the mobile phase was a gradient system using 10% to 100% methanol (0.1% formic acid) for 40 minutes. The flow rate was analyzed as 1 mL/min and detected at a wavelength of 254 nm. Other compounds isolated from *C. lanceolata* in this study could not be qualitatively evaluated due to their low yield. The extract was dissolved at 5 mg/mL and injected, and leptosidine was injected to compare the retention time (RT). The RT of Leptosidin was detected at 27.00 min and also in *C. lanceolata* 70% ethaol extract (Cl-70%E) at the same RT (Fig. 17).

Then leptosidin was injected at 7 different concentrations to detect the area values and calculate the calibration curve. As a result of quantitative evaluation for each compound, leptosidin contained in Cl-70%E was 0.438 (± 0.015) % (Table 3).

As a result, it suggested that leptosidin is the major compound of Cl-70%E.

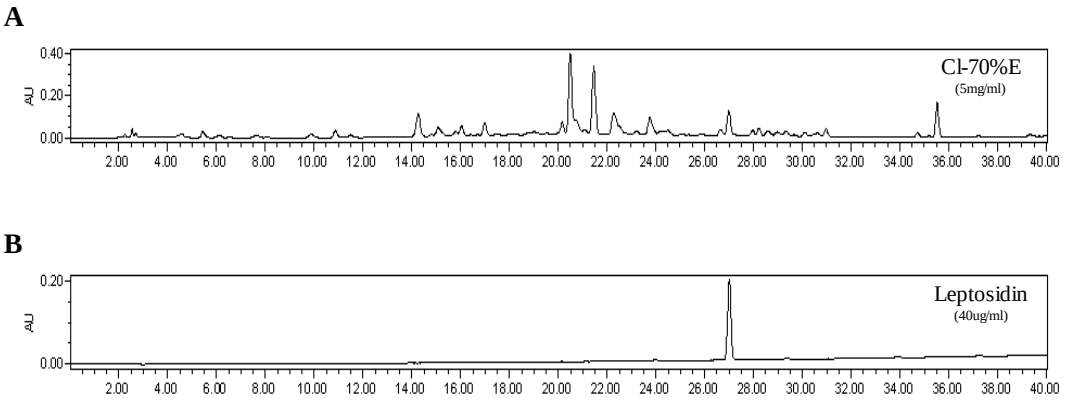

Fig. 17: Qualitative analysis of *C. lanceolata* and compounds in HPLC. *C. lanceolata* 70% EtOH extract (A) and the isolated compound leptosidin (B) were analyzed with the same mobile phase and column.

	1st	2nd	3rd	mean	O.D.
Cl-70E (uV*sec)	995693	939732	937272	957565.667	33042.1407
X (ug)	22.77775801	21.50142091	21.44531417	21.9081644	0.75361251
Content	0.46%	0.43%	0.43%	0.438%	0.015%

Table 3: Evaluation of the content of leptosidin isolated from *C. lanceolata*. Quantitative evaluations were calibrated through three independent analysis and the area values obtained through the analysis were calculated.

Ⅳ. Conclusion

The study has isolated nine known compounds from *R. bicolor* and *C. lanceolata* 70% EtOH extracts through various chromatographic steps including Column Chromatography and HPLC. Compounds isolated from *R. bicolor* 70% EtOH extract were structurally identified as patulitrin, eupatolitin-3-*O*-glucoside, eupatolin, and beta-amyrin. All compounds were first isolated in *R. bicolor*. In addition, it was quantified that patulin, eupatolitin-3-*O*-glucoside and eupatolin were contained in 0.628%, 1.045%, and 0.65%, respectively, as marker compounds.

The compounds isolated from *C. laceolata* 70% EtOH extract were structurally identified as phenylheptatriyne, 2'-hydroxy-3,4,4'-trimethoxy chalcone, 4', 7-dimethoxyflavanone, 8-methoxybutin, and leptosidin. Phenylheptatriyne was first isolated in *C. laceolata*. In addition, it was quantified that it contained 0.438% leptosidin as an marker compound of *C. laceolata*. In this study, the content evaluation of each of the five components and marker compounds included in the *R. bicolor* and *C. lanceolata* 70% EtOH of Compositae was quantified.

Chapter 3.

Anti-aging activity of extracts, fractions and compounds from *R. bicolor* and *C. lanceolata* in the various in vitro models

Ⅰ. Introduction

As the average life span of humans is increasing, an aging society is rapidly entering and the attitude to prevent aging is actively changing worldwide. Anti-aging measures include functional foods, anti-aging agents, cosmetics, and surgery. Diseases associated with aging include neurodegenerative diseases and skin aging [92, 93]. Aging has been linked to immune regulation, oxidative stress, and free radical products [94]. In addition, it is accompanied by a decrease in organ function and loss of regeneration ability in the Biology [95]. Among these dysfunctions, oxidative stress contributes to an aging-related chronic inflammatory process, namely "inflammatory aging" [96]. Inflammation is a phenomenon in which pro-inflammatory mediators, such as cytokines and chemokines, are synthesized and released [97]. Chronic inflammation is a condition in which inflammatory cytokines and chemokines are increased in response to physiological and environmental factors, allowing the immune system to continue functioning at low levels [98]. Causes of chronic inflammation include genetic susceptibility, visceral obesity, chronic infection, and cellular aging [99]. Oxidative stress contributes to the development of age-related diseases, causes imbalance in the body, and directly causes oxidative damage to cells, resulting in an inflammatory response in which local tissues resist invasion of chemical or biological factors [100-103]. During the inflammatory reaction of oxidative stress, unnecessary reactive oxygen species (ROS), such as singlet oxygen ($^1O_2$), superoxide (O_2^-), hydroxy radical (OH), and hydroxy peroxide (H_2O_2), cause disorders of nucleic acids, proteins, and lipids, and block normal functions [104, 105]. Furthermore, in this process, inflammation occurs due to DNA damage and cell death, and aging-related diseases, such as degenerative brain disease, cardiovascular disease, and thereby causing skin aging [106]. Plants of the Compositae family has long been used to treat cold, headache, and high blood

pressure. Numerous natural compounds have been isolated from the Compositae family, and most of them flavonoid-type compounds have been reported. However, there are no studies on the anti-aging effects of *R. bicolor* and *C. lanceolata.* Therefore, I investigated the anti-aging effects by extracts, fractions and compounds from *R. bicolor* and *C. lanceolata* using the various in vitro models including BV2 microglia, RAW264.7 macrophage, HT22 hippocampal, and HaCaT keratinocyte cells.

Ⅱ. Materials and Methods

1. Materials

(1) Samples preparation

R. bicolor (RB19-001) was collected at the Chosun University Herb Garden, Gwangju, Republic of korea and *C. lanceolata* (CL19-001) was collected in Bulgap-myeon, Yeonggwang, Jeollanam-do, Republic of korea. Both were collected in August 2012 and extracted with 70% EtOH. Four fractions were obtained from each extract using solvent by solvent fractionation. The solvents used were dichloromethane, ethyl acetate, butanol and distilled water. The names of the fractions obtained through the fractionation method are as follows: *R. bicolor* 70% ethanol extract (Rb-70%E), *R. bicolor* dichloromethane fraction (Rb-CH_2Cl_2), *R. bicolor* ethyl acetate fraction (Rb-EtOAc), *R. bicolor* butanol fraction (Rb-BuOH), and *R. bicolor* distilled water fraction (Rb-H_2O), *C. lanceolata* 70% ethanol extract (Cl-70%E), *C. lanceolata* dichloromethane fraction (Cl-CH_2Cl_2), *C. lanceolata* ethyl acetate fraction (Cl-EtOAc), *C. lanceolata* butanol fraction (Cl-BuOH) and *C. lanceolata* distilled water fraction (Cl-H_2O). Patulitrin and beta-amyrin were isolated from *R. bicolor*, and phenylheptatryine, 8-methoxybutin, and leptosidin were isolated from *C. lanceolata*.

(2) Chemicals and reagents for cell culture

Phosphate-buffered saline (PBS) [10 mM phosphate buffer (pH 7.4), 137 mM NaCl, 2 mM KCl], and fetal bovine serum (FBS) were purchased from Gibco (Grand Island,

NY, USA). All other chemicals were purchased from Sigma-aldrich (Saint Louis, MO, USA) unless otherwise specified.

2. Methods

(1) Cell culture

Mouse hippocampal HT22 cells, murine microglia BV2 cells, and RAW264.7 cells were donated by Prof. Youn-Chul Kim, Wonkwang University (Iksan, Korea). HaCaT human keratinocyte cells were donated by Prof. Hyeon-sook Cheong, Chosun University (Gwangju, Korea). Cells (5×10^6 cells/dish) were seeded in 100 mm dishes in dulbecco's modified eagle's medium (DMEM) (HT22), α-minimum essential medium (α-MEM) (BV2), roswell park memorial institute (RPMI)-1640 (RAW264.7), DMEM $^{+}$GlutaMAX^{TM} (HaCaT) containing streptomycin (100 μg/mL), 10% heat-inactivated FBS, and penicillin G (100 units/mL), and then incubated at 37 °C in a humidified atmosphere (5% CO_2 and 95% air).

(2) MTT assay

To determine cell viability, cells were maintained at 2×10^4 cells/well and then treated with samples in the absence or presence of glutamate (5 mM). After incubation for the indicated times, the cell culture medium was removed from each well and replaced with 200 μL of fresh medium in each well. Cells were incubated with 0.5 mg/mL of 3-(4,5-dimethylthiazol-2-yl)-2,5-diphenyltetrazolium bromide (MTT) for 1 h, and the formed formazan was resolved in dimethyl sulfoxide (DMSO). Next, the dissolved formazan was measured for absorbance at a wavelength of 540 nm using a ELISA microplate reader from Molecular Devices (San Jose, CA, USA).

(3) Nitrite assay

To determine the nitric oxide (NO) levels, the concentration of nitrite was assessed by the Griess reaction. The supernatant (100 μL) was mixed with Griess reagent (100 μL), and the absorbance was determined at 570 nm using an ELISA microplate reader from Molecular Devices (San Jose, CA, USA).

(4) Western blot analysis

The cells were harvested and pelleted by centrifugation at 200 × g for 3 min. Next, the cells were washed with PBS and lysed in 20 mM Tris-HCl buffer (pH 7.4) containing a protease inhibitor mixture (0.1 mM phenylmethanesulfonyl fluoride, 5 mg/mL aprotinin, 5 mg/mL pepstatin A, and 1 mg/mL chymostatin). Protein concentration was determined using a Lowry protein assay kit (Sigma-aldrich, Saint Louis, MO, USA). Protein (30 mg) from each sample was resolved using 7.5% and 12% sodium dodecyl sulfate-polyacrylamide gel electrophoresis (SDS-PAGE), and then electrophoretically transferred onto a Hybond enhanced chemiluminescence (ECL) nitrocellulose membrane (Bio-Rad, Hercules, CA, USA). The membrane was blocked with 5% skimmed milk and sequentially incubated with the primary antibody (Santa Cruz Biotechnology, Dallas, TX, USA and Cell Signaling Technology, Danvers, MA, USA) and a horseradish peroxidase-conjugated secondary antibody, followed by ECL detection (Amersham Pharmacia Biotech, Piscataway, NJ, USA).

(5) Prostaglandin (PGE_2) assay

The culture medium was collected, and the level of PGE_2 present in each sample was determined using a commercially available kit from R&D Systems. (Minneapolis, MN, USA). The assays were performed according to the manufacturer's instructions.

(6) IL-6 and IL-8 assay

The culture medium was collected, and the level of IL-6 and IL-8 present in each sample was determined using a commercially available kit from BioLegend (San Diego, CA, USA). The assays were performed according to the manufacturer's instructions.

(7) DNA binding activity assay

The DNA binding activity of nuclear factor kappa B (NF-κB) in nuclear extracts was measured using the NF-κB transcription factor assay kit from Cayman Chemical (Ann Arbor, MI, USA). The measurement method was carried out according to the manufacturer's instructions.

(8) Statistical Analysis

Data are expressed as the mean ± SD of three independent experiments. Statistical analysis was conducted using GraphPad Prism software version 3.03 (GraphPad Software Inc., San Diego, CA, USA). The differences between means were assessed by one-way analysis of variance (ANOVA), followed by Newman-Keuls post hoc test, and statistical significance was defined at $P < 0.05$.

Ⅲ. Results and Discussion

1. Anti-aging effect of *R. bicolor* and *C. lanceolata*

(1) Neuroprotective effect of extracts and fractions in HT22 hippocampal cells

Glutamate is the main excitatory neurotransmitter in the central nervous system. Glutamate instability is a major cause of neuronal cell death and is considered to cause chronic neurodegenerative diseases, such as Alzheimer's and Parkinson's disease [107]. Excessive excretion of glutamate results in excitotoxicity and oxidative stress [108]. However, there are reports that HT22 hippocampal cells lack functional ionotropic glutamate receptors [109]. Thus, excitotoxicity was excluded with respect to glutamate-induced HT22 hippocampal cells. During oxidative stress, ROS are overproduced and excessive ROS disrupts the balance of the antioxidant system, resulting in cell death [110]. Therefore, it was confirmed that *R. bicolor* has a neuroprotective effect against cells damaged by oxidative stress in HT22 hippocampal cells induced by glutamate. *R. bicolor* and *C. lanceolata* extracted with 70% EtOH and fractions derived from them were treated at each concentration to confirm the neuroprotective effect. Individual concentrations of *R. bicolor* were treated with Rb-70% E (10-100 μg/mL), Rb-CH_2Cl_2 (10-100 μg/mL), Rb-EtOAc (1-20 μg/mL), Rb-BuOH (25-200 μg/mL), and Rb-H_2O (25-200 μg/mL). The results showed neuroprotective effects in all fractions except in the Rb-H_2O fraction (Fig. 18A).

Subsequently, the individual concentrations of *C. lanceolata* were treated with Cl-70% E (10-100 μg/mL), Cl-CH_2Cl_2 (1-20 μg/mL), Cl-EtOAc (25-200 μg/mL), Cl-BuOH (25-200 μg/mL), and Cl-H_2O (25-200 μg/mL). The results indicated

neuroprotective effects in all fractions except in the Cl-CH_2Cl_2 and Cl-H_2O fractions (Fig. 18B).

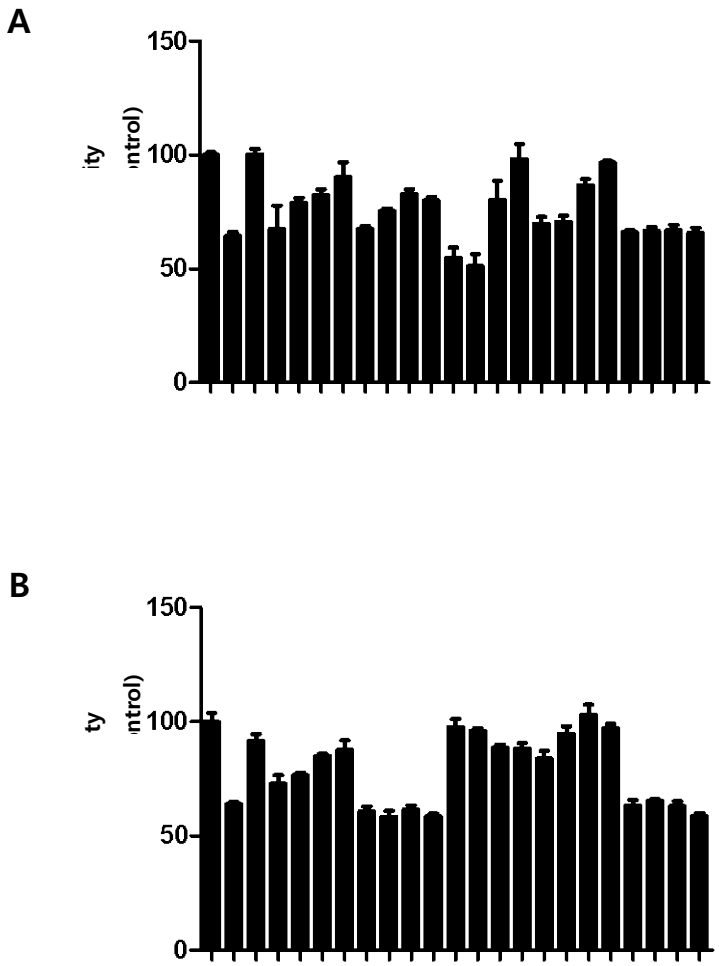

Fig. 18: Neuroprotective effect on HT22 hippocampal cells of *R. bicolor* and *C. lanceolata* extract & fraction. HT22 cells were treated with extract and fractions and then incubated for 12 h with glutamate (20 mM). Data are presented as mean ± SD values of 3 independent experiments. Trolox (100 μM) was used as the positive control. $^{*}P < 0.05$, $^{**}P < 0.01$, $^{***}P < 0.001$ vs. glutamate.

(2) Inhibitory Effect of extracts and fractions on neuroinflammation in BV2 Microglia

Microglia, which are macrophages present in the brain, are activated in the presence of harmful factors, and play an important role in maintaining homeostasis by eliminating adverse reactions in the body. However, when abnormally activated by external stimuli, pro-inflammatory mediators, ROS, and inflammatory cytokines are secreted [111]. When inflammatory mediators are secreted, cell damage and brain damage can occur, leading to degenerative brain diseases, such as Alzheimer's and Parkinson's disease [112, 113]. Unusually activated microglia are characterized as being found in a variety of neurodegenerative diseases. The pro-inflammatory mediators, NO and PGE_2, are inflammatory active substances secreted by macrophages during inflammation in the central nervous system and are rapidly produced when lipopolysaccharides (LPS) or pathogens are injected into the macrophages [114]. The secretion of inflammatory active substances eventually leads to nerve cell death, and inhibition of these inflammatory substances can be used to reduce nerve cell damage in cases of brain injury due to various causes [115, 116]. Therefore, in this study, the inhibitory effect of the extract and fractions on LPS-induced BV2 microglia was observed. First, a toxicity assessment was performed to establish the concentration of the compound. Individual concentrations were treated at 50-200 μg/mL for all the treatment groups except Rb-CH_2Cl_2 (25-100 μg/mL), Rb-EtOAc (12.5-50 μg/mL), Cl-CH_2Cl_2 (12.5-50 μg/mL), and Cl-EtOAc (12.5-50 μg/mL). Toxicity was observed to be present only in Rb-EtOAc among a total of 10 treatment groups (Fig. 19).

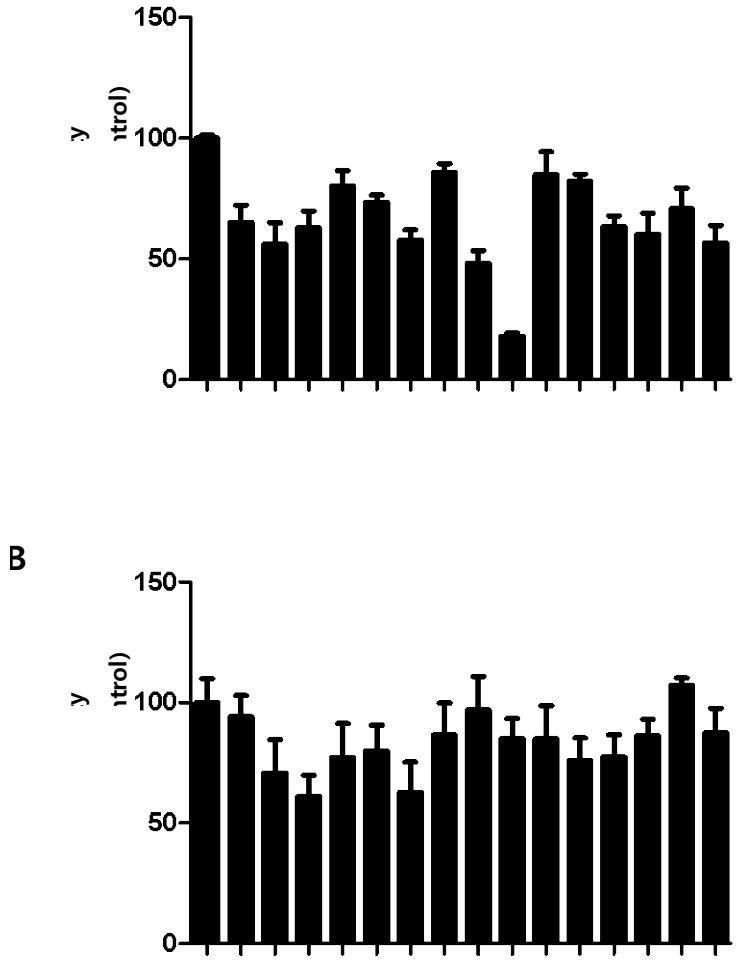

Fig. 19: Toxicity evaluation of *R. bicolor* and *C. lanceolata* extracts and fractions in BV2 microglia. BV2 cells were treated with extract and fractions and then incubated for 18 h. Data are presented as mean ± SD values of 3 independent experiments. $^{*}P < 0.05$, $^{**}P < 0.01$, $^{***}P < 0.001$ vs. control group.

The concentration setting based on the toxicity assessment was used to confirm the effect of inhibiting NO production. Extracts and fractions were pretreated at individual concentrations for 3 h and stimulated with 0.5 μg/mL of LPS for 18 h to observe NO production using the Griess reagent reaction. Sulfuretin (20 μg/mL) was used as a positive control. Individual concentrations of *R. bicolor* were treated with Rb-70% E (5-25 μg/mL), Rb-CH_2Cl_2 (2-10 μg/mL), Rb-EtOAc (2-10 μg/mL), Rb-BuOH (5-20 μg/mL), and Rb-H_2O (5-25 μg/mL). The results suggested concentration-dependent NO inhibitory effects in all treatment groups, and Rb-EtOAc showed a significant NO inhibitory effect (Fig. 20A).

Subsequently, the individual concentrations of *C. lanceolata* were treated with Cl-70% E (10-50 μg/mL), Cl-CH_2Cl_2 (2-10 μg/mL), Cl-EtOAc (10-50 μg/mL), Cl-BuOH (10-50 μg/mL), and Cl-H_2O (50-200 μg/mL). Concentration-dependent NO inhibitory effects were observed in all the treatment groups, and Cl-H_2O showed a significant NO inhibitory effect (Fig. 20B).

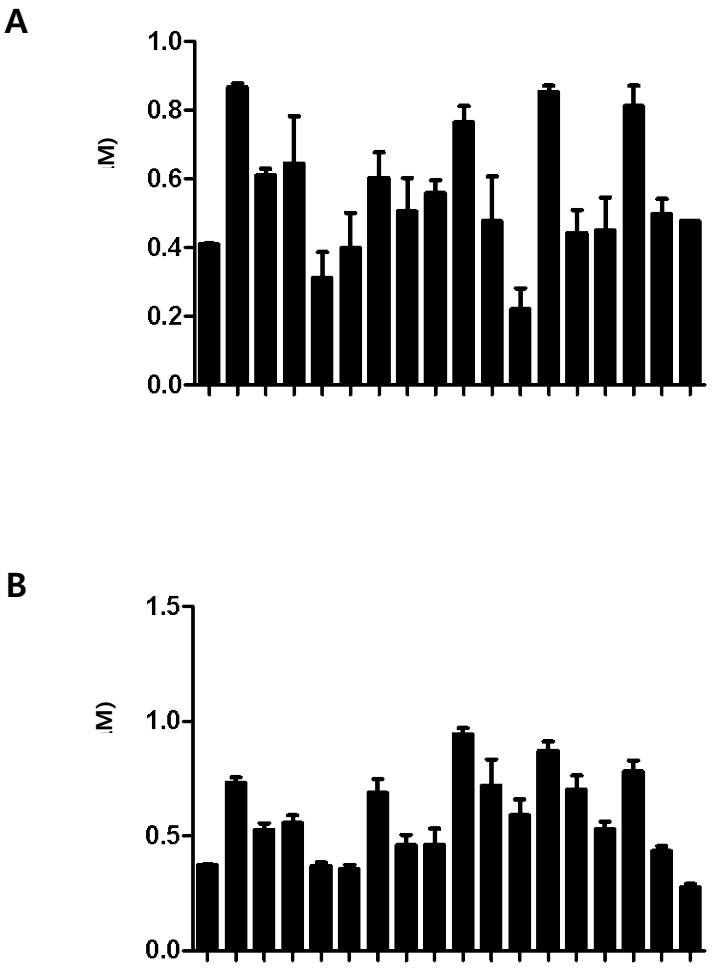

Fig. 20: Inhibitory Effect of *R. bicolor* and *C. lanceolata* extracts and fractions on NO production in BV2 microglia. BV2 cells were treated with extract and fractions and then incubated for 18 h with LPS (0.5 μg/mL). Data are presented as mean ± SD values of 3 independent experiments. Sulfuretin (20 μM) was used as the positive control. $^{*}P < 0.05$, $^{**}P < 0.01$, $^{***}P < 0.001$ vs. LPS.

(3) Inhibitory Effect of extracts and fractions on inflammation in RAW264.7 Macrophage

Macrophages are immune cells involved in the inflammatory response. Inflammation is a biological defense response to pathogens or external stimuli, and various mediators, such as cytokines, PGE_2, ROS, and free radicals are involved in the inflammatory process [117, 118]. During an inflammatory reaction, various tissue cells and immune cells secrete inflammatory mediators. However, chronic inflammatory disease occurs when inflammatory mediators are excessively produced in cells involved in the inflammatory response [119, 120]. When macrophages respond to external stimuli, they overproduce pro-inflammatory mediators, such as NO, PGE_2, and cytokines, which leads to chronic inflammatory responses, such as tissue damage and genetic mutations [121-123]. Therefore, in this study, I have observed the inhibitory effect of the extract and fraction on the production of pro-inflammatory mediators in RAW264.7 macrophages induced by LPS. First, a toxicity assessment was performed to establish the concentration of the compound. Individual concentrations were treated at 50-200 μg/mL for all treatment groups except Rb-CH_2Cl_2 (25-100 μg/mL), Rb-EtOAc (12.5-50 μg/mL), Cl-CH_2Cl_2 (12.5-50 μg/mL), and Cl-EtOAc (12.5-50 μg/mL). The results showed toxicity in Rb-70%E, Rb-CH_2Cl_2, Rb-EtOAc, and Cl-70%E among the 10 treatment groups (Fig. 21).

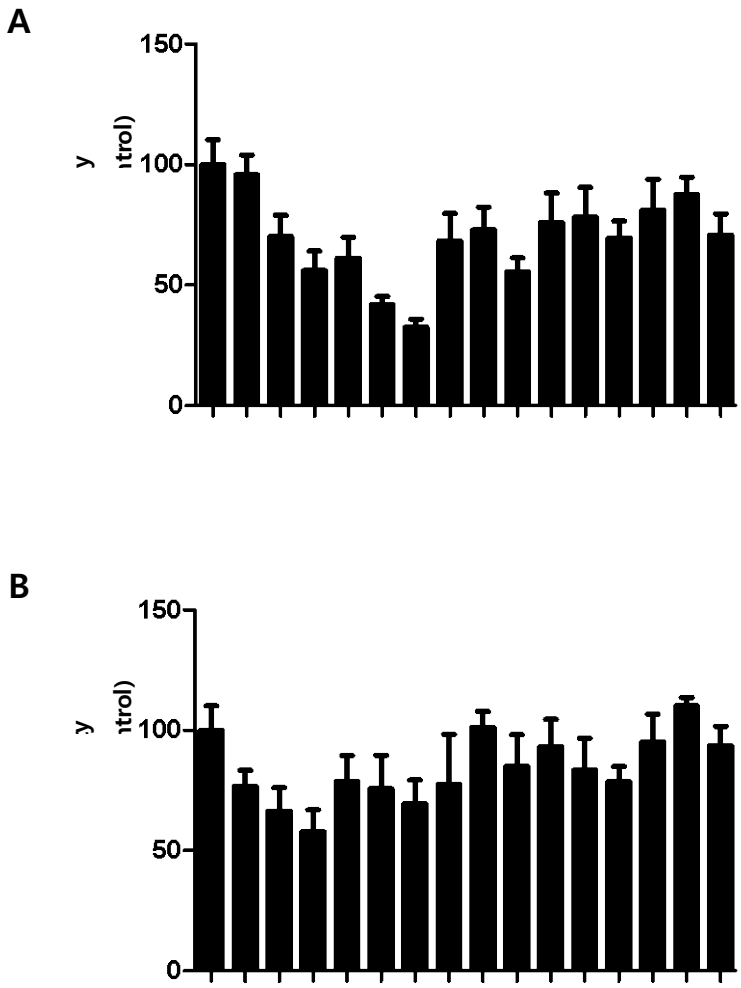

Fig. 21: Toxicity evaluation of *R. bicolor* and *C. lanceolata* extracts and fractions in RAW264.7 macrophage. RAW264.7 cells were treated with extract and fractions and then incubated for 18 h. Data are presented as mean ± SD values of 3 independent experiments. $^{*}P < 0.05$, $^{**}P < 0.01$, $^{***}P < 0.001$ vs. control group.

The concentration setting according to the toxicity assessment was used to confirm the effect of inhibiting NO production. Extracts and fractions were pretreated at individual concentrations for 3 h and stimulated with 0.5 μg/mL of LPS for 18 h to observe NO production using a Griess reagent reaction. Sulfuretin (20 μg/mL) was used as a positive control. Individual concentrations of *R. bicolor* were treated with Rb-70% E (5-25 μg/mL), Rb-CH_2Cl_2 (2-10 μg/mL), Rb-EtOAc (2-10 μg/mL), Rb-BuOH (5-20 μg/mL), and Rb-H_2O (5-25 μg/mL). The results indicated concentration-dependent NO inhibitory effects in all the treatment groups except Rb-BuOH, and Rb-EtOAc showed a significant NO inhibitory effect (Fig. 22A).

Subsequently, the individual concentrations of *C. lanceolata* were treated with Cl-70% E (10-50 μg/mL), Cl-CH_2Cl_2 (2-10 μg/mL), Cl-EtOAc (10-50 μg/mL), Cl-BuOH (10-50 μg/mL), and Cl-H_2O (50-200 μg/mL). Concentration-dependent NO inhibitory effects were observed in all treatment groups exept Cl-BuOH, and Cl-H_2O showed a significant NO inhibitory effect (Fig. 22B).

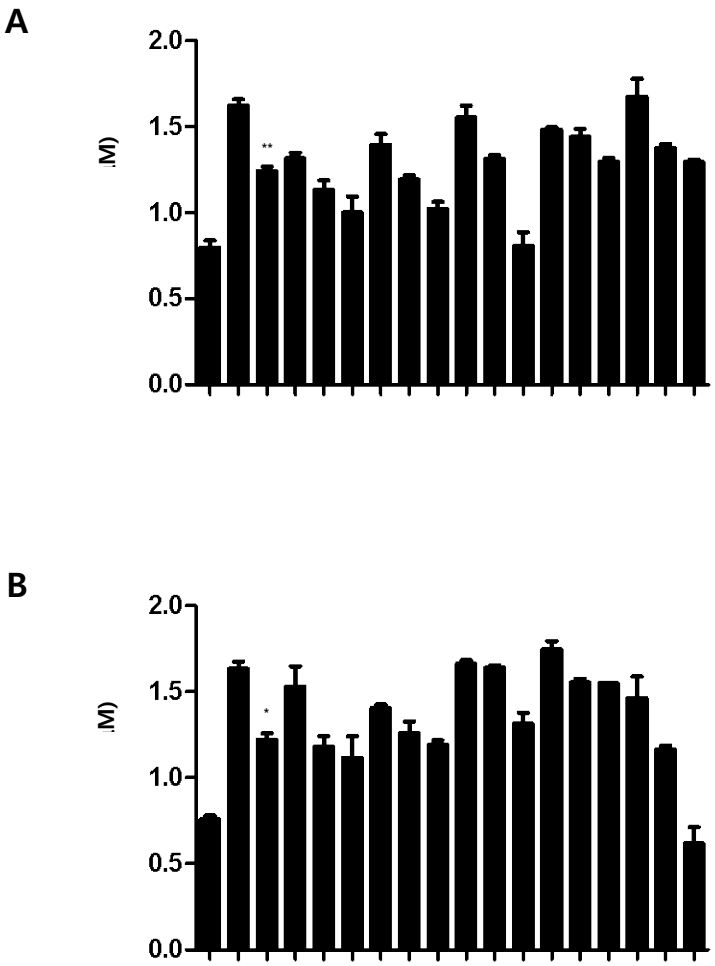

Fig. 22: Inhibitory Effect of *R. bicolor* and *C. lanceolata* extracts and fractions on NO production in RAW264.7 macrophage. RAW264.7 cells were treated with extract and fractions and then incubated for 18 h with LPS (0.5 μg/mL). Data are presented as mean ± SD values of 3 independent experiments. Sulfuretin (20 μM) was used as the positive control. $^{*}P < 0.05$, $^{**}P < 0.01$, $^{***}P < 0.001$ vs. LPS.

(4) Anti-skin inflammatory effects of extracts and fractions in HaCaT human keratinocytes

The keratinocytes of the epidermis are the main cells that make up the skin, forming the stratum corneum, and forming an effective skin barrier system against physical and chemical stimuli and external microorganisms. Keratinocytes are also involved in inflammatory and immune responses as well as protecting the skin in a variety of ways, such as from penetration and UV rays, and functioning as a moisturizer and antioxidant [124, 125]. However, constant exposure of the keratinocytes to physiological and environmental stresses leads to the activation of the inflammatory response producing various pro-inflammatory cytokines, such as tumor necrosis factor (TNF)-α, interleukin (IL)-6, and IL-8 [126]. Excessive production of pro-inflammatory cytokines damages keratinocytes and causes skin aging, leading to inflammatory skin diseases, such as psoriasis and atopic dermatitis [127]. Therefore, to treat skin damage and inflammatory diseases, it is necessary to regulate the inflammatory response of keratinocytes. Thus, in this study, I have attempted to observe the inhibitory effect of the extract and fraction on skin inflammation in HaCaT keratinocytes induced by recombining TNF-α and interferon (IFN)-γ. First, a toxicity assessment was performed to establish the concentration of the compound. Individual concentrations were Rb-CH_2Cl_2, Rb-EtOAc, and Cl-CH_2Cl_2 treated with 2.5-10 μg/mL, Rb-70%E, Rb-BuOH, and Rb-H_2O treated with 10-50 μg/mL, Cl-70%E, Cl-EtOAc, and Cl-BuOH treated with 25-100 μg/mL, and Cl-H_2O with 50-200 μg/mL. The results showed no toxicity in all the 10 treatment groups (Fig. 23).

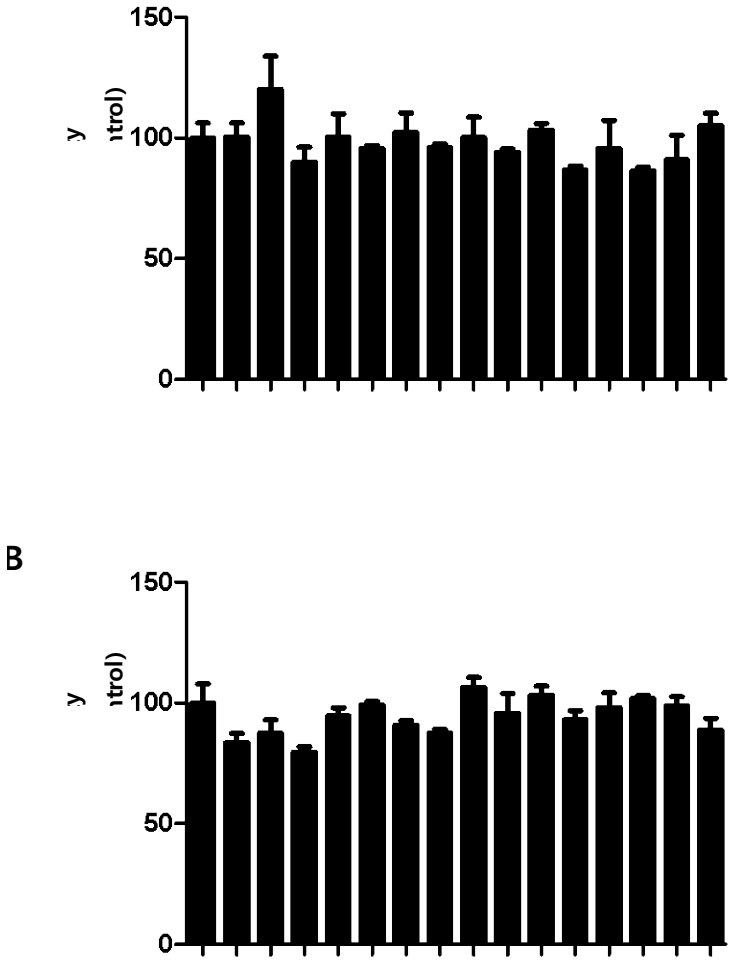

Fig. 23: Toxicity evaluation of *R. bicolor* and *C. lanceolata* extracts and fractions in HaCaT Human Keratinocytes. HaCaT cells were treated with extract and fractions and then incubated for 18 h. Data are presented as mean ± SD values of 3 independent experiments.

Subsequently, the concentration that was set based on the toxicity evaluation was used to confirm the inhibitory effect of IL-6 production. Extracts and fractions were pretreated at individual concentrations for 3 h and stimulated with 20 ng/mL TNF-α + IFN-γ for 24 h to observe IL-6 production. Individual concentrations of *R. bicolor* were treated with Rb-70% E (10-50 μg/mL), Rb-CH_2Cl_2 (2.5-10 μg/mL), Rb-EtOAc (2.5-10 μg/mL), Rb-BuOH (10-50 μg/mL), Rb-H_2O (10-50 μg/mL). Inhibition of IL-6 production was observed only in Rb-EtOAc (Fig. 24A).

Then, the individual concentrations of *C. lanceolata* were treated with Cl-70% E (25-100 μg/mL), Cl-CH_2Cl_2 (2.5-10 μg/mL), Cl-EtOAc (25-100 μg/mL), Cl-BuOH (25-100 μg/mL), and Cl-H_2O (50-200 μg/mL). The results suggested that Cl-70%E and Cl-EtOAc showed a concentration-dependent inhibitory effect on IL-6 production (Fig. 24B).

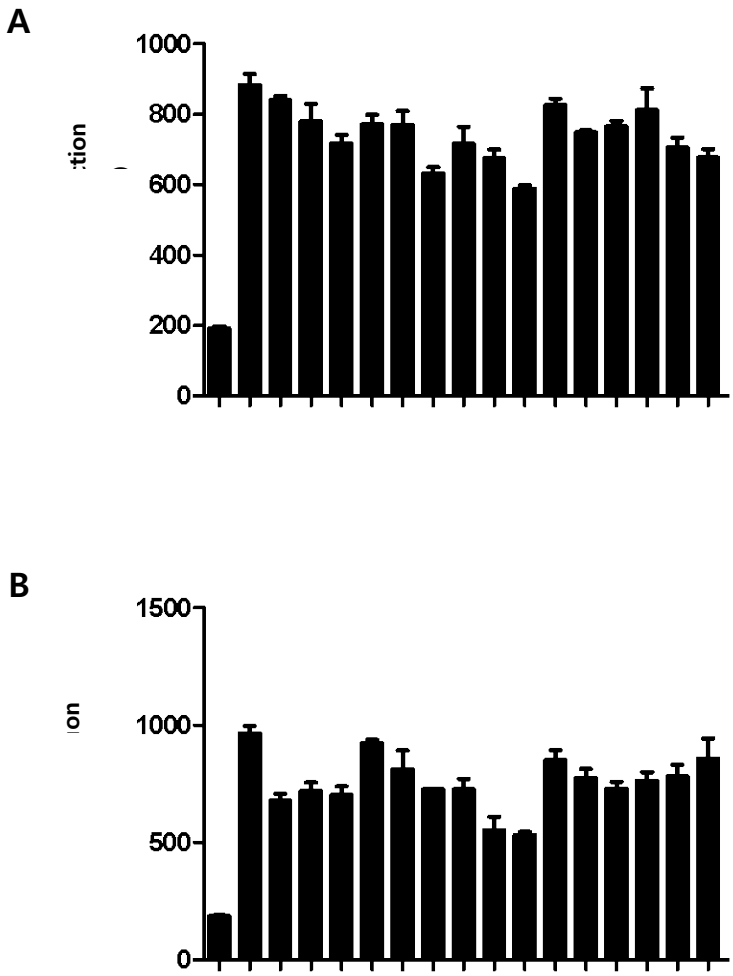

Fig. 24: Inhibitory Effect of *R. bicolor* and *C. lanceolata* extracts and fractions on IL-6 Production in HaCaT Human Keratinocytes. HaCaT cells were treated with extract and fractions and then incubated for 18 h with TNF-α/IFN-γ (20 ng/mL). Data are presented as mean ± SD values of 3 independent experiments. $^{*}P < 0.05$, $^{**}P < 0.01$, $^{***}P < 0.001$ vs. TNF-α/IFN-γ.

The concentration that was set based on the toxicity evaluation was used to confirm the inhibitory effect of IL-8 production. Extracts and fractions were pretreated at individual concentrations for 3 h and stimulated with 20 ng/mL TNF-α + IFN-γ for 24 h to observe IL-8 production. Individual concentrations of *R. bicolor* were treated with Rb-70% E (10-50 μg/mL), Rb-CH_2Cl_2 (2.5-10 μg/mL), Rb-EtOAc (2.5-10 μg/mL), Rb-BuOH (10-50 μg/mL), and Rb-H_2O (10-50 μg/mL). A concentration-dependent inhibitory effect on IL-8 production was observed in all the treatment groups exept Rb-CH_2Cl_2, among which Rb-70%E and Rb-BuOH significantly inhibited IL-8 production (Fig. 25A).

Subsequently, the individual concentrations of *C. lanceolata* were treated with Cl-70% E (25-100 μg/mL), Cl-CH_2Cl_2 (2.5-10 μg/mL), Cl-EtOAc (25-100 μg/mL), Cl-BuOH (25-100 μg/mL), Cl-H_2O (50-200 μg/mL). A concentration-dependent inhibitory effect on IL-8 production was observed in all the treatment groups exept Cl-BuOH, of which Cl-70%E and Cl-H_2O significantly inhibited IL-8 production (Fig. 25B).

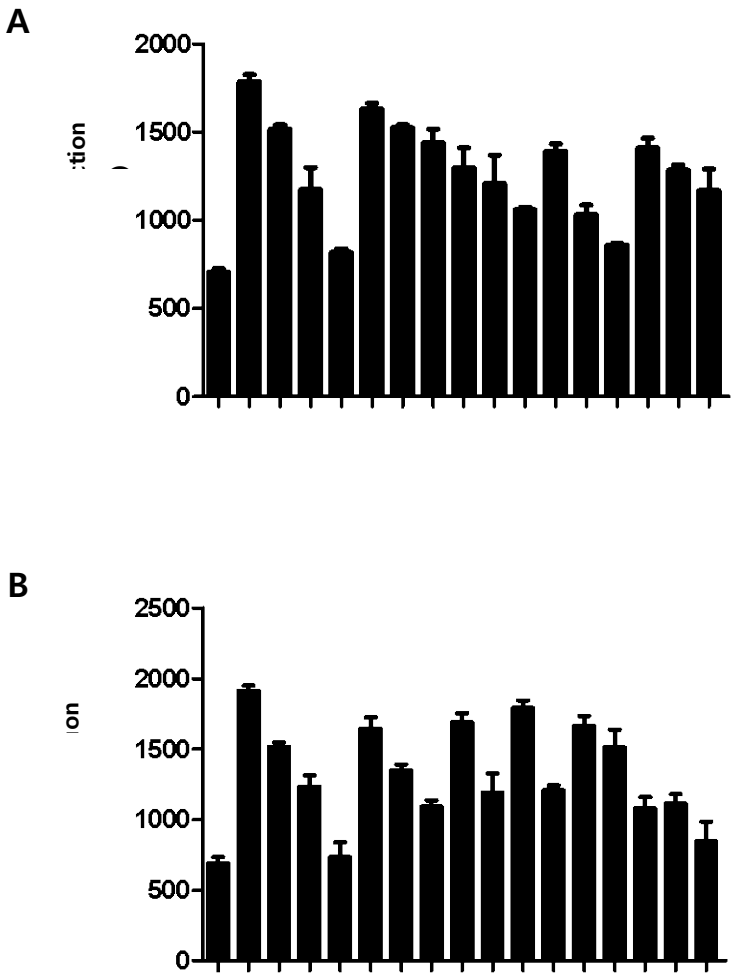

Fig. 25: Inhibitory Effect of *R. bicolor* and *C. lanceolata* extracts and fractions on IL-8 Production in HaCaT Human Keratinocytes. HaCaT cells were treated with extract and fractions and then incubated for 18 h with TNF-α/IFN-γ (20 ng/ml). Data are presented as mean ± SD values of 3 independent experiments. $^{*}P < 0.05$, $^{**}P < 0.01$, $^{***}P < 0.001$ vs. TNF-α/IFN-γ.

2. Anti-aging effect of compounds isolated from *R. bicolor* and *C. lanceolata*

(1) Structure of compounds isolated from *R. bicolor* and *C. lanceolata*

The compounds used in this study consisted of five compounds isolated from *R. bicolor* and *C. lanceolata* (Compositae). Patulitrin and beta-amyrin were isolated from *R. bicolor*, and phenylheptatryine, 8-methoxybutin, and leptosidin were isolated from *C. lanceolata*. The structure of the compound is shown in the figure (Fig. 26). Patulitrin is a flavonol type compound with a molecular weight of 494.4 g/mol. Beta-amyrin is a triterpenoid-type compound with a molecular weight of 426.7 g/mol, while phenylheptatryine has a molecular weight of 164.2 g/mol. 8-methoxybutin is a flavanone compound with a molecular weight of 302.28 g/mol. Leptosidin is an aurone type compound with a molecular weight of 300.26 g/mol. Each compound was used for in vitro analysis by calculating its molarity through molecular weight and then diluting with DMSO.

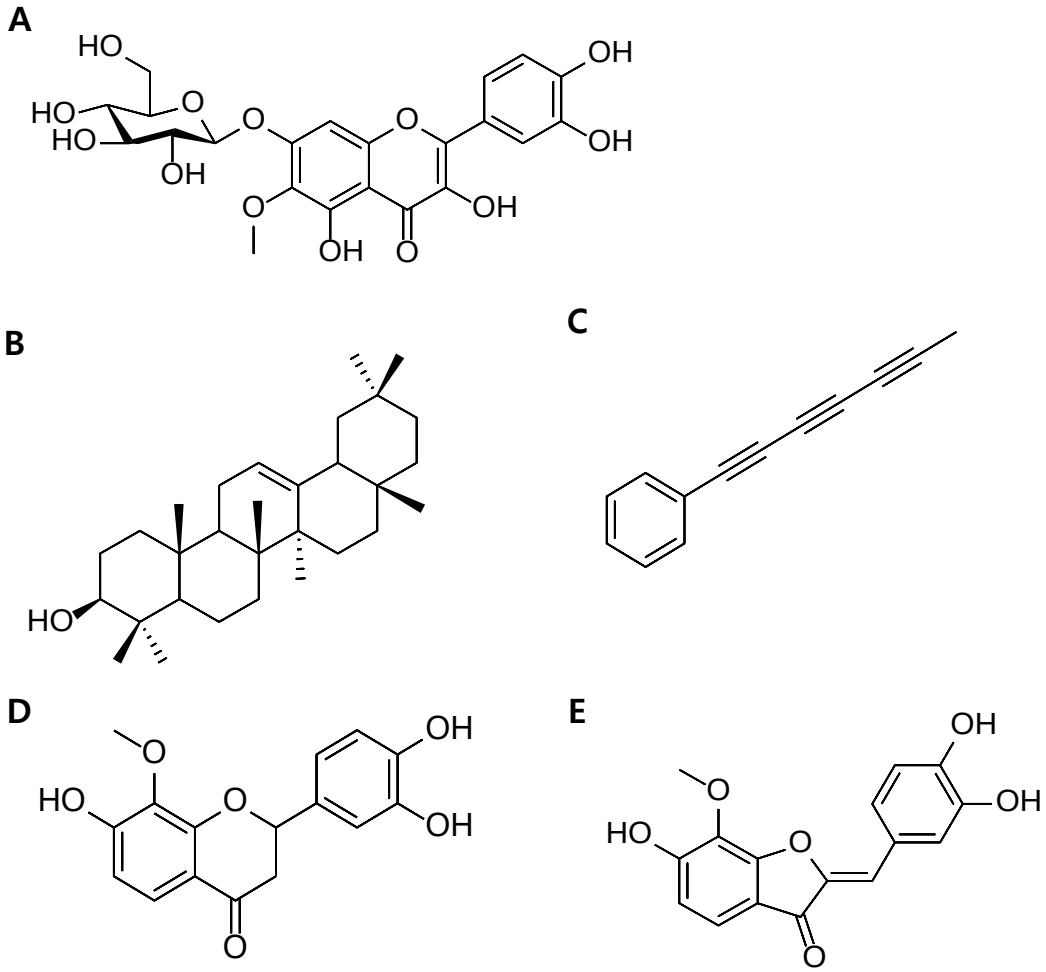

Fig. 26: Structure of compounds isolated from *R. bicolor* and *C. lanceolata*

(2) Neuroprotective effect of compounds in HT22 hippocampal cells

Excessive excretion of glutamate causes excitatory toxicity and oxidative stress [108]. However, there are reports that HT22 hippocampal cells lack functional ionotropic glutamate receptors [109]. Therefore, I have evaluated the oxidative stress-related cytotoxic and brain cell protective effects of HT22 hippocampal cells induced by glutamate.

By treating the cells with 5-20 μM of each of the five compounds isolated from two Compositae plants, cytotoxicity was observed at 20 μM concentrations of 8-methoxybutin and leptosidin (Fig. 27A).

Based on the toxicity evaluation, the maximum concentration of 8-methoxybutin and leptosidin were set to 10 μM, and neuroprotective effects were observed in HT22 hippocampal cells induced by glutamate. Each compound was treated for 6 h, with 20 mM glutamate and 100 μM Trolox as positive controls. Absorbance measurements from the MTT assay after 12 h showed no neuroprotective effects in all the compounds (Fig. 27B).

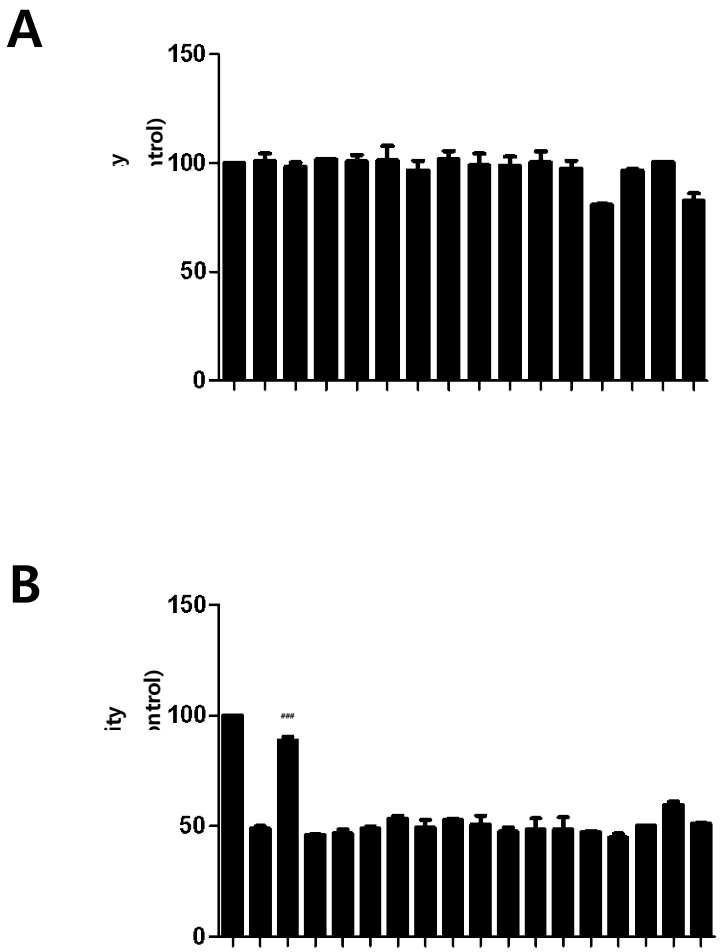

Fig. 27: Neuroprotective effect on HT22 hippocampal cells of compounds isolated *R. bicolor* and *C. lanceolata.* HT22 cells were treated with five compounds and then incubated for 12 h (A). HT22 cells were treated with five compounds and then incubated for 12 h with glutamate (20 mM) (B). Data are presented as mean ± SD values of three independent experiments. Trolox (100 μM) was used as the positive control. $^{***}P < 0.001$ vs. glutamate (A); $^{###}P < 0.001$ vs. glutamate (B).

(3) Anti-neuroinflammatory Effect of compounds in BV2 Microglia

Microglia, which are macrophages present in the brain, are activated in the presence of harmful factors, and play an important role in maintaining homeostasis by eliminating adverse reactions in the body. However, when abnormally activated by external stimuli, pro-inflammatory mediators, ROS, and inflammatory cytokines are secreted [111]. The secretion of inflammatory mediators can lead to cell damage and brain damage, leading to degenerative brain diseases, such as Alzheimer's and Parkinson's disease [112, 113]. When microglial cells are overactivated by external stimuli, pro-inflammatory substances, such as NO and PGE_2 and inflammatory cytokines, such as TNF-α, IL-6, and IL-1β are secreted. Suppressing the secretion of active inflammatory substances can prevent cell damage. Thus, the neuroinflammation inhibitory effect of the compounds on BV2 microglia induced by LPS was observed.

First, a toxicity assessment was performed on the compound. The results showed toxicity at the maximum concentrations of the four compounds except for patulitrin (Fig. 28A). Based on the toxicity assessment, the maximum concentration of beta-amyrin, 8-methoxybutin, and leptosidin was set to 10 μM, and that of phenylheptatryine to 20 μM. The maximum concentration of patulitrin was set to 40 μM to confirm the inhibitory effect of nitrite production. Butein (10 μM) was used as a positive control. As for the NO production inhibitory effect of the compounds, four compounds, except patulitrin, suppressed NO production in a concentration-dependent manner, and beta-amyrin, 8-methoxybutin, and leptosidin showed superior NO production inhibitory effects than the positive control (Fig. 28B).

Subsequently, the inhibitory effect on IL-6 production was confirmed for the three compounds having an excellent inhibitory effect on NO production. The IL-6 inhibitory effect of phenylheptatryine and 8-methoxybutin at the same concentration was found to be excellent (Fig. 28C).

In addition, results confirmed the inhibitory effect on TNF-α production, which was observed only in phenylheptatryine (Fig. 28D). Overall, among the five compounds, phenylheptatryine showed excellent anti-neuroinflammatory effects.

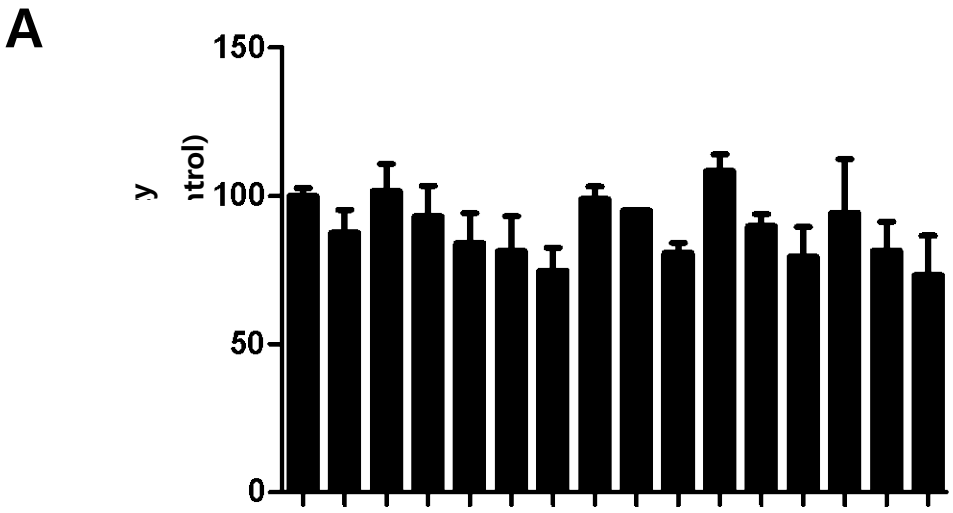

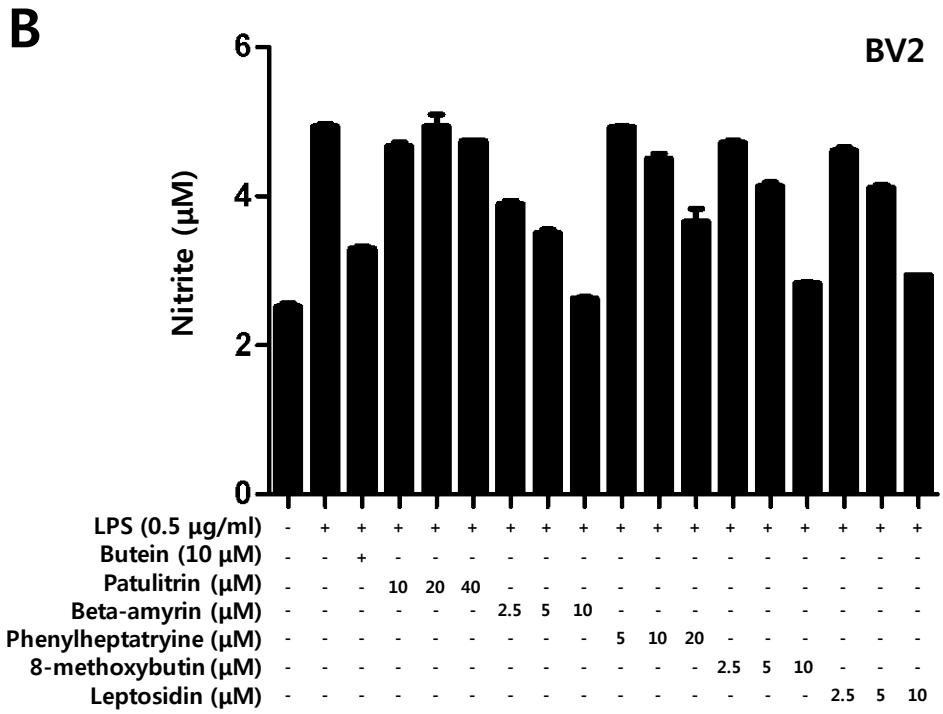

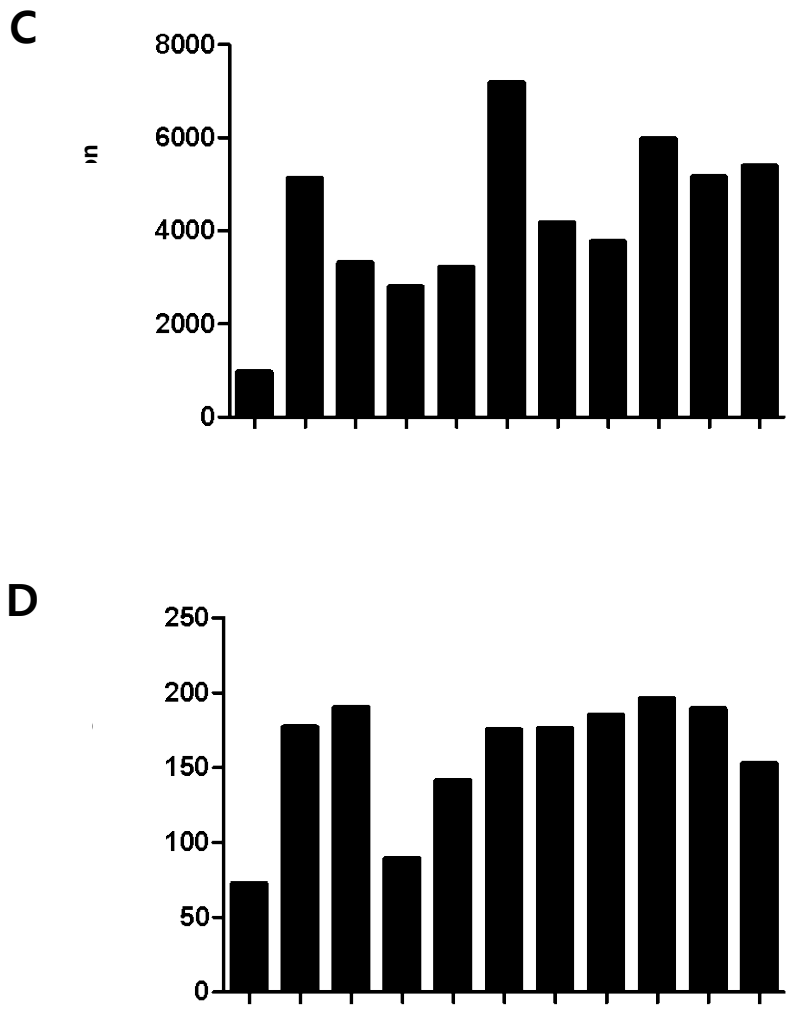

Fig. 28: Anti-neuroinflammatory effects of compounds isolated from *R. bicolor* and *C. lanceolata* on BV2 microglia. BV2 cells were treated with three compounds and then incubated for 18 h (A). BV2 cells were treated with three compounds and then incubated for 18 h with LPS (0.5 μg/mL) (B, C, D). Data are presented as mean ± SD values of 3 independent experiments. Butein (10 μM) was used as the positive control. $^{\#\#}P < 0.01$, $^{\#\#\#}P < 0.001$ vs. LPS.

(4) The inhibitory effects of compounds on the iNOS and COX-2 expression in BV2 microglia

Inflammatory cytokines and NO are active inflammatory substances that are rapidly produced when LPS or pathogens are injected into macrophages [114]. These substances are increased by the pro-inflammatory proteins inducible nitric oxide synthase (iNOS) and cyclooxygenase-2 (COX-2). Therefore, it was confirmed by Western blot analysis that the expression of pro-inflammatory proteins iNOS and COX-2 was inhibited for compounds that inhibit inflammatory cytokines. As a result, phenylheptatryine inhibited the expression of iNOS and COX-2 in a concentration-dependent manner (Fig. 29).

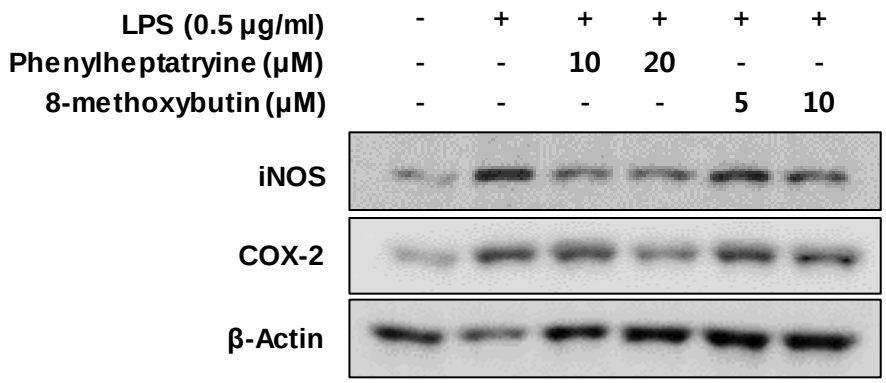

Fig. 29: Inhibitory effect of phenylheptatryine and 8-methoxybutin on the expression of iNOS and COX-2 proteins in LPS-induced BV2 microglia. BV2 cells were treated with two compounds and then incubated for 18 h with LPS (0.5 μg/mL).

(5) The inhibitory effects of compounds on NF-κB translocation in BV2 microglia

The transcription factor that regulates the expression of iNOS and COX-2 is known as NF-κB [128]. Normal NF-κB maintains its inactive form by forming complexes with proteins such as IκBα. However, when NF-κB is activated by LPS, the degradation of IκBα by phosphorylation is promoted and NF-κB tranlocated to the nucleus [129]. When NF-κB tranlocated to the nucleus, it binds to the promoter of the inflammatory mediator gene and induces the expression of the inflammatory mediator [130]. Therefore, it was confirmed that nuclear proteins were extracted from BV2 cells stimulated with LPS for compounds that inhibit inflammatory cytokines, thereby inhibiting NF-κB activation. As a result, it was confirmed that phenylheptatryine inhibited p-IκBα phosphorylation in a concentration-dependent manner. Additionally, the translocation of p65 to the nucleus was inhibited in a concentration-dependent manner (Fig. 30). In this study, it was confirmed that phenylheptatryine inhibited the degradation of IκBα and the activation by LPS.

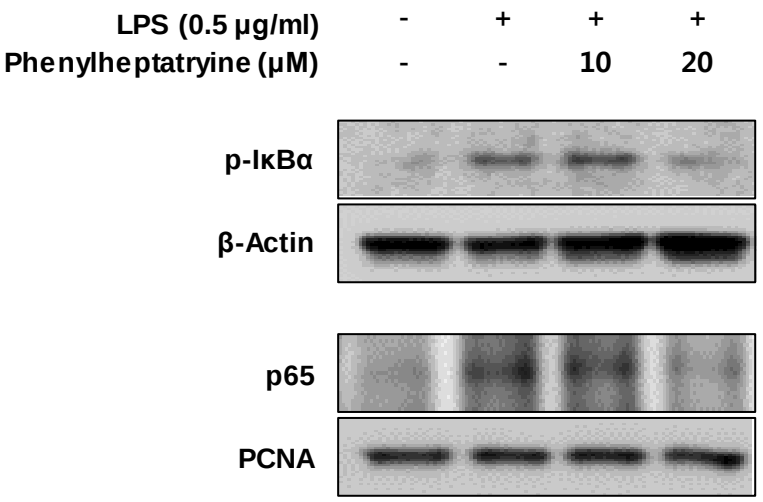

Fig. 30: Inhibitory effect of phenylheptatryine on the Nuclear NF-κB translocation in LPS-induced BV2 microglia. Cells were pretreated with the indicated concentrations of phenylheptatryine for 3 h and stimulated with LPS (0.5 μg/mL) for 1 h. Nuclear NF-κB translocation was analyzed using western blotting as described in the Materials and Methods section.

(6) Anti-inflammatory effects of compounds in RAW264.7 Macrophage

Macrophages are immune cells involved in the inflammatory response. However, when macrophages respond to external stimuli, they overproduce pro-inflammatory mediators, such as NO, PGE_2, and cytokines, leading to chronic inflammatory reactions, such as tissue damage and genetic mutations [121-123]. Therefore, in this study, I have observed the inhibitory effect of extracts and fractions on the production of pro-inflammatory mediators in RAW264.7 macrophages induced by LPS.

First, a toxicity assessment was performed on the compound. Results showed toxicity at the maximum concentration of all compounds. In particular, leptosidin was toxic even at 10 μM (Fig. 31A). Based on the toxicity assessment, the maximum concentrations of beta-amyrin, 8-methoxybutin, and leptosidin was set to 10 μM, and that of phenylheptatryine to 20 μM. The maximum concentration of patulitrin was set to 40 μM to confirm the inhibitory effect on nitrite production. Butein (10 μM) was used as a positive control. The inhibitory effect of the compound on NO production in LPS-induced RAW264.7 macrophages was observed only in groups treated with beta-amyrin and leptosidin (Fig. 31B). Subsequently, the inhibitory effect on IL-6 production was confirmed for the three compounds having an excellent inhibitory effect on NO production in RAW264.7 macrophages. An excellent IL-6 inhibitory effect of phenylheptatryine and 8-methoxybutin at the same concentration was observed (Fig. 31C). In addition, phenylheptatryine and 8-methoxybutin showed inhibitory effect on TNF-α production (Fig. 31D).

Overall, among the five compounds, phenylheptatryine and 8-methoxybutin showed excellent anti-inflammatory effects.

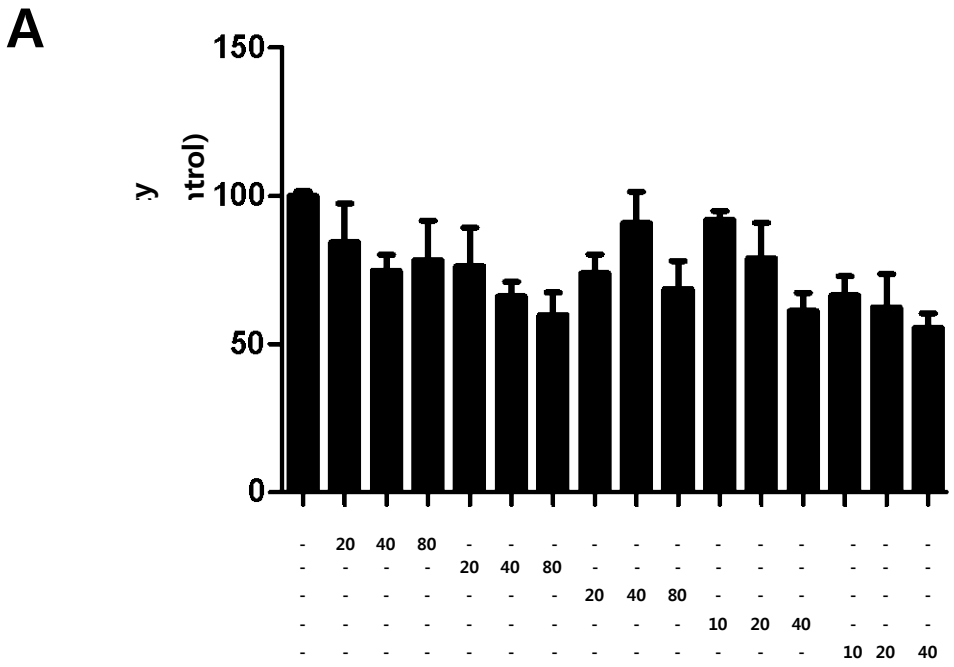

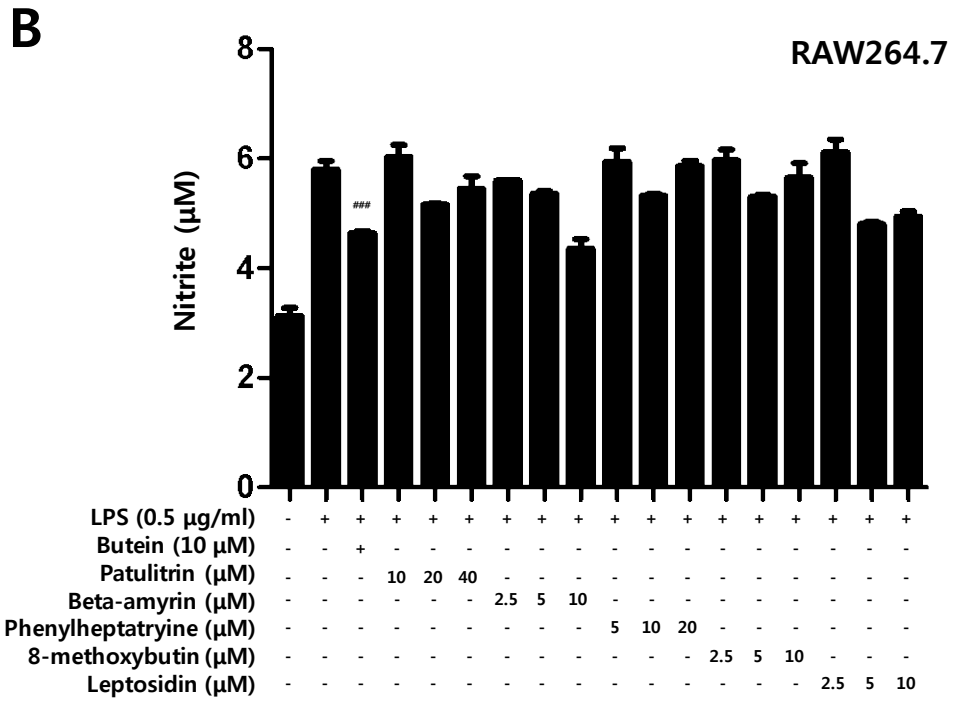

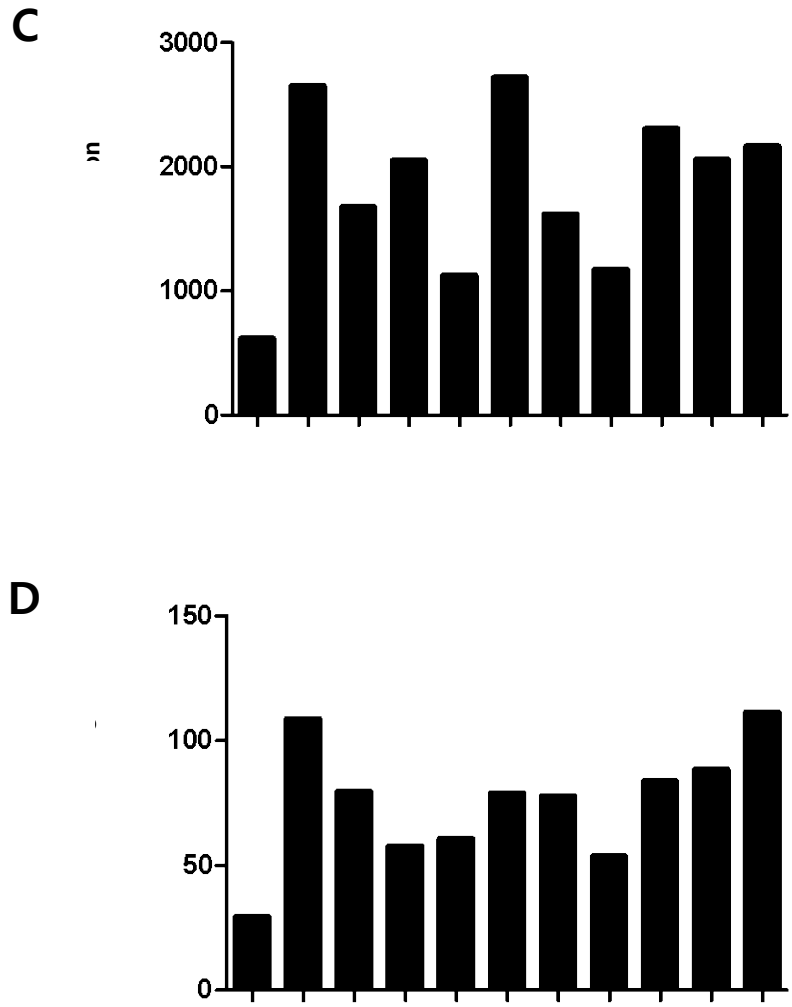

Fig. 31: Anti-inflammatory effects of compounds isolated from *R. bicolor* and *C. lanceolata* on RAW264.7 macrophage. RAW264.7 cells were treated with three compounds and then incubated for 18 h (A). RAW264.7 cells were treated with three compounds and then incubated for 18 h with LPS (0.5 μg/mL) (B, C, D). Data are presented as mean ± SD values of 3 independent experiments. $^{*}P < 0.05$, $^{**}P < 0.01$ vs. control group (A); $^{\#\#}P < 0.01$, $^{\#\#\#}P < 0.001$ vs. LPS (B).

(7) The inhibitory effects of compounds on the iNOS and COX-2 expression in RAW264.7 macrophage

Inflammatory cytokines and NO are active inflammatory substances that are rapidly produced when LPS or pathogens are injected into macrophages [114]. These substances are increased by the pro-inflammatory proteins iNOS and COX-2. Therefore, it was confirmed by Western blot analysis that the expression of pro-inflammatory proteins iNOS and COX-2 was inhibited for compounds that inhibit inflammatory cytokines. As a result, phenylheptatryine inhibited the expression of COX-2 in a concentration-dependent manner, and 8-methoxybutin inhibited the expression of iNOS and COX-2 (Fig. 32).

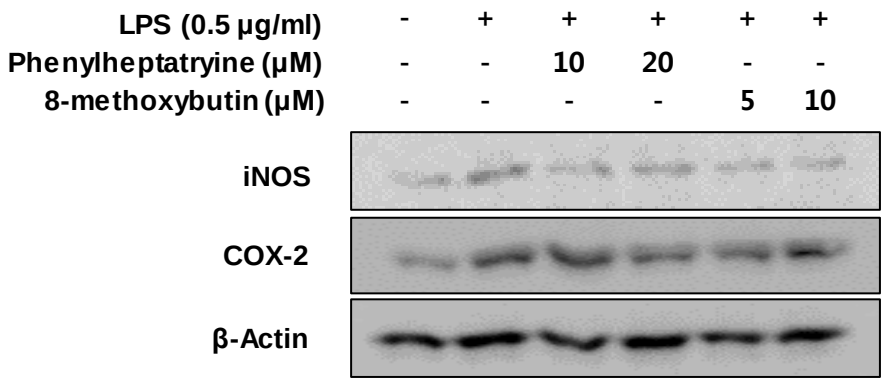

Fig. 32: Inhibitory effect of phenylheptatryine and 8-methoxybutin on the expression of iNOS and COX-2 proteins in LPS-induced RAW264.7 macrophage. RAW264.7 macrophage was treated with two compounds and then incubated for 18 h with LPS (0.5 μg/mL).

(8) The inhibitory effects of compounds on NF-κB translocation in RAW264.7 macrophage

The transcription factor that regulates the expression of iNOS and COX-2 is known as NF-κB [128]. Normal NF-κB maintains its inactive form by forming complexes with proteins such as IκBα. However, when NF-κB is activated by LPS, the degradation of IκBα by phosphorylation is promoted and NF-κB tranlocated to the nucleus [129]. When NF-κB tranlocated to the nucleus, it binds to the promoter of the inflammatory mediator gene and induces the expression of the inflammatory mediator [130]. Therefore, it was confirmed that nuclear proteins were extracted from RAW264.7 cells stimulated with LPS for compounds that inhibit inflammatory cytokines, thereby inhibiting NF-κB activation. As a result, it was confirmed that phenylheptatryine inhibited p-IκBα phosphorylation in a concentration-dependent manner. Additionally, the translocation of p65 to the nucleus was inhibited in a concentration-dependent manner (Fig. 33). In this study, it was confirmed that phenylheptatryine inhibited the degradation of IκBα and the activation by LPS.

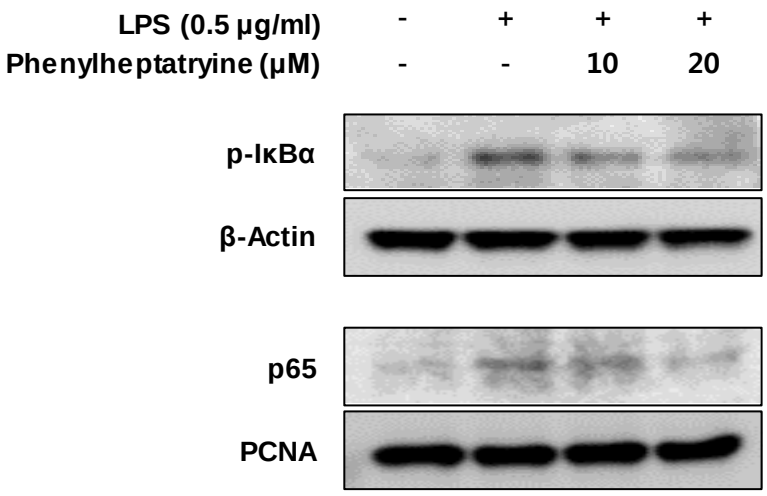

Fig. 33: Inhibitory effect of phenylheptatryine on the Nuclear NF-κB translocation in LPS-induced RAW264.7 macrophage. Cells were pretreated with the indicated concentrations of phenylheptatryine for 3 h and stimulated with LPS (0.5 μg/mL) for 1 h. Nuclear NF-κB translocation was analyzed using western blotting as described in the Materials and Methods section.

(9) Anti-skin inflammatory effects of compounds in HaCaT human keratinocytes

The keratinocytes of the epidermis are the main cells that make up the skin, forming the stratum corneum, and forming an effective skin barrier system against physical and chemical stimuli and external microorganisms. However, continuous exposure of keratinocytes to physiological and environmental stress activates the inflammatory response, producing a variety of pro-inflammatory cytokines, including TNF-α, IL-6, and IL-8. Excessive production of pro-inflammatory cytokines damages keratinocytes and causes skin aging, leading to inflammatory skin diseases such as psoriasis and atopic dermatitis. Therefore, it is necessary to control the inflammatory response of keratinocytes to treat skin damage and inflammatory diseases. In this study, I have attempted to observe the inhibitory effect of extracts and fractions on skin inflammation of HaCaT keratinocytes induced by the recombination of TNF-α and IFN-γ. First, a toxicity assessment was performed to determine the concentration of the compound. All compounds were treated at the same concentration (5-80 μM), and toxicity was confirmed. Results showed toxicity in a concentration-dependent manner in 8-methoxybutin and leptosidin (Fig. 34A). Next, the inhibitory effect of IL-6 production was confirmed using the concentration setting based on the toxicity evaluation. Compounds were pretreated at individual concentrations for 3 h and stimulated with 20 ng/mL TNF-α + IFN-γ for 24 h to observe IL-6 production. The inhibitory effect on IL-6 and -8 production was not observed in any of the compounds (Fig. 34B, C).

A

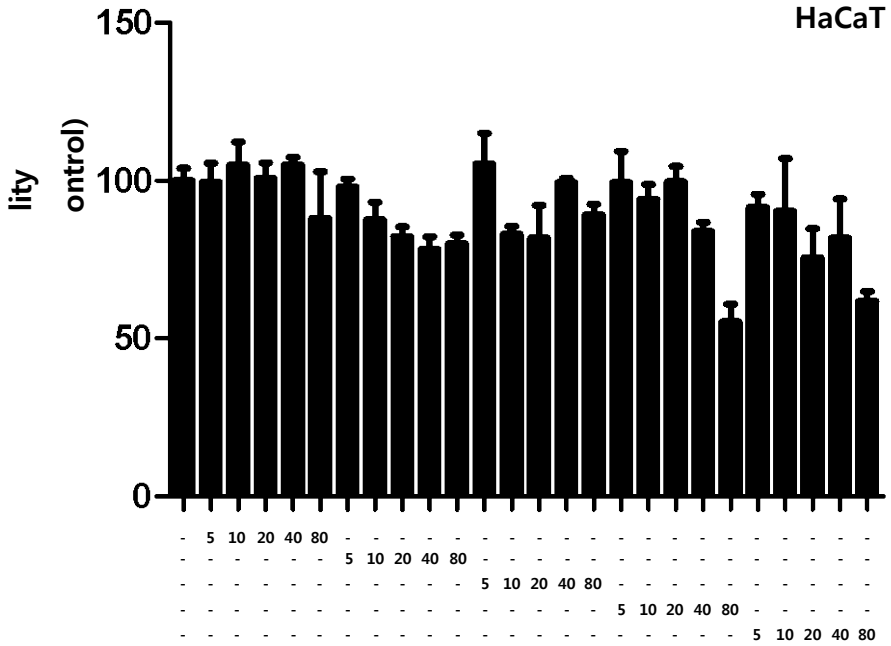

B

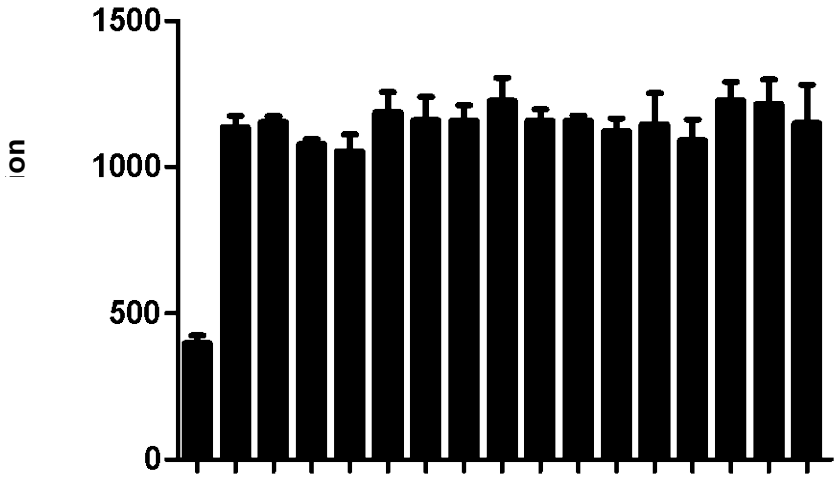

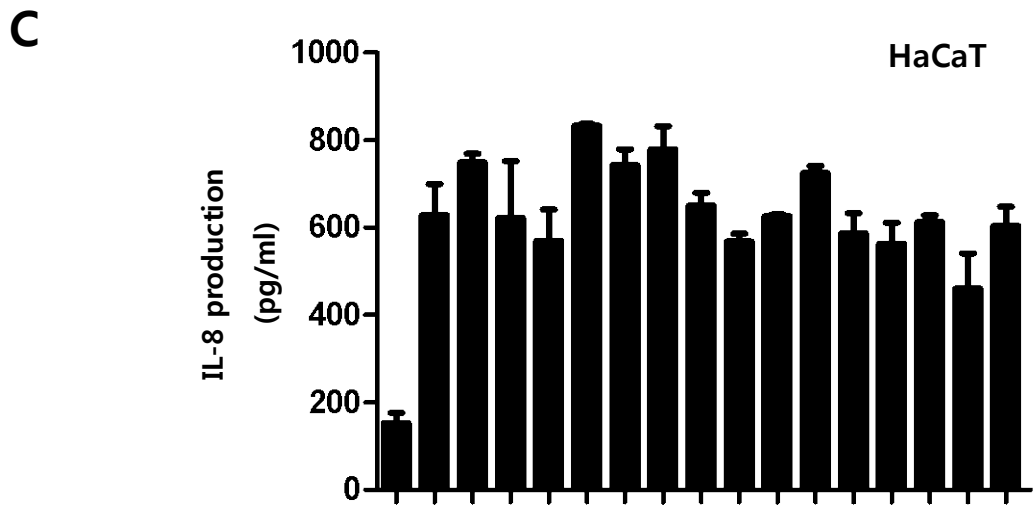

Fig. 34: Anti-skin inflammatory effects of compounds isolated from *R. bicolor* and *C. lanceolata* in HaCaT human keratinocytes. HaCaT cells were treated with extract and fractions and then incubated for 18 h (A). HaCaT cells were treated with extract and fractions and then incubated for 18 h with TNF-α/IFN-γ (20 ng/mL) (B and C). Data are presented as mean ± SD values of 3 independent experiments. **P* < 0.05, ***P* < 0.01 vs. control group (A); $^{\#}$*P* < 0.001 vs. TNF-α/IFN-γ (C).

Ⅳ. Conclusion

The purpose of this study was to investigate the treatment mechanisms used for anti-aging-related diseases, such as the neuroprotective effect of *R. bicolor* and *C. lanceolata*, and the inhibitory effects of neuroinflammation and skin inflammation. In particular, the potential effects of *R. bicolor* and *C. lanceolata* extracted with 70% ethanol on anti-aging-related diseases were confirmed, and the anti-inflammatory effects of the isolated compounds were compared. In this study, treatment group concentration settings were established through toxicity assessment. The neuroprotective effects of glutamate-induced HT22 hippocampal cells of extracts and fractions were observed in all treatment groups except in Rb-H_2O, Cl-CH_2Cl_2, and Cl-H_2O. Next, anti-neuronal inflammatory effects were observed in all treatment groups. Anti-inflammatory effects were observed in all treatment groups except Rb-BuOH and Cl-BuOH. In HaCaT human keratinocytes induced by TNF-α + IFN-γ, Rb-EtOAc and all *C. lanceolata* treatment groups except in Cl-CH_2Cl_2 inhibited IL-6 production. In addition, all *C. lanceolata* treatment groups except in Cl-BuOH inhibited IL-8 production. By investigating the neuroprotective effect, neuroinflammation, and skin inflammation inhibitory effect of the five compounds isolated from these extracts, phenylheptatriyne showed the best anti-neuroinflammatory effect. In addition, phenylheptatriyne and 8-methoxybutin also showed excellent anti-inflammatory effects. In this study, the anti-aging evaluation of extract, fractions and compounds from *R. bicolor* and *C. lanceolata* were performed. As the results, 70% EtOH extracts and EtOAc fractions of *R. bicolor* and *C. lanceolata*, and phenylheptatriyne was identified as the best anti-aging active component among the isolated five compounds.

References

1. MK Kim, HR Kwak, SJ Ko, SH Lee, JS Kim, KH Kim, BJ Cha and HS Choi (2010) First Report of Cucumber mosaic virus Infecting Pinewood Coneflower (*Rudbeckia bicolor*) in Korea. *Plant Pathol. J*. 26(1): 93-98

2. IJ An, JK Kwon, JS Lee, HS Park, DC Kim, BJ Choi, KM Lee, YJ Park and JY Jung (2012) Induction of Apoptosis in Human Cancer Cells with Compositae Extracts. *J. Korean Soc. Food Sci. Nut*. 41(5): 584-590

3. NY Park, JH Kown and HK Kim (1998) Optimization of extraction conditions for ethanol extracts from Chrysanthemum morifolium by response surface methodology. *Korean J. Food Sci. Technol*. 31: 1189-1196

4. SH Choi, SI Im and JE Bae (2006) Analysis of aroma components from flower tea of German chamomile and *Chrysantehmum boreale* Makino. *Korea J. Food Cookery Sci.* 22: 768-773

5. JR Kang, MK Lee and SM Kang (2008) Anti-oxidant property and tyrosinase inhibition activity of various extracts from plants in compositae plants. *J. Korea Soc. Appl. Biol. Chem*. 51: 321-328

6. Michael BR, Gedara SR, Amer MM, Stevenson L and Ahmed AF. (2014) Evidence-based medicinal value of *Rudbeckia hirta* L. flowers. *Nat. Prod. Res.* 28(12): 909-13

7. Lawson SK, Sharp LG, Powers CN, McFeeters RL, Satyal P and Setzer WN (2020) Volatile Compositions and Antifungal Activities of Native American Medicinal Plants: Focus on the Asteraceae. *Plants* (Basel). 9(1): 126

8. Pardede A, Mashita K, Ninomiya M, Tanaka K and Koketsu M (2016) Flavonoid profile and antileukemic activity of *Coreopsis lanceolata* flowers. *Bioorg. Med. Chem. Lett.* 26(12): 2784-2787

9. Bolek D and Gutschow M (2005) Preparation of 4,6,30,40-tetrasubstituted aurones via aluminium oxide-catalyzed condensation. *J. Heterocycl. Chem*. 42: 1399-1403

10. Quattrocchi U (2000) CRC World Dictionary of Plant Names: A-C. *CRC Press*. 615

11. SC Kim, JC Daniel, T Mesfin, B Mary, RG Fred, P Mona and JE Elizabeth (1999) ITS sequences and phylogenetic relationships in Bidens and Coreopsis (Asteraceae). *Syst. Bot.* 24: 480-493

12. Y Zhang, A Mourboul and ZY Li (2013) Research advance in medicinal plants from genus Coreopsis. *Zhongguo Zhong Yao Za Zhi*. 38(16): 2633-8

13. L Yao, J Li, L Li, X Li, R Zhang, Y Zhang and X Mao (2019) *Coreopsis tinctoria* Nutt ameliorates high glucose-induced renal fibrosis and inflammation via the TGF-β1/SMADS/AMPK/NF-κB pathways. *BMC Complement Altern. Med*. 19(1): 14

14. T Dias, MR Bronze, PJ Houghton, H Mota-Filipe and A Paulo (2010) The flavonoid-rich fraction of *Coreopsis tinctoria* promotes glucose tolerance regain through pancreatic function recovery in streptozotocin-induced glucose-intolerant rats. *J. Ethnopharmacol.* 132(2): 483-90

15. Derr JF (1994) Weed control in container-grown herbaceous perennials. *HortScience*. 29(2): 95-97

16. Pardede A, Adfa M, Kusnanda AJ, Ninomiya M and Koketsu M (2018) Chemical Constituents of *Coreopsis lanceolata* Stems and Their Antitermitic Activity Against the Subterranean Termite *Coptotermes curvignathus*. *J. Econ. Entomol*. 111(2): 803-807

17. Y Okada, M Okita, Y Murai, Y Okano and M Nomura (2014) Isolation and identification of flavonoids from *Coreopsis lanceolata* L. petals. *Nat. Prod. Res*. 28(3): 201-204

18. D Nakabo, Y Okano, N Kandori, T Satahira, N Kataoka, J Akamatsu and Y Okada (2018) Convenient Synthesis and Physiological Activities of Flavonoids in *Coreopsis lanceolata* L. Petals and Their Related Compounds. *Molecules*. 23(7): 1671

19. HG Kim, YS Jung, SM Oh, HJ Oh, JH Ko, DO Kim, SC Kang, YG Lee, DY Lee and NI Baek (2020) Coreolanceolins A-E, New Flavanones from the Flowers of *Coreopsis lanceolate*, and Their Antioxidant and Anti-inflammatory Effects. *Antioxidants* (Basel). 9(6): 539

20. HG Kim, HJ Oh, JH Ko, HS Song, YG Lee, SC Kang, DY Lee and NI Baek (2019) Lanceoleins A-G, hydroxychalcones, from the flowers of *Coreopsis lanceolata* and their

chemopreventive effects against human colon cancer cells. *Bioorg. Chem*. 85: 274-281

21. L Qu, W Zou, Z Zhou, T Zhang, JV Greef and M Wang (2014) Non-European traditional herbal medicines in Europe: A community herbal monograph perspective. *J. Ethnopharmacol*. 156: 107-114

22. DS Hage and R Matsuda (2015) Affinity chromatography: a historical perspective. *Methods Mol. Biol*. 1286: 1-19

23. KM Witherup, SA Look, MW Stasko, TJ Ghiorzi, GM Muschik and GM Cragg (1990) Taxus spp. Needles Contain Amounts of Taxol Comparable to the Bark of *Taxus brevifolia*: Analysis and Isolation. *J. Nat. Prod*. 53(5): 1249-1255

24. Y Hou, X Dan, M Babbar, Y Wei, SG Hasselbalch, DL Croteau and VA Bohr (2019) Ageing as a risk factor for neurodegenerative disease. *Nat. Rev. Neurol*. 15(10): 565-581

25. H Phatnani and T Maniatis (2015) Astrocytes in neurodegenerative disease. *Cold Spring Harb Perspect Biol*. 7(6): a020628

26. HM Schipper, W Song, A Tavitian and M Cressatti (2019) The sinister face of heme oxygenase-1 in brain aging and disease. *Prog. Neurobiol*. 172: 40-70

27. RM Ransohoff, D Schafer, A Vincent, NE Blachere and A Bar-Or (2015) Neuroinflammation: ways in which the immune system affects the brain. *Neurotherapeutics*. 12: 896-909

28. MB Graeber, W Li and ML Rodriguez (2011) Role of microglia in CNS inflammation. *FEBS Lett*. 585: 3798-3805

29. J Gehrmann, Y Matsumoto and GW Kreutzberg (1995) Microglia: intrinsic immuneffector cell of the brain. *Brain Res. Rev*.20(3): 269-287

30. KS Kirkley, KA Popichak, MF Afzali, ME Legare and RB Tjalkens (2017) Microglia amplify inflammatory activation of astrocytes in manganese neurotoxicity. *J. Neuroinflammation*.14(1): 99

31. JB Koprich, C Reske-Nielsen, P Mithal and O Isacson (2008) Neuroinflammation mediated by IL-1beta increases susceptibility of dopamine neurons to degeneration in an

animal model of Parkinson's disease. *J. neuroinflammation.* 5: 8

32. MA Mines, E Beurel and RS Jope (2011) Regulation of cell survival mechanisms in Alzheimer's disease by glycogen synthase kinase-3. *Int. J. Alzheimers Dis.* 2011: 861072

33. Z Chen and C Zhong (2014) Oxidative stress in Alzheimer's disease. *Neurosci. Bull.* 30: 271-281

34. MA Daulatzai (2017) Cerebral hypoperfusion and glucose hypometabolism: Key pathophysiological modulators promote neurodegeneration, cognitive impairment, and Alzheimer's disease. *J. Neurosci. Res.* 95: 943-972

35. N Tyagi, AV Ovechkin, D Lominadze, KS Moshal and SC Tyagi (2006) Mitochondrial mechanism of microvascular endothelial cells apoptosis in hyperhomocysteinemia. *J. Cell Biochem*. 98: 1150-1162

36. N Kushairi, CW Phan, V Sabaratnam, P David and M Naidu (2019) Lion's Mane Mushroom, Hericium erinaceus (Bull.: Fr.) Pers. Suppresses H 2 O 2-Induced Oxidative Damage and LPS-Induced Inflammation in HT22 Hippocampal Neurons and BV2 Microglia. *Antioxidants (Basel).* 8(8): 261

37. MY Huang, CE Tu, SC Wang, YL Hung, CC Su, SH Fang, CS Chen, PL Liu, WC Cheng, YW Huang and CY Li (2018) Corylin inhibits LPS-induced inflammatory response and attenuates the activation of NLRP3 inflammasome in microglia. *BMC Complement Altern. Med.* 18(1): 221

38. I Garate, , B García-Bueno, JLM Madrigal, JR Caso, L Alou, ML Gómez-Lus and JC Leza (2014) Toll-like receptor inhibitor TAK242 decreases neuroinflammation in rat brain frontal cortex after stress. *J. Neuroinflammation*. 11: 8

39. Q Han, Q Yuan, X Meng, J Huo, Y Bao and G Xie (2017) 6-Shogaol attenuates LPS-induced inflammation in BV2 microglia cells by activating PPAR-γ. *Oncotarget*. 8(26): 42001-42006

40. J Zhang, Y Zheng, Y Luo, Y Du, X Zhang and J Fu (2019) Curcumin inhibits LPS-induced neuroinflammation by promoting microglial M2 polarization via TREM2/ TLR4/ NF-κB pathways in BV2 cells. *Mol. Immunol*. 116: 29-37

41. M Takashima, K Ichihara and Y Hirata (2019) Neuroprotective effects of Brazilian green propolis on oxytosis/ferroptosis in mouse hippocampal HT22 cells. *Food Chem. Toxicol*. 132: 110669

42. Olney JW (1969) Brain lesions, obesity, and other disturbances in mice treated with monosodium glutamate. *Science*. 164(3880): 719-721

43. P Nagakannan, Md I Islam, S Karimi-Abdolrezaee and E Eftekharpour (2019) Inhibition of VDAC1 Protects Against Glutamate-Induced Oxytosis and Mitochondrial Fragmentation in Hippocampal HT22 Cells. *Cell Mol. Neurobiol*. 39(1): 73-85

44. Y Shao, T He, G J Fisher, J J Voorhees and T Quan (2017) Molecular basis of retinol anti-ageing properties in naturally aged human skin in vivo. *Int. J. Cosmet. Sci*. 39(1): 56-65

45. GJ Fisher, S Kang, J Varani, Z Bata-Csorgo, Y Wan, S Datta and JJ Voorhees (2002) Mechanisms of photoaging and chronological skin aging. *Arch. Dermatol*. 138(11): 1462-1470

46. L Rittie and GJ Fisher (2002) UV-light-induced signal cascades and skin aging. *Ageing Res. Rev.* 1: 705-720

47. Makrantonaki E and Zouboulis CC (2007) Molecular mechanisms of skin aging: State of the art. *Ann. N. Y. Acad. Sci*. 1119: 40-50

48. QL Pham, HJ Jang and KB Kim (2017) Antiwrinkle effect of fermented black ginseng on human fibroblasts. *Int. J. Mol. Med.* 39: 681-686

49. YH Kim, HR Park, SY Cha, SH Lee, JW Jo, JN Go, KH Lee, SY Lee and SS Shin (2020) Effect of red ginseng NaturalGEL on skin aging. *J. Ginseng Res*. 44(1): 115-122

50. JN Barker, RS Mitra, CE Griffiths, VM Dixit and BJ Nickoloff (1991) Keratinocytes as initiators of inflammation. *Lancet*. 337(8735): 211-214

51. C Albanesi, C Scarponi, ML Giustizieri and G Girolomoni (2005) Keratinocytes in inflammatory skin diseases. *Curr. Drug Targets Inflamm. Allergy*. 4(3): 329-334

52. T Banno, A Gazel and M Blumenberg (2004) Effects of tumor necrosis factor-alpha (TNF alpha) in epidermal keratinocytes revealed using global transcriptional profiling. *J. Biol.*

Chem. 279(31): 32633-32642

53. GJ Kang, NJ Kang, SC Han, DH Koo, HK Kang, BS Yoo and ES Yoo (2012) The Chloroform Fraction of *Carpinus tschonoskii* Leaves Inhibits the Production of Inflammatory Mediators in HaCaT Keratinocytes and RAW264.7 Macrophages. *Toxicol. Res.* 28(4): 255-62

54. EJ An, Y Kim, SH Lee, SH Choi, WS Chung and HJ Jang (2020) Ophiopogonin D ameliorates DNCB-induced atopic dermatitis-like lesions in BALB/c mice and TNF-α-inflamed HaCaT cell. *Biochem. Biophys. Res. Commun*. 522(1): 40-46

55. AJ Lewis and AM Manning (1999) New targets for anti-inflammatory drugs, *Curr. Opin. Chem. Biol*. 3: 489-494

56. M Wufuer, G Lee, W Hur, B Jeon, BJ Kim, TH Choi and S Lee (2016) Skin-on-a-chip model simulating inflammation, edema and drug-based treatment. *Sci. reps*. 6: 37471

57. JH Yang, YH Hwang, MJ Gu, WK Cho and JY Ma (2015) Ethanol extracts of *Sanguisorba officinalis* L. Suppress TNF-alpha/IFN-gamma-induced pro-inflammatory chemokine production in HaCaT cells. *Phytomedicine*. 22: 1262-1268

58. JH Yang, E Lee, B Lee, WK Cho, JY Ma and KI Park (2018) Ethanolic Extracts of *Artemisia apiacea* Hance Improved Atopic Dermatitis-Like Skin Lesions In Vivo and Suppressed TNF-Alpha/IFN-Gamma - Induced Proinflammatory Chemokine Production In Vitro. *Nutrients*. 10(7): 806

59. TH Pham, MS Kim, MQ Le, YS Song, Y Bak, HW Ryu, SR Oh and DY Yoon (2017) Fargesin exerts anti-inflammatory effects in THP-1 monocytes by suppressing PKC-dependent AP-1 and Nf-kB signaling. *Phytomedecine*. 24: 96-103

60. SI Jeong, BM Choi and SI Jang (2010) Sulforaphane suppresses TARC/CCL17 and MDC/CCL22 expression through heme oxygenase-1 and NF-kappaB in human keratinocytes. *Arch. Pharm. Res*. 33: 1867-1876

61. JS Lee, IS Kim, JS Ryu and CY Yun (2008) House dust mite, dermatophagoides pteronissinus increases expression of MCP-1, IL-6, and IL-8 in human monocytic THP-1 cells. *Cytokine*. 42: 365-371

62. K Tanaka, MH Roberts, N Yamamoto, H Sugiura, M Uehara and JM Hopkin (2006) Upregulating promoter polymorphisms of rantes relate to atopic dermatitis. *Int. J. Immunogenet*. 33: 423-428

63. RF Langston, CH Stevenson, CL Wilson, I Saunders and ER Wood (2010) The role of hippocampal subregions in memory for stimulus associations. *Behav. Brain Res*. 215(2): 275-91

64. M He, JLiu, S Cheng, Y Xing and WZ Suo (2013) Differentiation renders susceptibility to excitotoxicity in HT22 neurons. *Neural. Regen. Res*. 8(14): 1297-306

65. CH Park, JH Song, SN Kim, JH Lee, HJ Lee, KS Kang and HH Lim (2019) Neuroprotective Effects of Tetrahydrocurcumin against Glutamate-Induced Oxidative Stress in Hippocampal HT22 Cells. *Molecules*. 25(1): 144

66. E O'Loughlin, C Madore, H Lassmann and O Butovsky (2018) Microglial Phenotypes and Functions in Multiple Sclerosis. *Cold Spring Harb Perspect Med*. 8(2): a028993

67. Skaper SD, Facci L and Giusti P (2014) Neuroinflammation, microglia and mast cells in the pathophysiology of neurocognitive disorders: a review. *CNS Neurol Disord Drug Targets*. 13: 1654-1666

68. CH Kang, YH Choi, SK Moon, WJ Kim and GY Kim (2013) Quercetin inhibits lipopolysaccharide-induced nitric oxide production in BV2 microglial cells by suppressing the NF-kappaB pathway and activating the Nrf2-dependent HO-1 pathway. *Int. Immunopharmacol*. 17: 808-813

69. Saliba E and Henrot A (2001) Inflammatory mediators and neonatal brain damage. *Biol. Neonat.* 79: 224-227

70. T Roger, AL Chanson, M Knaup-Reymond and T Calandra (2005) Macrophage migration inhibitory factor promotes innate immune responses by suppressing glucocorticoidinduced expression of mitogen-activated protein kinase phosphatase-1. *Eur. J. Immunol*. 35: 3405-3413

71. A Baroni, E Buommino, VD Gregorio, E Ruocco, V Ruocco and R Wolf (2012) Structure and function of the epidermis related to barrier properties. *Clin. Dermatol*. 30(3): 257-262

72. Y Liu, C Zhao, Q Ma and Y Li (2019) Sinomenine retards LPS-elicited inflammation via down-regulating CCAT1 in HaCaT cells. *Life Sci*. 233: 116703

73. VG Wilson (2014) Growth and differentiation of HaCaT keratinocytes. *Methods Mol. Biol*. 1195: 33-41

74. HJ Kim, J Baek, JR Lee, JY Roh and Y Jung (2018) Optimization of Cytokine Milieu to Reproduce Atopic Dermatitis-related Gene Expression in HaCaT Keratinocyte Cell Line. *Immune. Netw*. 18(2): e9.

75. Capasso L. (1998) 5300 years ago, the Ice Man used natural laxatives and antibiotics. *Lancet*. 352(9143): 1864

76. Wilt TJ, Ishani A, Stark G, MacDonald R, Lau J and Mulrow C (1998) Saw palmetto extracts for treatment of benign prostatic hyperplasia: a systematic review. *JAMA*. 280: 1604

77. Kaptchuk TJ (2002) Acupuncture: theory, efficacy, and practice. *Ann. Intern*. Med. 136: 374

78. Association of the European Self-Medication Industry (1999) Herbal medicinal products in the European Union. Pharmaceuticals Policy and Law 2: 55-199

79. TY Tang, FZ Li and J Afseth (2014) Review of the regulations for clinical research in herbal medicines in USA, *Chin. J. Integr. Med*. 20(12): 883-93

80. D Wang, V Hiebl, T Xu, A Ladurner, AG Atanasov, EH Heiss and VM Dirsch (2020) Impact of natural products on the cholesterol transporter ABCA1. *J. Ethnopharmacol*. 249: 112444

81. GM Cragg, and DJ Newman (2013) Natural Products: A Continuing Source of Novel Drug Leads. *Biochim. Biophys. Acta.* 1830: 3670-3695

82. T Rodrigues, D Reke, P Schneider and G Schneider (2016) Counting on Natural Products for Drug Design. *Nat. Chem.* 8(6): 531-541

83. S Faizi, H Siddiqi, A Naz, S Bano and Lubna. (2010). Specific deuteration in patuletin and related flavonoids via keto-enoltautomerism: Solvent- and temperaturedependent ^{1}H-NMR

studies. *Helvetica Chimica. Acta*. 93(3): 466-481

84. A Sosa and C Rosquete (2010) Flavonoids from *Urena sinuata* L. *Avances en Química*. 5(2): 95-98

85. WR Thompson, J Meinwald, D Aneshansley and T Eisner (1972) Flavonols: pigments responsible for ultraviolet absorption in nectar guide of flower. *Science*. 177(4048): 528-530

86. L Quijano, F Malanco and TirsoRíos (1970) The structures of eupalin and eupatolin. Two new flavonol rhamnosides isolated from Eupatorium ligustrinum D.C. *Tetrahedron*. 26(12): 2851-2859

87. LH Vázquez, J Palazon and A Navarro-Ocaña (2012) The Pentacyclic Triterpenes α-, β-amyrins: A Review of Sources and Biological Activities. *Phytochemicals*. 23: 487-502

88. R Wang, QX Wu and YP Shi (2010) Polyacetylenes and Flavonoids from the Aerial Parts of Bidens Pilosa. *Planta Medica*. 76(9): 893-896

89. J Zhang, XL Fu, N Yang and QA Wang (2013) Synthesis and Cytotoxicity of Chalcones and 5-Deoxyflavonoids. *ScientificWorldJournal*. 2013: 649485

90. FR Garcez, WS Garcez, ALBD Santana, MM Alves, MFC Matos and AM scaliante (2006) Bioactive flavonoids and triterpenes from *Terminalia fagifolia* (Combretaceae). *J. Braz. Chem. Soc.* 17(7): 1223-1228

91. D Nakabo, Y Okano, N Kandori, T Satahira, N Kataoka, J Akamatsu and Y Okada (2018) Convenient Synthesis and Physiological Activities of Flavonoids in *Coreopsis lanceolata* L. Petals and Their Related Compounds. *Molecules*. 23(7): 1671

92. E Gabandé-Rodríguez, L Keane and M Capasso (2020) Microglial phagocytosis in aging and Alzheimer's disease. *J. Neurosci. Res*. 98(2): 284-298

93. L Li, HTT Ngo, E Hwang, X Wei, Y Liu, J Liu and TH Yi (2019) Conditioned Medium from Human Adipose-Derived Mesenchymal Stem Cell Culture Prevents UVB-Induced Skin Aging in Human Keratinocytes and Dermal Fibroblasts. *Int. J. Mol. Sci.* 21(1): 49

94. Y Pan and Z Lin (2019) Anti-aging Effect of Ganoderma (Lingzhi) with Health and Fitness. *Adv. Exp. Med. Biol*. 1182: 299-309

95. J Neves and P Sousa-Victor (2020) Regulation of inflammation as an anti-aging intervention. *FEBS J*. 287(1): 43-52

96. R Zhang, J Chen, X Mao, P Qi and X Zhang (2019) Anti-Inflammatory and Anti-Aging Evaluation of Pigment-Protein Complex Extracted from Chlorella Pyrenoidosa. *Mar. Drugs*. 17(10): 586

97. JV Horssen, PV Schaik and M Witte (2017) Inflammation and mitochondrial dysfunction: A vicious circle in neurodegenerative disorders?. *Neurosci. Lett*. 710: 132931

98. S Salvioli, D Monti, C Lanzarini, M Conte, C Pirazzini, MG Bacalini, P Garagnani, C Giuliani, E Fontanesi, R Ostan, L Bucci, F Sevini, SL Yani, A Barbieri, L Lomartire, V Borelli, D Vianello, E Bellavista, M Martucci, E Cevenini, E Pini, M Scurti, F Biondi, A Santoro, M Capri and C Franceschi (2013) Immune system, cell senescence, aging and longevity--inflamm-aging reappraised. *Curr. Pharm. Des*. 19(9): 1675-1679

99. P Soysal, F Arik, L Smith, SE Jackson and AT Isik (2020) Inflammation, Frailty and Cardiovascular Disease. *Adv. Exp. Med. Biol*. 1216: 55-64

100. J Papaconstantinou (2019) The Role of Signaling Pathways of Inflammation and Oxidative Stress in Development of Senescence and Aging Phenotypes in Cardiovascular Disease. *Cells*. 8(11): 1383

101. Y Wang, R Branicky, A Noe and S Hekimi (2018) Superoxide dismutases: dual roles in controlling ROS damage and regulating ROS signaling. *J. Cell. Biol*. 217(6): 1915-1928

102. YM Lee, BC Song and KJ Yeum (2015) Impact of Volatile Anesthetics on Oxidative Stress and Inflammation. *Biomed Res. Int*. 2015: 242709

103. J Tang, P Diao, X Shu, L Li and L Xiong (2019) Quercetin and Quercitrin Attenuates the Inflammatory Response and Oxidative Stress in LPS-Induced RAW264.7 Cells: In Vitro Assessment and a Theoretical Model. *Biomed Res. Int*. 2019: 7039802

104. TY Zhou, XW Xiang, M Du, LF Zhang, NX Cheng, XL Liu, B Zheng and ZS Wen (2019) Protective effect of polysaccharides of sea cucumber *Acaudina leucoprocta* on hydrogen peroxide-induced oxidative injury in RAW264.7 cells. *Int. J. Biol. Macromol*. 139: 1133-1140

105. OI Aruoma, HKaur and B Halliwell (1991) Oxygen free radicals and human diseases. *J. R. Soc. Health*. 111(5): 172-177

106. F Anwar, N Shaheen, G Shabir, M Ashraf, KM Alkharfy and AH Gilani (2013) Variation in Antioxidant Activity and Phenolic and Flavonoid Contents in the Flowers and Leaves of Ghaneri (*Lantana camara* L.) as Affected by Different Extraction Solven. *Int. J. Pharmacol*. 9: 442-453

107. K Aoyama, M Watabe and T Nakaki (2008) Regulation of neuronal glutathione synthesis. *J. Pharmacol. Sci*. 108: 227-238

108. Lo EH, Dalkara T and Moskowitz MA (2003) Mechanisms, challenges and opportunites in stroke. *Nat. Rev. Neurosci*. 4: 399-415

109. B Kulawiak, and A Szewczyk (2012) Glutamate-induced cell death in HT22 mouse hippocampal cells is attenuated by paxilline, a BK channel inhibitor. *Mitochondrion*. 12: 169-172

110. RA Floyd and JM Carney (1992) Free radical damage to protein and DNA: mechanisms involved and relevant observations on brain undergoing oxidative stress. *Ann. Neurol*. 32: S22-7

111. SL Doyle and LA O'Neill (2006) Toll-like receptors: From the discovery of NFkappaB to new insights into transcriptional regulations in innate immunity. *Biochem. Pharmacol*. 72: 1102-1113

112. D Pratico and JQ Trojanowski (2000) Inflammatory hypotheses: novel mechanisms of Alzheimer's neurodegeneration and new therapeutic targets. *Neurobiol. Aging*. 21: 441-445

113. PF Good, P Werner, A Hsu, CW Olanow and DP Perl (1996) Evidence of neuronal oxidative damage in Alzheimer's disease. *Am. J. Pathol*. 149: 21-28

114. K Apple, P Honegger and PJ Gebicke-Haerter (1995) Expression of interleukin-3 and tumor necrosis factor-beta mRNAs in cultured microglia. *J. Neuroimmunol*. 60(1-2): 83-91

115. AK Cross and MN Woodroofe (2001) immunoregulatory of microglial functional

properties. *Microse. Res. Tech*. 54: 10-17

116. F González-Scarano and G Baltuch (1999) Microglia as mediators of inflammatory and degenerative diseases. *Annu. Rev. Neurosci*. 22: 219-240

117. M Storck, M Schilling, K Burkhardt, R Prestel, D Abendroth and C Hammer (1994) Production of proinflammatory cytokines and adhesion molecules in ex-vivo xenogeneic kidney perfusion. *Transpl. Int*. 1: S647-S649

118. S Han, JH Lee, C Kim, D Nam, WS Chung, SG Lee, KS Ahn, SK Cho, M Cho and KS Ahn (2013) Capillarisin inhibits iNOS, COX-2 expression, and proinflammatory cytokines in LPS-induced RAW 264.7 macrophages via the suppression of ERK, JNK, and NF-κB activation. *Immunopharmacol Immunotoxicol.* 35: 34-42

119. M Fujihara, M Muroi, K Tanamoto, T Suzuki, H Azuma and H Ikeda (2003) Molecular mechanisms of macrophage activation and deactivation by lipopolysaccharide: roles of the receptor complex. *Pharmacol. Ther.* 100: 171-194

120. PP Tak and GS Firestein (2001) NF-kappaB: a key role in inflammatory diseases. *J. Clin. Invest.* 107: 7-11

121. CE Muller, C Khoo and SS Percival (2010) Cranberry polyphenols down-regulate the toll-like receptor 4 pathway and NF-κB activation, while still enhancing tumor necrosis factor α secretion. *FASEB J*. 24: 332.2

122. Bodet C, Chandad F and Grenier D (2006) Anti-inflammatory activity of a high-molecular-weight cranberry fraction on macrophages stimulated by lipopolysaccharides from periodontopathogens. *J. Dent. Res*. 85: 235-239

123. McCartney-Francis N, Allen JB, Mizel DE, Albina JE, Xie QW, Nathan CF and Wahl SM (1993) Suppression of arthritis by an inhibitor of nitric oxide synthase. *J. Exp. Med.* 178: 749-754

124. Elias PM (2007) The skin barrier as an innate immune element. *Semin Immunopathol.* 29: 3-14

125. Beissert S, Cavazzana I, Mascia F, Meroni P, Pastore S, Tessari G and Girolomoni G

(2006) Mechanisms of immune-mediated skin diseases: an overview. *Clin. Exp. Rheumatol.* 24: S1-6

126. Maas-Szabowski N, Shimotoyodome A and Fusenig NE (1999) Keratinocyte growth regulation in fibroblast cocultures via a double paracrine mechanism. *J. Cell Sci.* 112: 1843-1853

127. WS Seo, HN Oh, WJ Park, SY Um and SM Kang (2014) Study for possibility of n,n,n-trimethylphytosphingosine (TMP) for management of chronic skin diseases. *Kor. Soc. Biotechnol. Bioeng. J.* 29: 36-41

128. YJ Surh, KS Chun, HH Cha, SS Han, YS Keum, KK Park and SS Lee (2001) Molecular mechanisms underlying chemopreventive activities of anti-inflammatory phytochemicals: down-regulation of COX-2 and iNOS through suppression of NF-κB activation. *Mutat. Res.* 480: 243-268

129. VJ Palombella, OJ Rando, AL Goldberg and Maniatis T (1994) The ubiquitin-proteasome pathway is required for processing the NF-κappa B1 precursor protein and the activation of NF-κappaB. *Cell.* 78(5): 773-785

130. DA Walsh (1999) Angoigenesis and arthritis. *Rheumatology (Oxford)*. 38: 103-112

APPENDIX

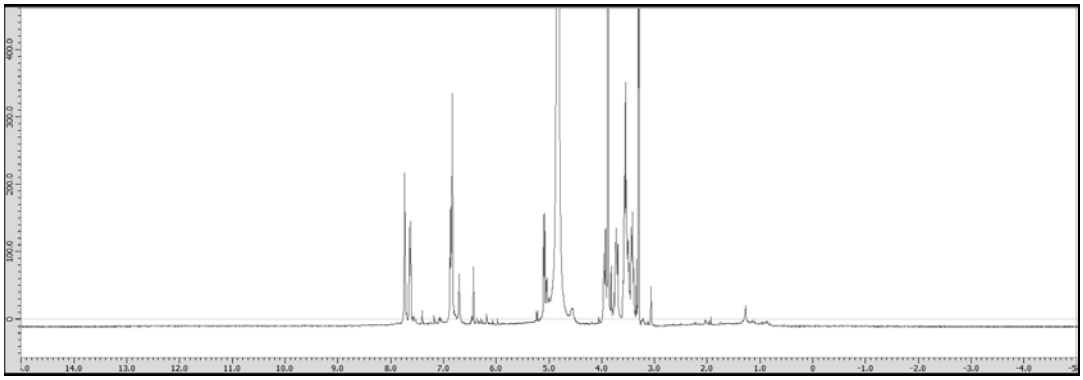

Fig. 35: ^{1}H-NMR spectrum of compound 1 (400 MHz, CD_3OD)

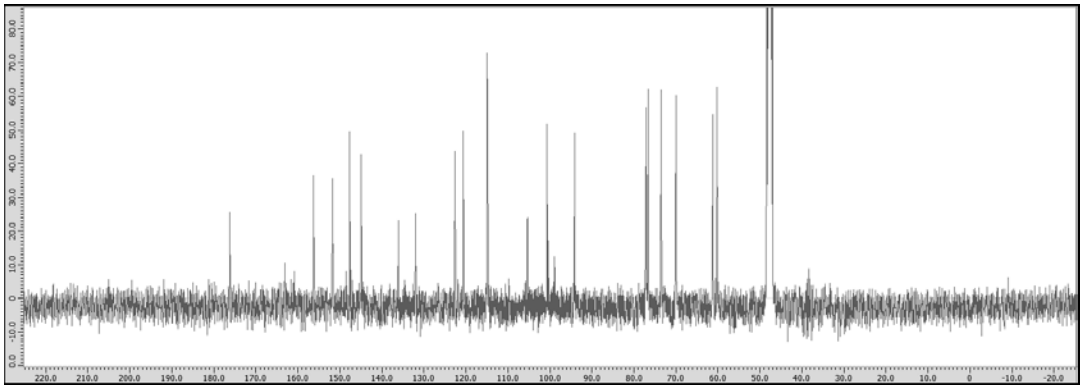

Fig. 36: ^{13}C-NMR spectrum of compound 1 (100 MHz, CD_3OD)

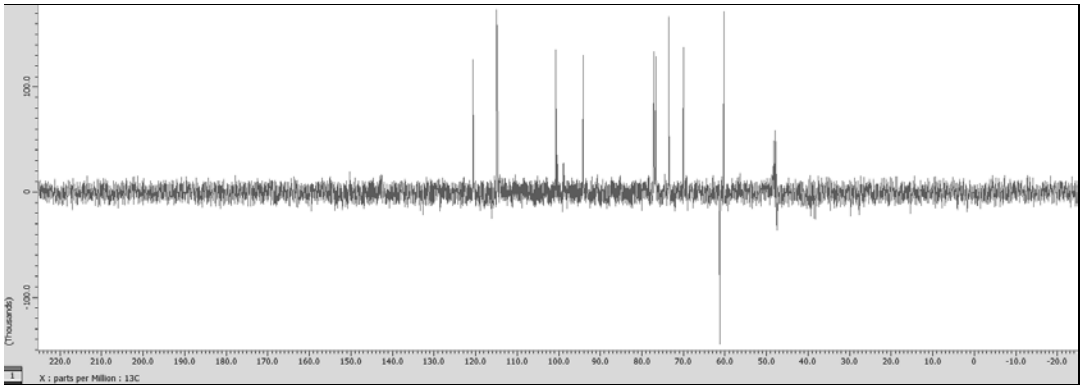

Fig. 37: DEPT spectrum of compound 1 (100 MHz, CD_3OD)

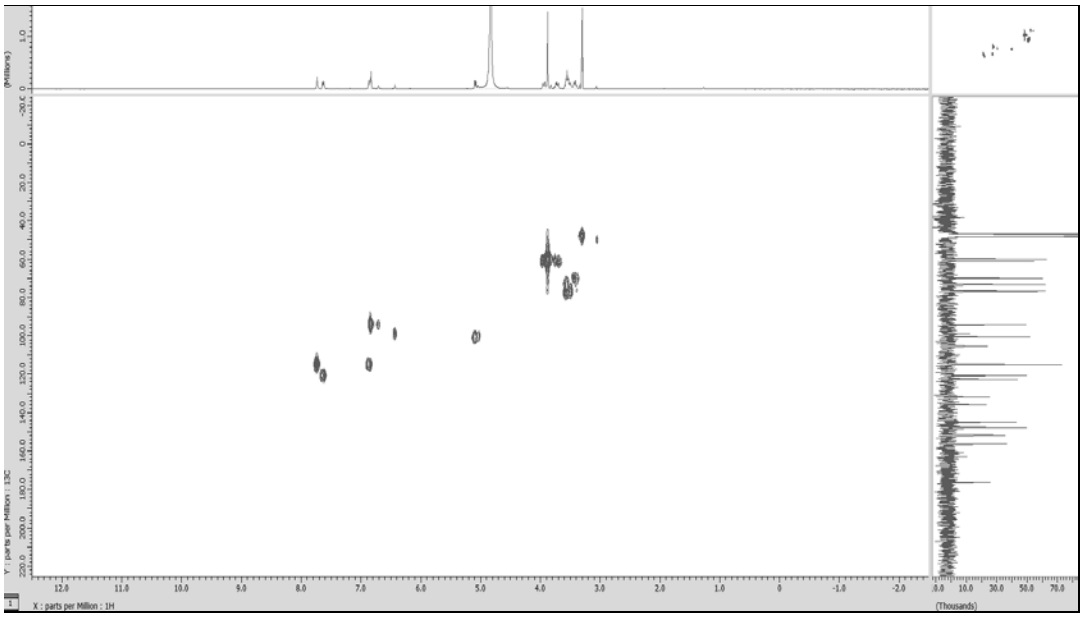

Fig. 38: HSQC spectrum of compound 1 (CD_3OD)

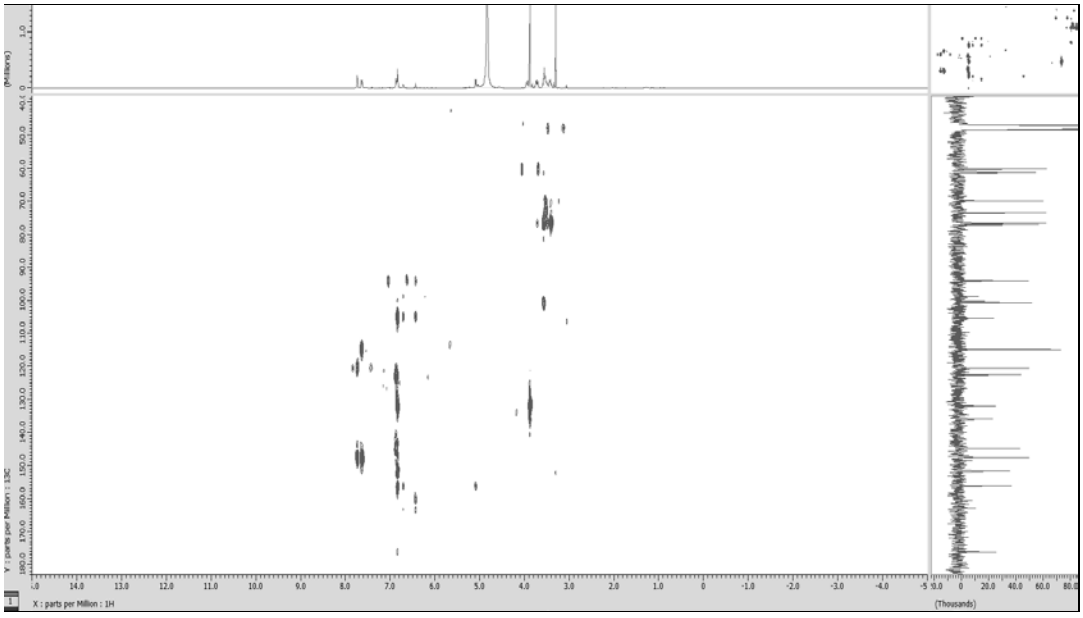

Fig. 39: HMBC spectrum of compound 1 (CD_3OD)

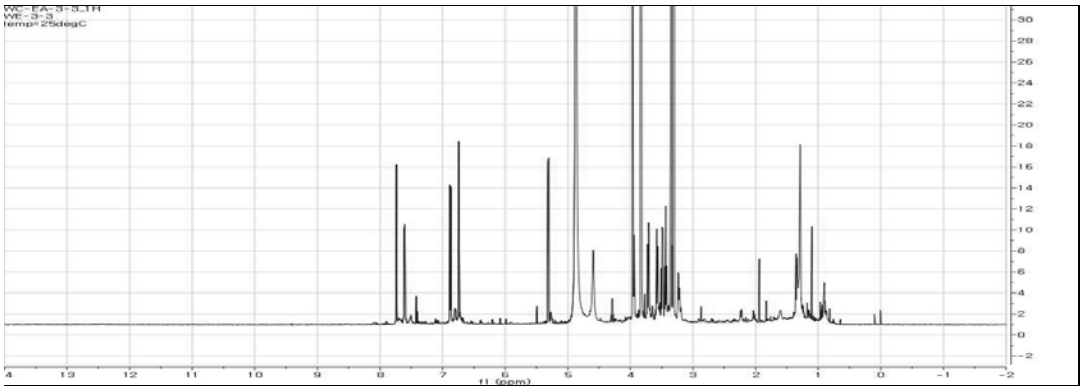

Fig. 40: ^{1}H-NMR spectrum of compound 2 (600 MHz, CD_3OD)

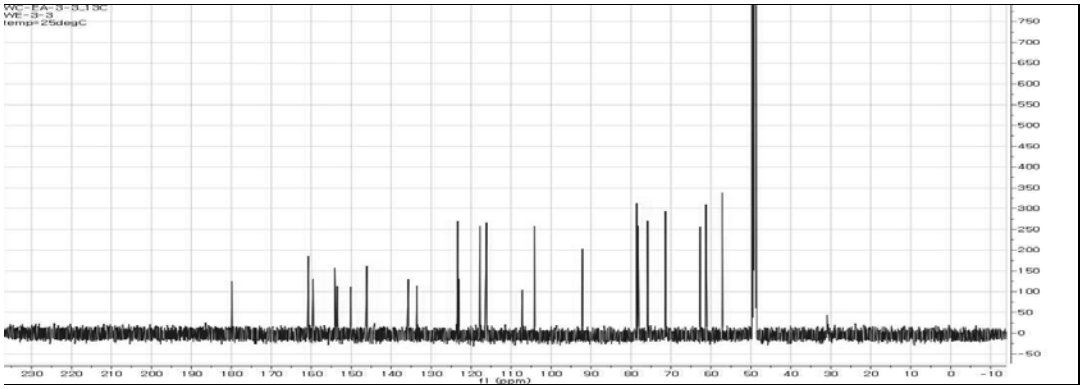

Fig. 41: ^{13}C-NMR spectrum of compound 2 (150 MHz, CD_3OD)

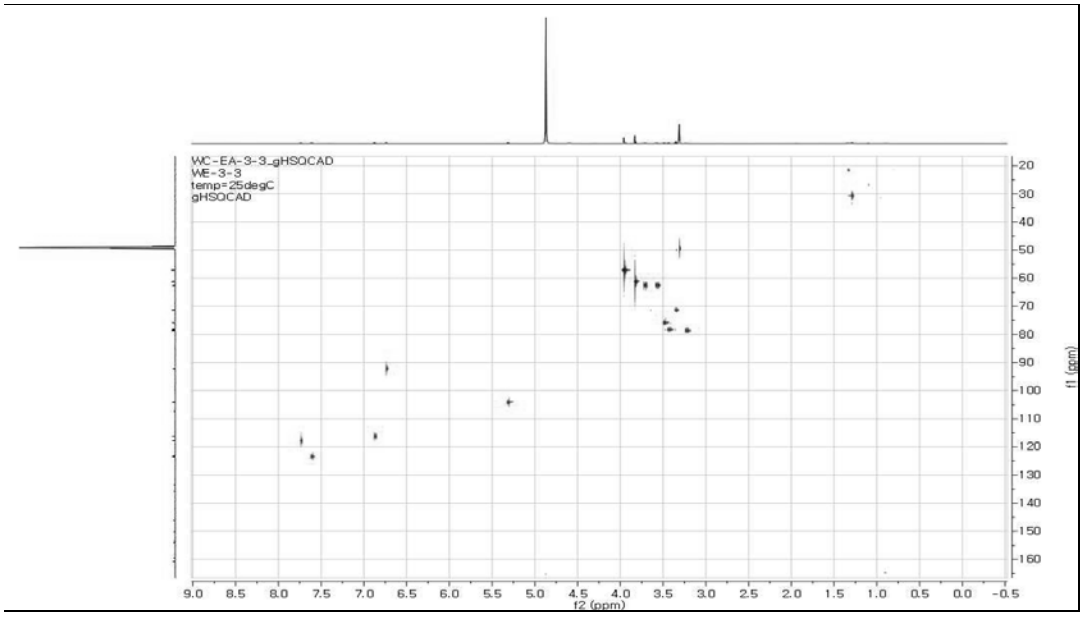

Fig. 42: HSQC spectrum of compound 2 (CD_3OD)

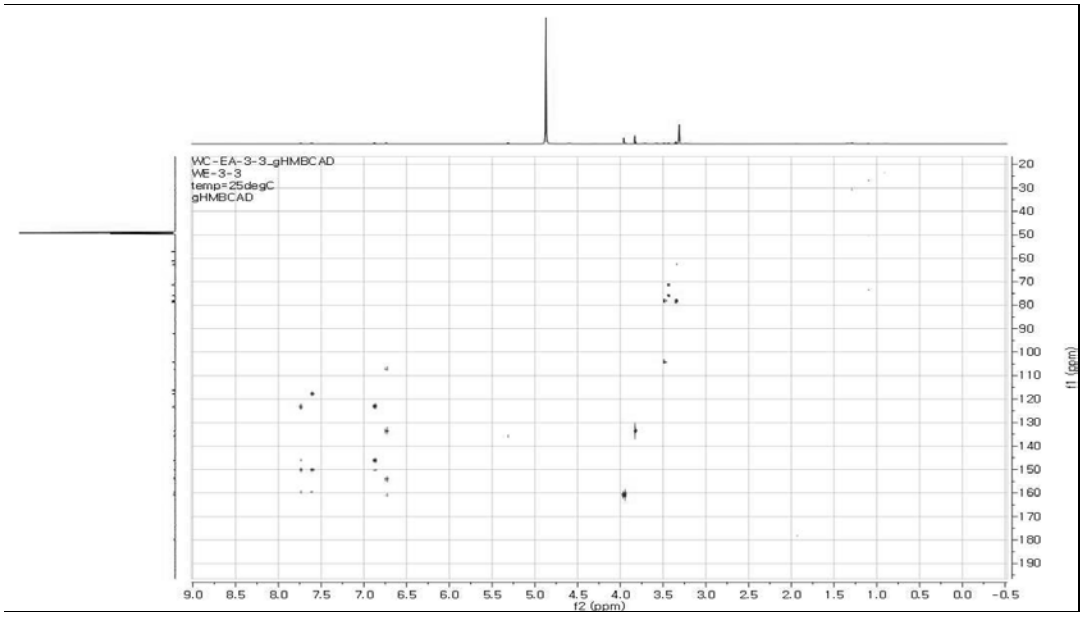

Fig. 43: HMBC spectrum of compound 2 (CD_3OD)

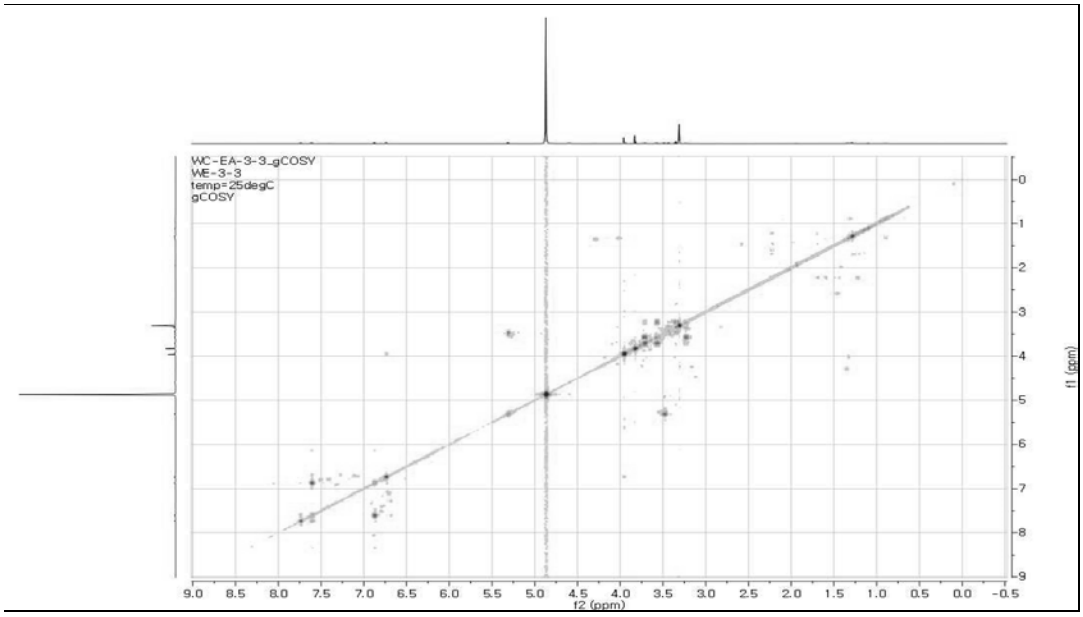

Fig. 44: COSY spectrum of compound 2 (CD_3OD)

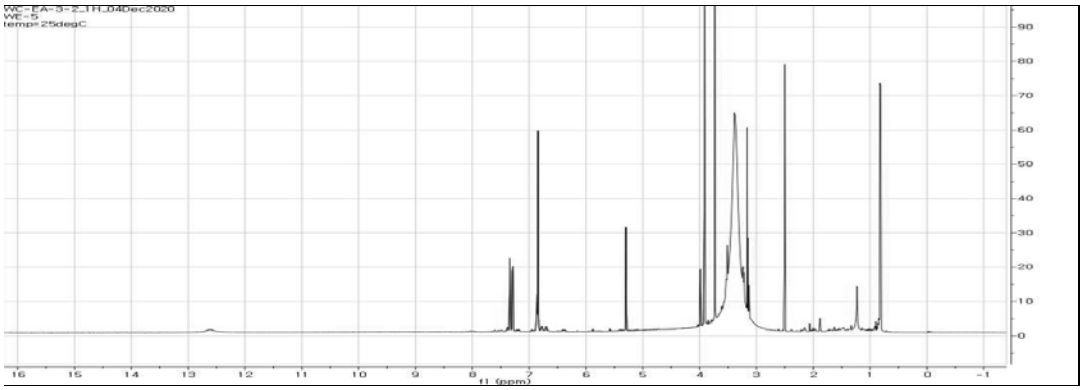

Fig. 45: ^{1}H-NMR spectrum of compound 3 (600 MHz, DMSO- d_6)

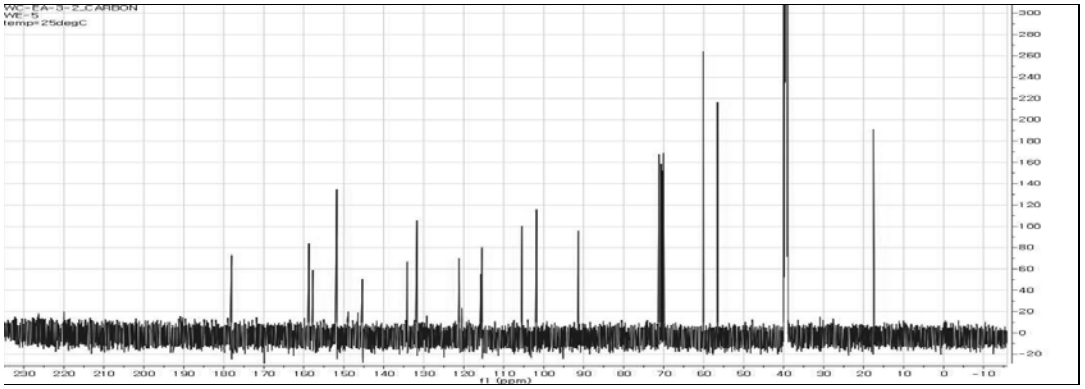

Fig. 46: ^{13}C-NMR spectrum of compound 3 (150 MHz, DMSO- d_6)

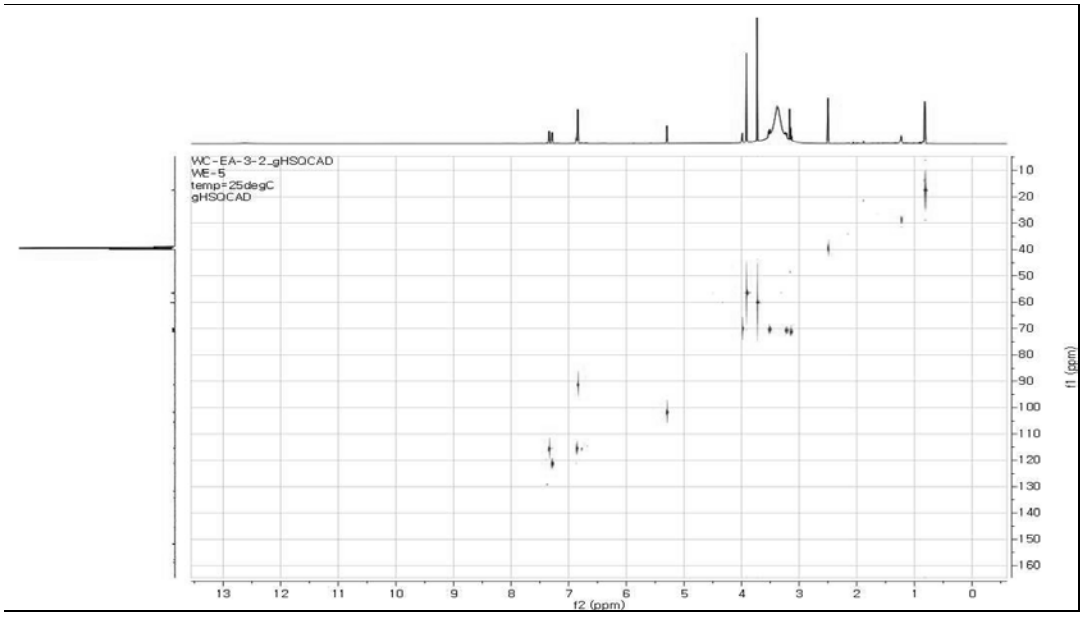

Fig. 47: HSQC spectrum of compound 3 (DMSO-d_6)

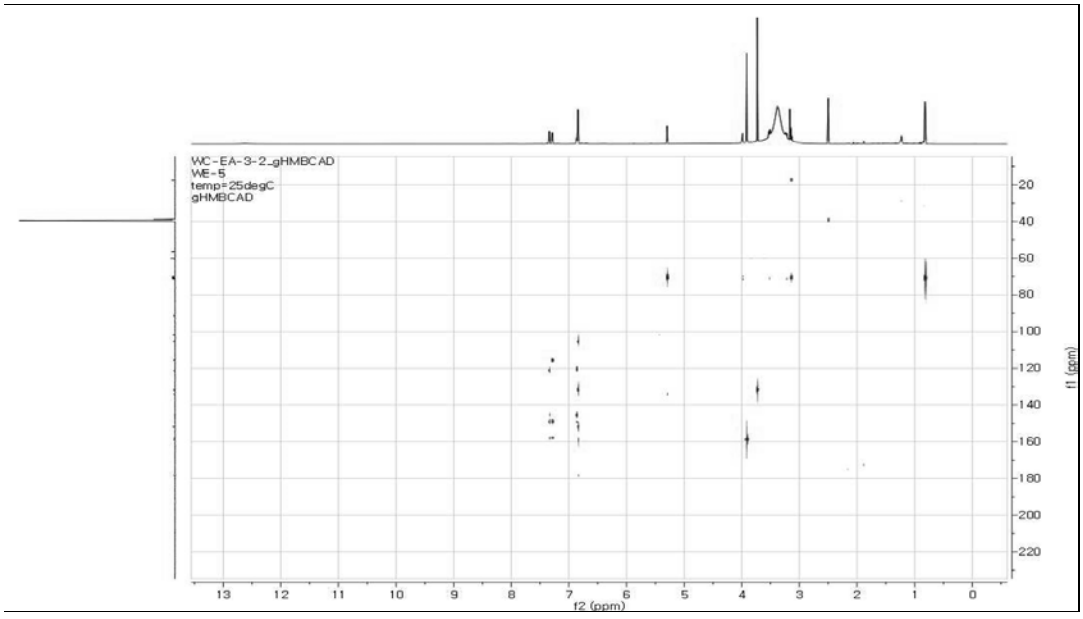

Fig. 48: HMBC spectrum of compound 3 (DMSO- d_6)

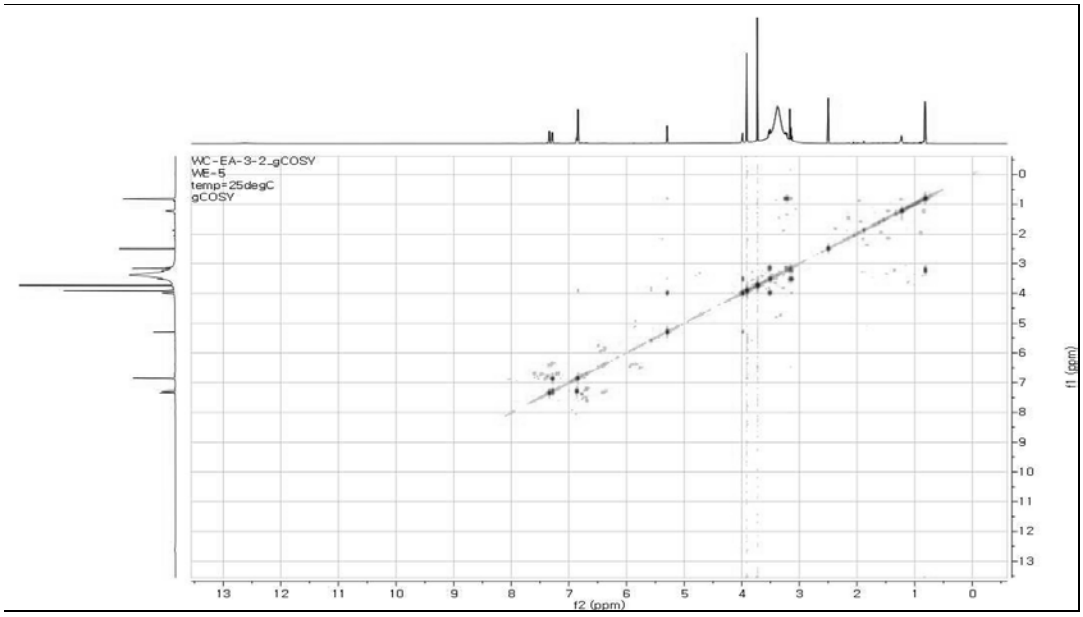

Fig. 49: COSY spectrum of compound 3 (DMSO-d_6)

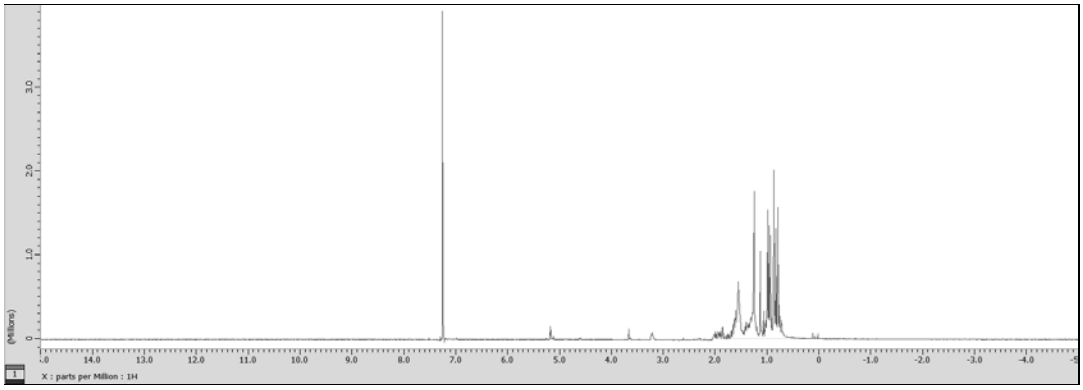

Fig. 50: ^{1}H-NMR spectrum of compound 4 (400 MHz, $CDCl_3$)

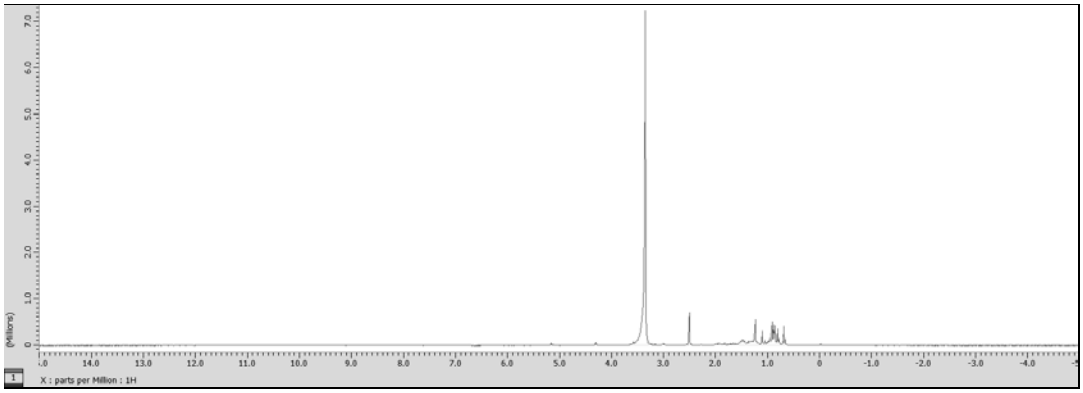

Fig. 51: ^{1}H-NMR spectrum of compound 4 (400 MHz, DMSO-d_6)

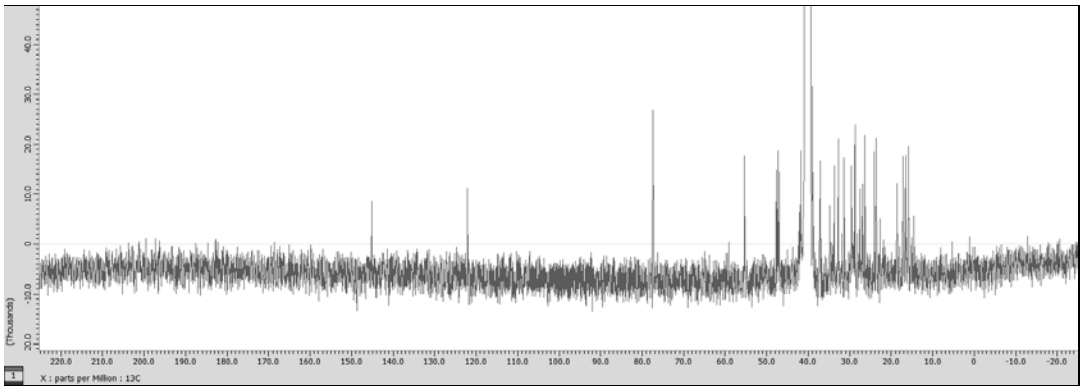

Fig. 52: ^{13}C-NMR spectrum of compound 4 (100 MHz, DMSO-d_6)

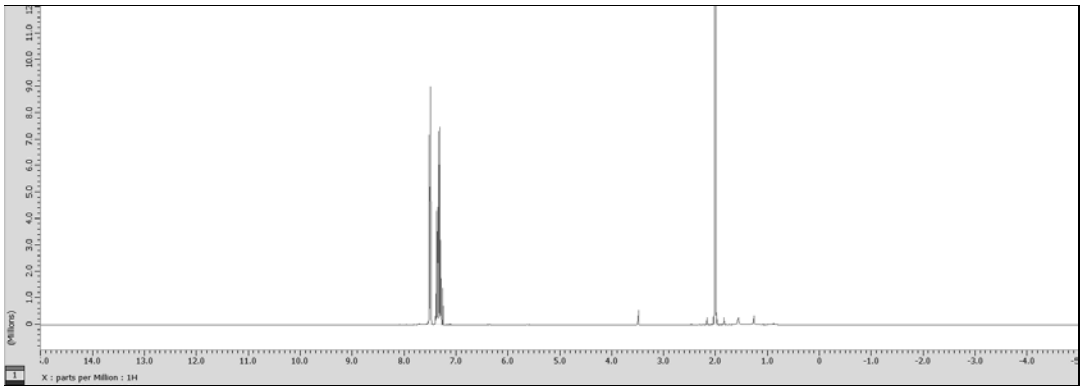

Fig. 53: ^{1}H-NMR spectrum of compound 5 (400 MHz, $CDCl_3$)

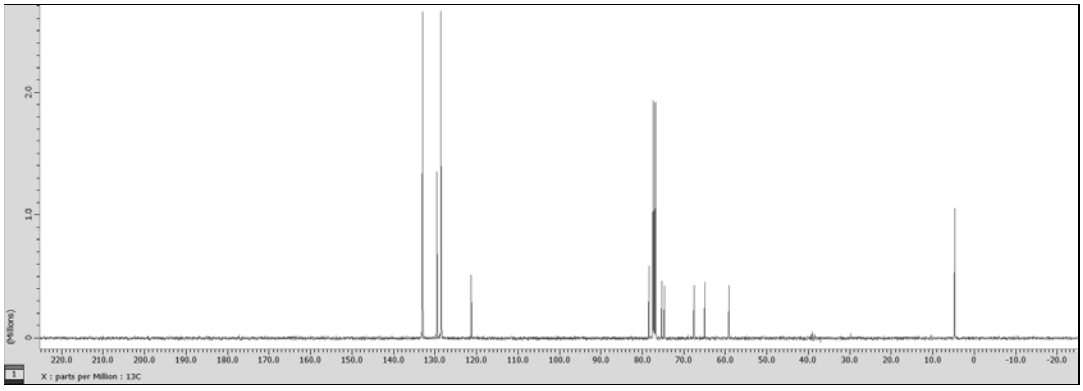

Fig. 54: ^{13}C-NMR spectrum of compound 5 (100 MHz, $CDCl_3$)

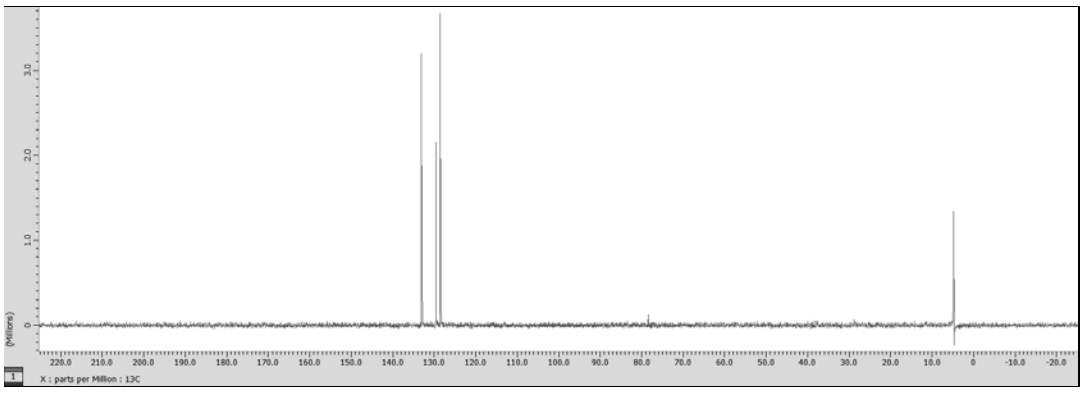

Fig. 55: DEPT spectrum of compound 5 (100 MHz, $CDCl_3$)

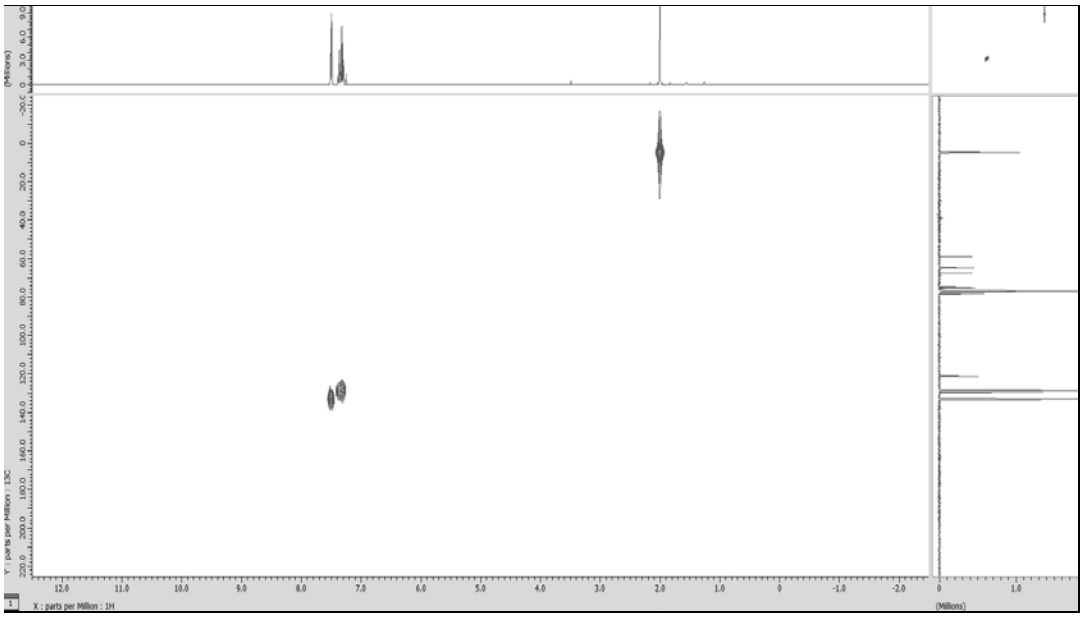

Fig. 56: HSQC-NMR spectrum of compound 5 ($CDCl_3$)

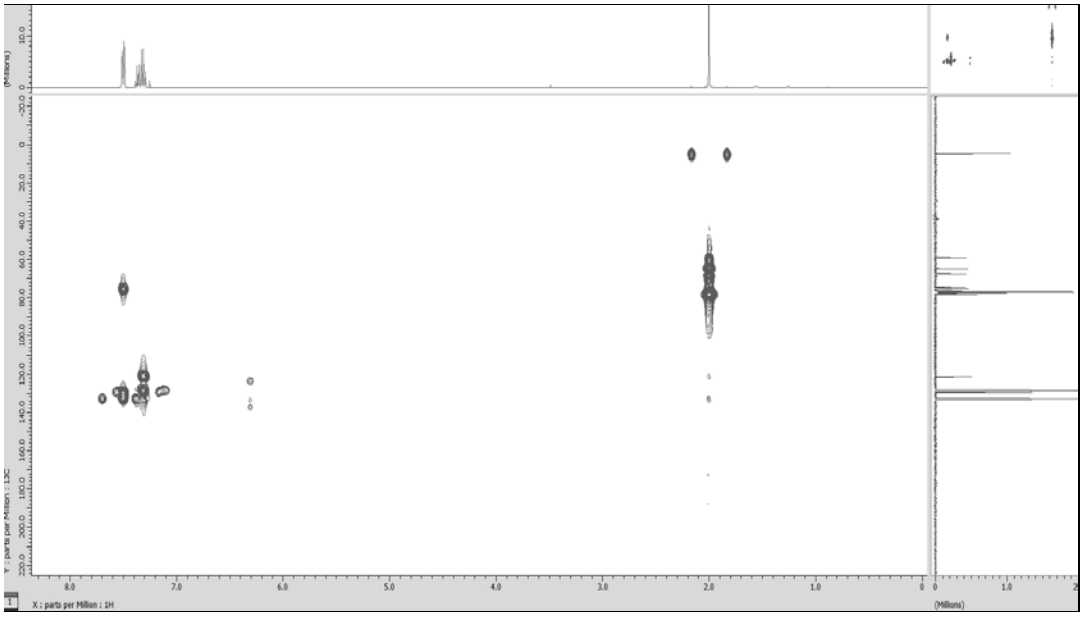

Fig. 57: HMBC-NMR spectrum of compound 5 ($CDCl_3$)

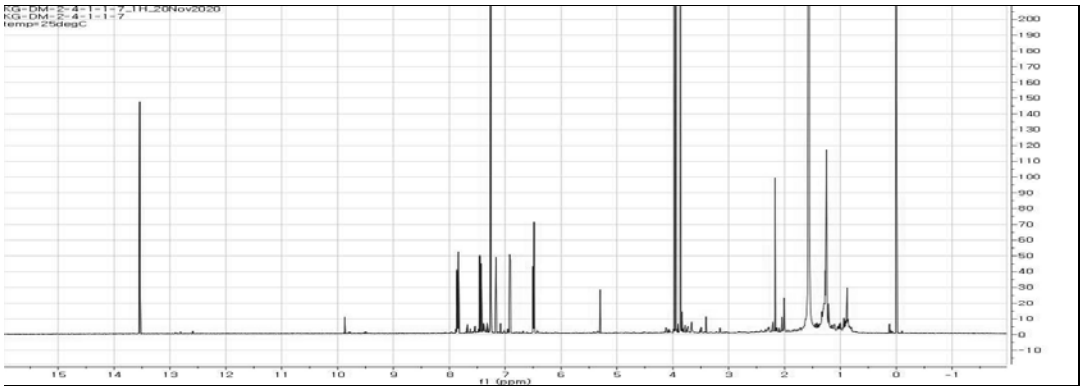

Fig. 58: ^{1}H-NMR spectrum of compound 6 (600 MHz, $CDCl_3$)

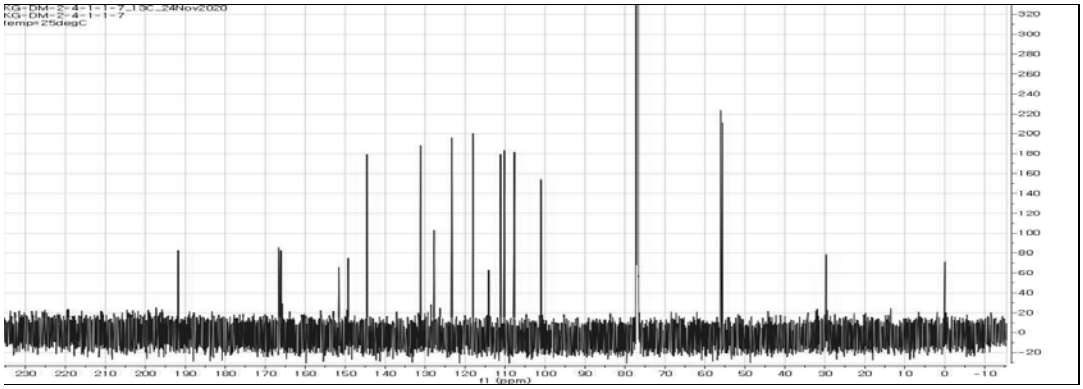

Fig. 59: ^{13}C-NMR spectrum of compound 6 (150 MHz, $CDCl_3$)

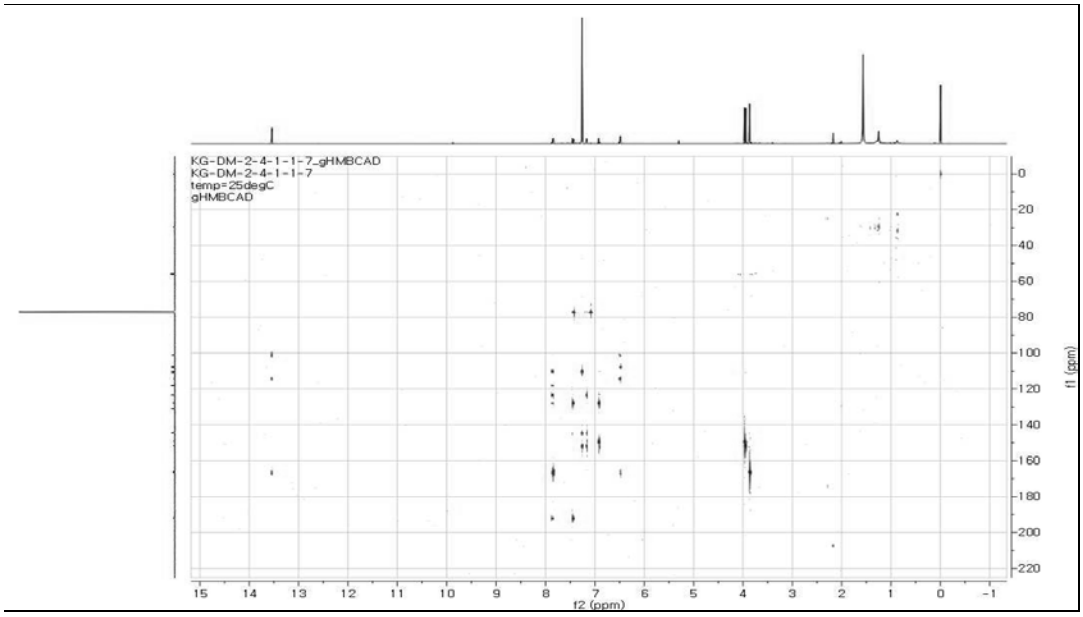

Fig. 60: HMBC-NMR spectrum of compound 6 ($CDCl_3$)

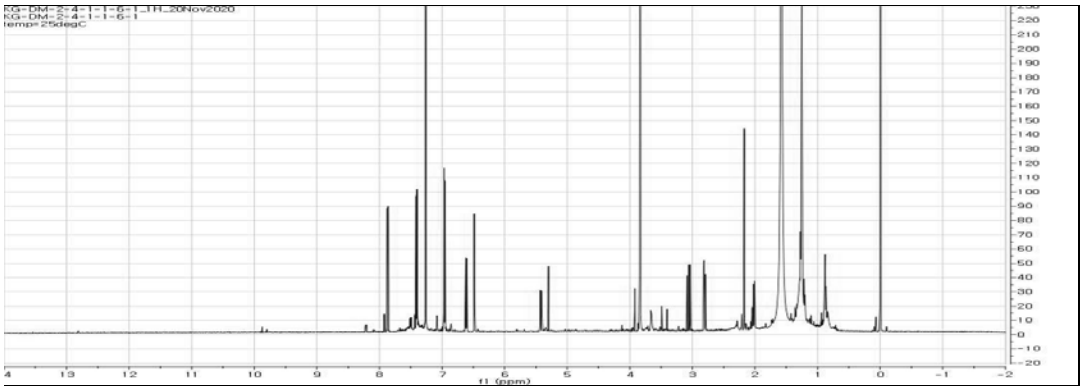

Fig. 61: ^{1}H-NMR spectrum of compound 7 (600 MHz, $CDCl_3$)

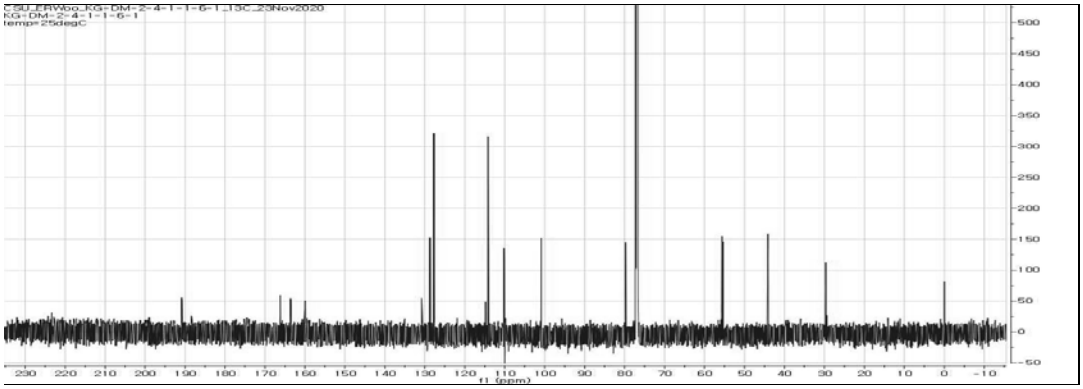

Fig. 62: ^{13}C-NMR spectrum of compound 7 (150 MHz, $CDCl_3$)

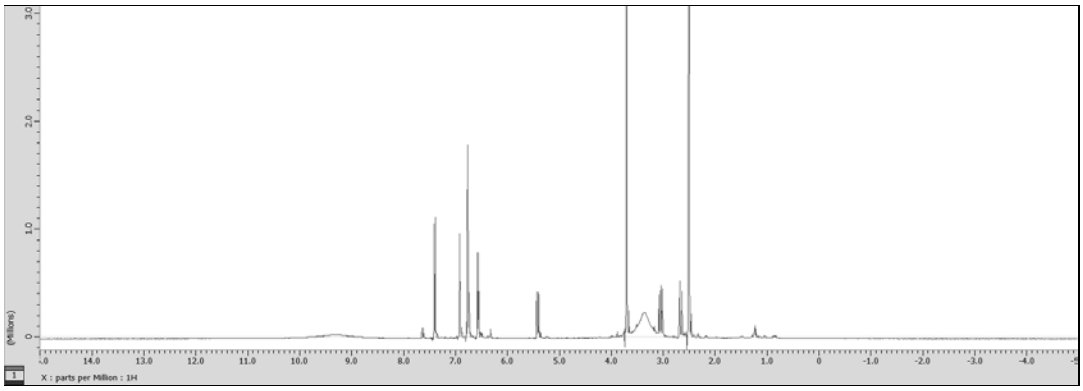

Fig. 63: ^{1}H-NMR spectrum of compound 8 (400 MHz, CD_3OD)

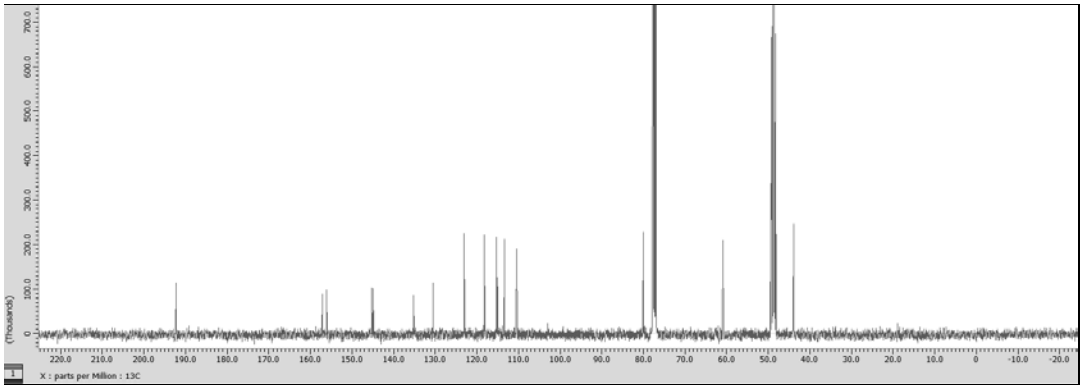

Fig. 64: ^{13}C-NMR spectrum of compound 8 (100 MHz, CD_3OD)

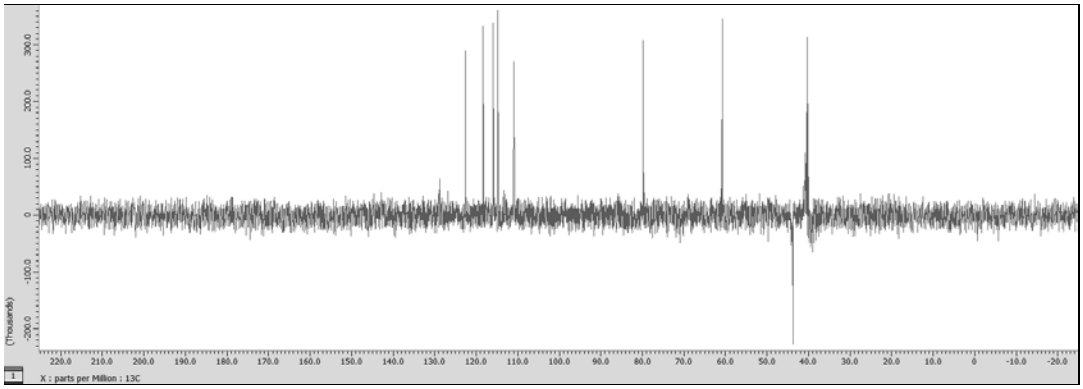

Fig. 65: DEPT spectrum of compound 8 (100 MHz, CD_3OD)

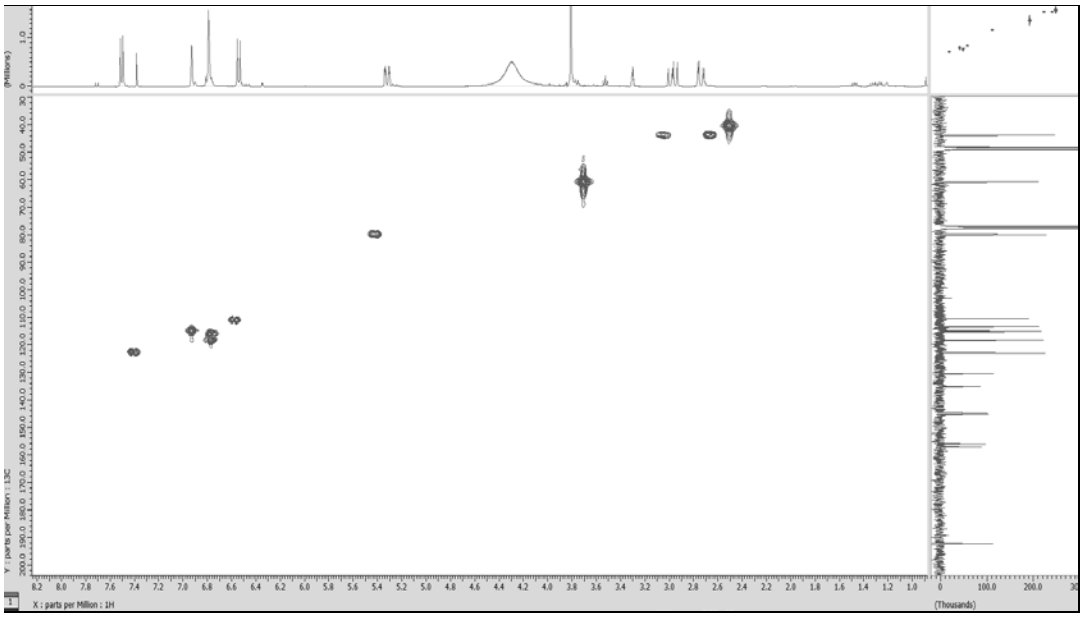

Fig. 66: HSQC spectrum of compound 8 (CD_3OD)

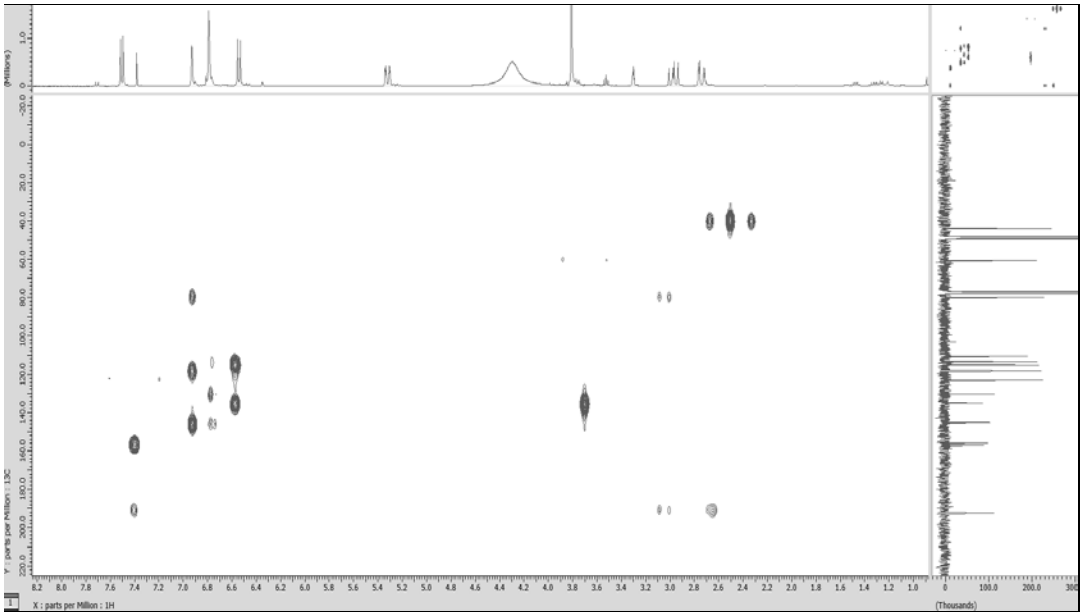

Fig. 67: HMBC spectrum of compound 8 (CD_3OD)

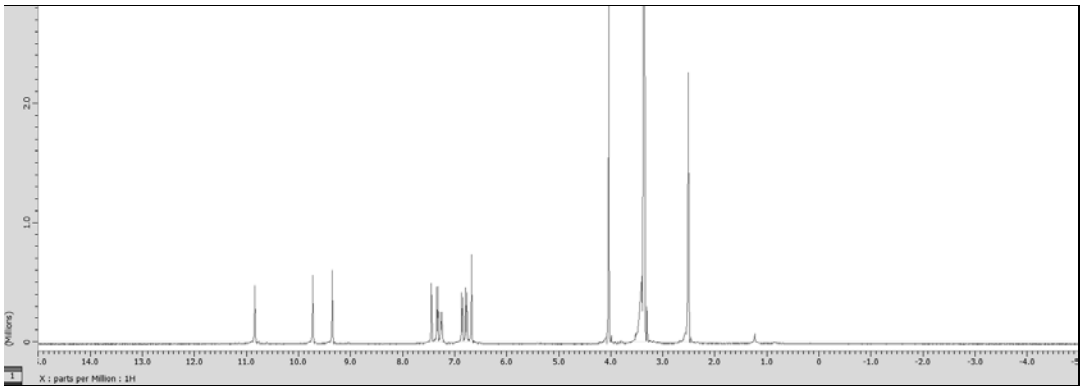

Fig. 68: ^{1}H-NMR spectrum of compound 9 (400 MHz, DMSO- d_6)

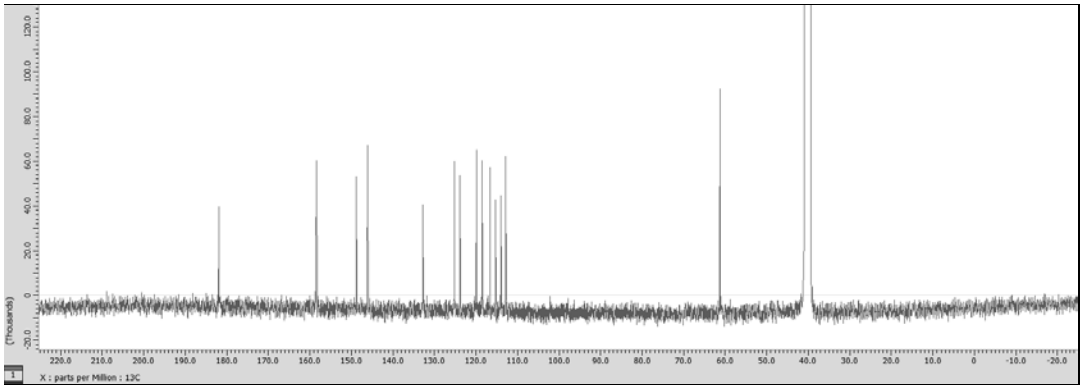

Fig. 69: ^{13}C-NMR spectrum of compound 9 (100 MHz, DMSO- d_6)

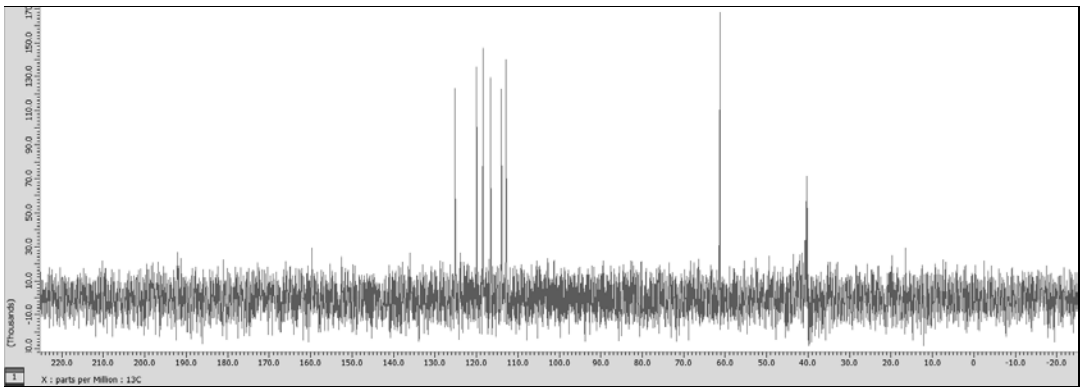

Fig. 70: DEPT spectrum of compound 9 (100 MHz, DMSO- d_6)

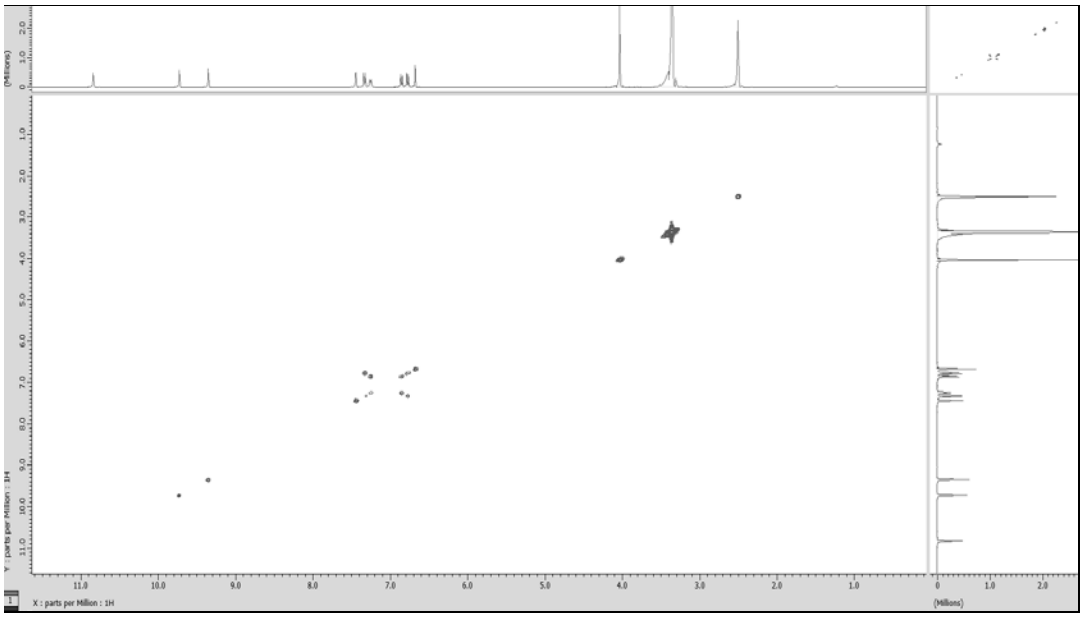

Fig. 71: COSY spectrum of compound 9 (DMSO- d_6)